NASA CR-168267

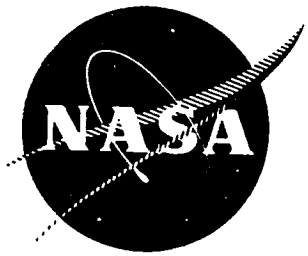

DYNAMIC GAS TEMPERATURE MEASUREMENT SYSTEM FINAL REPORT

VOLUME I
TECHNICAL EFFORTS

by
D. L. Elmore, W. W. Robinson and W. B. Watkins

Prepared for
National Aeronautics and Space Administration

NASA-Lewis Research Center
Contract NAS3-23154
Cleveland, Ohio 44135

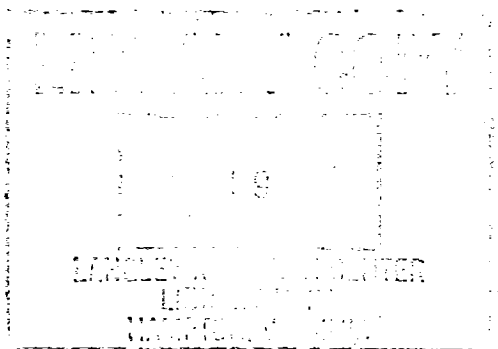

Printed in the United States of America

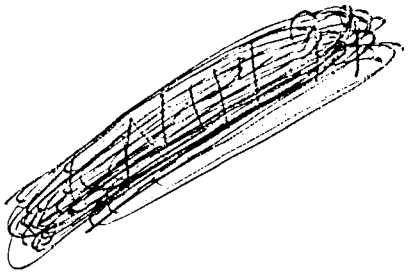

DISPLAY 02/2/1

84N16529*# ISSUE 7 PAGE 1007 CATEGORY 35

RPT#: NASA-CR-168267-VOL-1 NAS 1.26:168267-VOL-1 PWA/GPD-FR-17145-VOL-1

CNT#: NAS3-23154 83/05/10 138 PAGES UNCLASSIFIED DOCUMENT

UTTL: Dynamic gas temperature measurement system, volume 1

AUTH: A/ELMORE, D. L.; B/ROBINSON, W. W.; C/WATKINS, W. B.

CORP: Pratt and Whitney Aircraft, West Palm Beach, FL. AVAIL.CASI

SAP: Avail: CASI HC A07/MF A02

CIO: UNITED STATES

MAJS: /*COMBUSTION CHAMBERS/*EXHAUST GASES/*GAS TEMPERATURE/*GAS TURBINE ENGINES /*TEMPERATURE MEASUREMENT

MINS: / CONDUCTIVE HEAT TRANSFER/ CONVECTIVE HEAT TRANSFER/ DURABILITY/ THERMOCOUPLES

ABA: S.L.

ABS: A gas temperature measurement system with compensated frequency response of 1 kHz and capability to operate in the exhaust of a gas turbine engine combustor was developed. A review of available technologies which could attain this objective was done. The most promising method was identified as a two wire thermocouple, with a compensation method based on the responses of the two different diameter thermocouples to the fluctuating gas temperature field. In a detailed design of the probe, transient conduction effects were identified as significant. A compensation scheme was derived to include the effects of gas convection and wire conduction.

ENTER: MORE

1. Report Number	2. Govt Accession No.	3. Recipient's Catalog Number
NASA CR-168267		CR-168267

4. Title *(and Subtitle)*	5. Report Date
DYNAMIC GAS TEMPERATURE MEASUREMENT SYSTEM	10 May 1983
	6. Performing Organization Code

7. Author(s)	8. Performing Organization Report No.
D. L. Elmore, W.W. Robinson and W.B. Watkins	P&WA/GPD FR-17145

9. Performing Organization Name and Address	10. Work Unit No.
United Technologies Corporation Pratt & Whitney Aircraft Group Government Products Division P.O. Box 2691, West Palm Beach, FL 33402	11. Contract or Grant No. NAS3-23154

12. Sponsoring Agency Name and Address	13. Type of Report and Period Covered
National Aeronautics and Space Administration NASA-Lewis Research Center Cleveland, Ohio 44135	Final Report
	14. Sponsoring Agency Code

15. Supplementary Notes

3645

Project Manager, G. C. Fralick, Instrumentation and Fluid Mechanics Division, NASA-Lewis Research Center, Cleveland, Ohio 44135

16. Abstract

The objective of this contract was to develop a gas temperature measurement system with compensated frequency response of 1 kHz and capability to operate in the exhaust of a gas turbine engine combustor. A review of available technologies which could attain this objective was done. The most promising method was identified as a two-wire thermocouple, with a compensation method based on the responses of the two different diameter thermocouples to the fluctuating gas temperature field. In a detailed design of the probe, transient conduction effects were identified as significant. A compensation scheme was derived to include the effects of gas convection and wire conduction. The two-wire thermocouple concept was tested in a laboratory burner exhaust to temperatures of about 3000°F and in a gas turbine engine to combustor exhaust temperatures of about 2400°F. Uncompensated and compensated waveforms and compensation spectra are presented.

17. Key Words	18. Distribution Statement
	Unclassified – unlimited

19. Security Classif. (of this report)	20. Security Classif. (of this page)	21. No. of Pages	22. Price*
Unclassified	Unclassified	131	

*For sale by the National Technical Information Service, Springfield, Virginia 22151

TABLE OF CONTENTS

TABLE OF CONTENTS (Continued)

LIST OF ILLUSTRATIONS

LIST OF ILLUSTRATIONS (Continued)

LIST OF ILLUSTRATIONS (Continued)

LIST OF ILLUSTRATIONS (Continued)

LIST OF ILLUSTRATIONS (Continued)

LIST OF ILLUSTRATIONS (Continued)

SECTION I
SUMMARY

The objective of this contract was to develop a gas temperature measurement system with compensated frequency response of 1 kHz and capability to operate in the exhaust of a gas turbine engine combustor. A review of available technologies which could attain this objective was done. The most promising method was identified as a two-wire thermocouple, with a compensation method based on the responses of the two different diameter thermocouples to the fluctuating gas temperature field. In a detailed design of the probe, transient conduction effects were identified as significant. A compensation scheme was derived to include the effects of gas convection and wire conduction. The two-wire thermocouple concept was tested in a laboratory burner exhaust to temperatures of about 3000°F and in a gas turbine engine to combustor exhaust temperatures of about 2400°F. Uncompensated waveforms and compensation spectra are also presented.

SECTION II
INTRODUCTION

The objective of this contract was to develop a gas temperature measurement system with compensated frequency response of 1 kHz and capabiliiy to operate in the exhaust of a gas turbine combustor. This contract was accomplished in five technical tasks:

Task 1: Study and Selection of Methods
Task 2: Analysis of Methods and Selection of the Most Promising Method
Task 4: System Design and Test Plan Formulation
Task 5: Fabrication and Tests
Task 6: Analysis of Results.

In Task 1, several methods were identified through literature searches using NASA RECON, Lockheed Dialog and Defense Technical Information Center Systems. References to methods are listed in Appendix A. Methods were evaluated against criteria for geometry, temperature, frequency response, pressure, flow conditions, gas composition, sensor life, accuracy, spatial resolution, and vibration. Each method was rated either satisfactory or unsatisfactory. Results of the evaluation are shown in Table II. Two concepts, both bare wire thermocouples, were identified in this evaluation for further study.

The two concepts identified for Task 2, analysis of methods and selection of the most promising method, were a single-wire pulse heated thermocouple and a dual wire passive thermocouple. Both concepts use unique data analysis methods to measure the convective heat transfer coefficient, h_g, in-situ, to derive a compensation spectrum. Both concepts were analyzed for mechanical, thermal and data acquisition/reduction system characteristics to determine which concept would be chosen for detailed design and test. In the mechanical analysis, concepts are very similar, and the same design satisfies structural requirements. It was discovered in the thermal analysis that the effects of the transient heat conduction were significant in the range of wire length-to-diameter ratios required by the mechanical analysis. A compensation method would therefore necessarily include the effects of transient heat conduction. In the data acquisition/reduction system analysis, several problems in pulse heating the single wire thermocouple were identified, including switching from pulsing to recording circuits, zero stability, measurement accuracy, and number of data records required. The two-wire technique did not involve these difficulties and was selected for detailed design and testing.

In Task 4, System Design and Test Plan Formulation, detailed mechanical design of probes was done and a test plan which addressed environmental criteria was formulated. In addition, an analysis method which compensates measured waveforms and includes the effects of transient conduction was computerized and checked out.

The design of the two-wire probe which was used in the subscale combustor tests is shown in Figure 7. The probe was designed to operate in aerodynamic loads encountered in an atmospheric pressure, Mach = 0.25, high temperature combustion stream. Vibratory load design cirteria of 500g's were imposed. The thermocouple elements are beadless junctions fabricated using a proprietary Pratt & Whitney Aircraft (P&WA) method. Use of a beadless junction simplifies analysis considerably, since the thermocouple is then a cylinder in crossflow.

The design of the probe used in the gas turbine engine tests is shown in Figures 5 and 6. The probe is designed to operate at aerodynamic loads encountered in a 20-atmosphere pressure, Mach = 0.3, high temperature combustion stream. Vibratory load design criteria of 500g's were imposed. This probe also uses beadless junction thermocouples.

A summary of the test plan is shown in Table IV. The test plan addresses all of the environmental factors specified by NASA.

The data analysis method is described in detail in Task 4. This method was computer coded and implemented on a Hewlett-Packard 5451C Fourier Analyzer System. The key feature of the method is determination of the gas heat transfer coefficient (h_g) from measured thermocouple response. Compensation for thermal lag and conduction effects may then be done numerically. The computer model uses a finite-element breakup of the thermocouple wire, support posts and ceramic body and is shown in Figure 11.

In Task 5, Fabrication and Tests, two-wire probes were built and tested. The probe design in Figure 7 was fabricated for test in a laboratory subscale combustor. The probe as built is shown in Figure 16. Figure 18 is a photographic record of the 76 μm (0.003 in.) and 250 μm (0.010 in.) diameter thermocouple junctions. These photographs verify that the junctions are indeed beadless. Figure 41 is a photograph of the subscale combustor probe in the high-temperature exhaust of the laboratory combustor. Approximately two hours of test time were accumulated on this probe at temperatures ranging from about 1050K (~1900°F) to 1650K (~3000°F). Erosion effects were not significant on this probe.

Figure 17 is a photograph of the probe built for testing in the gas turbine engine. This probe used beadless thermocouple junctions similar to those shown in Figure 18. The probe was installed and tested in a gas turbine engine. After approximately one hour of testing, the 76 μm element signal became intermittent, and post-test inspection of the probe revealed the 76 μm element to be missing. The intermittent nature of the signal suggests that the element failed at test point No. 6, at a temperature of ~1225K (~1750°F). Since the structural design criteria exceed any loads present in the engine, and from the durability of the subscale combustor probe, the most likely failure mechanism has been determined to be particulate bombardment in the engine, especially during engine transients.

In Task 6, subscale combustor data and gas turbine engine data were compensated. Figure 47 is a plot of waveforms observed from 76 μm (3 mil) and 250 μm (10 mil) thermocouples in the highest temperature subscale combustor test point. Figure 15 is a plot of the 76 μm compensation spectrum derived using the data analysis method from Task 4. Figure 51 is the compensated waveform for a 100 millisecond portion of waveform. Frequency response for an instantaneous spectrum was demonstrated to be in excess of 1 kHz, and for an averaged spectrum, in excess of 1.2 kHz.

Figure 59 is a time waveform of the 76 μm output in the gas turbine engine test at temperature of ~1225K(~1745°F). Figure 65 is the compensation spectrum for the 76 μm thermocouple derived using the data analysis method from Task 4. Figure 67 is a 50 millisecond record of the compensated 76 μm waveform.

Overall accuracy of the compensation technique was studied by fabricating electrical circuit analogs to the finite element model of Figure 26. One such model is shown in Figure 27. Input and output waveforms could be compared in the computer to calculate directly the compensation spectrum. The data analysis method was also used to calculate a compensation spectrum. Comparisons between the two compensation methods yielded a key portion of the total method uncertainty. Uncertainties due to signal to noise ratio and thermocouple wire diamaters were propagated to give a total error. Table XI is the error stackup for the ensemble averaged frequency spectra of various types of temperature waveforms. From Table XI, where the most representative waveforms for actual combustors are 15K peak-to-peak/ $\sqrt{\text{Hz}}$ from 0 to 1 kHz, the error in the 0-200 Hz bandwidth is 6.1%, which exceeds the contract goal of 5%. In the 200-1000 Hz bandwidth, the error is 7.6%, which is less than the contract goal of 10 percent. Table XII is the error stackup for the same waveforms presented as the compensated instantaneous time waveforms. For the 15K peak-peak/ $\sqrt{\text{Hz}}$ waveform, the error in the 0-200 Hz bandwidth is 7.4% and in the 200-1000 Hz bandwidth the error is 12.9%.

SECTION III
TECHNICAL EFFORTS

A. TASK 1 — STUDY AND SELECTION OF METHODS

1. Summary

A study of methods for measuring rapidly varying gas temperature in a gas turbine combustor environment was completed. Principal results of this study were (1) a literature search of temperature measuring methods, (2) conceptual ideas that lend themselves to development of a prototype instrument, and (3) consultation with recognized authorities in the field of temperature measurement. All methods accumulated in this task were evaluated against criteria set forth in NASA RFP 3-355995, Exhibit B, and are listed in Table I. Two methods were found acceptable using these criteria. The first method found acceptable, a single wire pulse-heated thermocouple concept, was specified in the request for proposal (RFP). A second method, a dual wire passive thermocouple which had been attempted by P&WA, was also found acceptable. These two methods were selected for further study in Task 2.

TABLE I. — SENSOR ENVIRONMENTAL GUIDELINES

Geometry:	Annular combustor, $2\text{ cm} < H < 8\text{ cm}$
Temperature:	$T \sim 1400\text{K}$ (2060°F); $T' \sim 500\text{K}$ (900°F)
Frequency response:	1 kHz
Pressure:	$1.01 \times 10^6\text{N/M}^2$(10 ATM) $< P < 2.02 \times 10^6\text{N/M}^2$(20 ATM)
Flow:	$v \sim 150\text{ m/s}$; $v' \sim 50\text{ m/s}$
Gas composition:	Fuel (nominal jet A) and air
Sensor life:	5 hr minimum
Accuracy:	Temperature uncertainty $\leq 5\%$ for $f \leq 200$ Hz Temperature uncertainty 10% for 200 Hz $< f <$ 1 kHz
Spatial resolution:	$D \leq 0.5\text{ cm}$
Vibration:	10g

2. Concept Identification

Literature surveys were conducted and consisted of searches using the NASA RECON, Lockheed Dialog, Defense Technical Information Center (DTIC), and United Technologies Research Center (UTRC) Library. From the several hundred title abstract listings obtained, copies of 92 references were received. Additional references and concepts were also obtained and reviewed through consultation with P&WA instrumentation specialists at the Government Products Division (GPD) and Commercial Products Division (CPD). Copies of these references were made and are listed in Appendix A. In a few cases the references were in Russian and were translated.

3. Evaluation/Screening

The final list of candidate measurement systems is presented in Table II, with the results of the evaluation of each candidate given with respect to each of the evaluation criteria. The

candidate measurement systems were classified as optical or physical techniques. Each candidate was judged either acceptable or unacceptable in terms of the evaluation criteria in Table I. Many of the techniques listed in Table II have obvious deficiencies in response and accuracy. However, two of the techniques warrant further discussion because they are currently being studied at P&WA and other United Technologies Corporation (UTC) divisions and may in the future be applicable. These are the Coherent Anti-Stokes Raman Spectroscopy (CARS), and high-speed photography through fiber optics.

Recent experimental demonstrations using the CARS technique indicate this technique should be considered as a combustion temperature diagnostic; however, when used as a dynamic sensor the effective frequency response is limited by the Nyquist sampling criteria to a maximum of one-half the sampling rate. At present, CARS employs pulsed lasers at repetition rates of between 10 and 50 pulses per second, which implies maximum frequency response of 5 to 25 Hz. An additional drawback is its requirement for direct line of sight between the laser source and the receiver. The CARS technique therefore seems unsuited to this particular application at its present stage of development. Once probe lasers with rates of 1 to 2 kHz are developed, the CARS technique might become a technically superior approach because of its nonintrusive nature.

Studies of combustion processes using fiber optics and high-speed (5000 frames per second) photography indicate it is possible to measure dynamic gas temperatures to the frequency response required; however, the accuracy and spatial resolution requirements would be difficult to meet at the present state of development.

Based on the results of the evaluation in Table II the single pulse-heated and dual passive compensated thermocouple systems were acceptable by all criteria and therefore were selected for further study in Task 2. The pulse-heated dual concept was a third possible candidate (the only other candidate found acceptable by all criteria). This concept is more complicated than the other two concepts and would have been considered only if the other two candidates had failed to meet the program requirements during later studies.

The single pulse-heated concept, described by Yule (reference 1 p. 95), uses one thin-wire thermocouple to determine a compensation time constant for local flow conditions and is an improvement over previous methods which used one time constant over a wide range of conditions. Evaluation of the time constant is made by electrically pulse heating the thermocouple wire and measuring the resulting decay rates.

The dual passive thermocouple concept suggested by Dils (reference 4 p. 95) employs two thermocouple wires of different sizes to obtain data necessary for evaluation of the time constant for each wire. If two thermocouples are positioned in close proximity such that both are exposed to the same instantaneous temperature and velocity, the difference in their thermal responses will be governed by their relative diameters. These responses can then be used to obtain time constants for compensating the thermocouples.

TABLE II. — CANDIDATE SCREENING EVALUATION

Measurement Technique	*Evaluation Criteria*									
	Geometry	*Temperature*	*Response*	*Pressure*	*Flow*	*Gas Composition Compatibility*	*Sensor Life*	*Accuracy*	*Spatial Resolution*	*Vibration*
Optical Techniques										
Coherent Anti-Stokes Raman Spect (CARS)	S	S	U	S	S	S	S	S	S	S
High Speed Photography	S	S	S	S	S	S	S	S	U	S
Through Fiber Optics Radiation Pyrometry	S	S	U	S	S	S	S	S	S	S
Physical Techniques										
Thermocouples										
Single — Passive — Compensated	S	S	U	S	S	S	S	U	S	S
Single — Pulsed Cooled — Compensated	S	S	U	S	S	S	S	S	S	S
Single — Pulse Heated — Compensated	S	S	S	S	S	S	S	S	S	S
Dual — Passive — Compensated	S	S	S	S	S	S	S	S	S	S
Dual — Pulse Heated — Compensated	S	S	S	S	S	S	S	S	S	S
Resistance Thermocouples										
Single Wire — Compensated	S	S	U	S	S	S	S	U	S	S
Film on Cooled Glass Tube — Compensated	S	S	S	S	S	S	U	S	S	U
Ultrasonic Thermometry	S	S	U	S	S	S	S	S	U	S
Fluid Oscillator (Edge Tone Resonator)	S	S	U	S	S	S	S	U	S	S
Gas Sampling Probe	S	S	U	S	S	S	S	U	S	S
Johnson Noise Thermometry	S	S	U	S	S	S	S	S	S	S
Vibrating Wire	S	U	U	S	S	S	U	S	S	U
Piezoelectric Resonator	U	U	U	S	S	U	S	S	S	S

Key:
S — Satisfactory
U — Unsatisfactory

B. TASK 2 — ANALYSIS OF METHODS AND SELECTION OF THE MOST PROMISING METHOD

1. Summary

The Task 2 effort consisted of detailed analysis of the two methods selected in Task 1. The principal thrust of the Task 2 analysis was to evaluate how well each method could be made into a reliable, fast responding, high-temperature measuring device. Factors considered are listed in the Task 2 paragraph of the contract Statement of Work, and generally fall into the two categories of structural adequacy/durability and measurement accuracy. The detailed analysis was therefore subdivided into three major subanalyses relating to structural adequacy/durability and measurement accuracy: (1) a structural/material/fabrication analysis, (2) a transient thermal analysis, and (3) a data acquistion/reduction system analysis. Evaluation factors from Task 2 and Table I were applied to the results of the analyses to identify the most promising method.

The results of the structural/material/fabrication analysis showed that both conceptual designs are acceptable Type B thermocouple wire was selected based on a review of available materials. A stress analysis of this type B material revealed that the maximum length-to-diameter ratio for the small wires was 20 to 1. The stress analysis performed on the probe support structure revealed than an Al_2O_3 ceramic material was acceptable.

The thermal analysis predicted the transient response of different size thermocouple wires for various gas temperature fluctuations and frequencies. In addition, pulse heating cycles were analyzed to define the heating and cooling rates required. The effects of radiation and end conduction losses to the support wires were also evaluated. Conduction losses were found to be sufficiently large ($\pm$67K) at the low frequencies and maximum gas temperature fluctuations ($\pm$500K); correction for these losses must be provided. A method for correcting was identified for each concept.

The data acquistion/reduction systems for the two concepts were refined and modeled to predict noise levels. Both concepts were evaluated and found to meet accuracy specifications for the 1000K peak-to-peak fluctuations at discrete frequencies up to 1 kHz (neglecting end conduction and radiation). For the more realistic case of 1000K peak-to-peak white noise, the dual wire technique was found to produce much more accurate results. The dual wire was also judged to be superior in its ease of application. This is primarily due to the difficulty in maintaining a stable zero calibration reference for the pulse-heated thermocouple, which is due to off-position leakage currents in the solid state relays required to pulse heat.

A final evaluation was conducted and resulted in the selection of the dual passive thermocouple concept as the most promising concept.

2. Structural/Material/Fabrication Analysis

This analysis consisted of reviewing thermocouple wire materials and stresses, probe structural support materials and stresses, and fabrication requirements. The results are applicable to both concepts because the preliminary conceptual probe configurations shown in Figures 1 and 2 are very similar.

The results of a review of possible high-temperature thermocouple wire materials showed that only the platinum/rhodium alloys have the required high temperature (1900K) capabilities along with good oxidation resistance characteristics. Nickel-base alloys such as chromel/alumel do not have high enough melting temperatures. Tungsten/rhenium alloys have high melting temperatures but can be used only in vacuum and inert atmospheres because of very poor oxidation properties. The iridium/rhodium alloys have higher melting temperatures than platinum/rhodium alloys; however, NBS data and P&WA experience with these thermocouples in typical combustion environments reveal a problem with the wires vaporizing and failing. A detailed review of the platinum/rhodium alloys commercially available was made. Tensile strength, melting temperature, emf output, thermal conductivity, stress to rupture, and specific heat were reviewed. Tensile and stress-rupture values are higher for increasing rhodium content, indicating the best thermocouple should have a high rhodium content. The Type B (platinum — 6% rhodium/platinum — 30% rhodium) was selected over the other commercially available thermocouple material with rhodium in both alloys (platinum — 20% rhodium/platinum — 40% rhodium) based on its higher emf output, availability, and known fabrication characteristics.

A stress analysis of the small thermocouple probe wires was performed, assuming that each of the wires was a beam supported at both ends. The maximum allowable wire lengths for various diameter wires were calculated based on the stresses due to aerodynamic loading and vibration. The wire material was assumed to be ISA Type B. The allowable g-loads due to vibration were also assumed to be 500g. The results show that the maximum length/diameter ratio (for different wire diameters) is a constant 20 to 1.

A review of the probe structural support requirements revealed that the support needs to operate uncooled in the gas stream to minimize thermal conduction losses in the thermocouple wires. The only materials identified which would meet these requirements were the platinum/rhodium alloys and ceramics such as Al_2O_3. A stress analysis of the proposed structures based on aerodynamic loading and vibration showed that the maximum stress would be 4.042×10^7 Newton/meter^2 (5863 psi) and is again based on a 500g vibration criterion. A review of the properties of a platinum/30% rhodium alloy and an Al_2O_3 ceramic such as Coors AD-99 shows that either would be acceptable; however, the ceramic could be obtained at considerably less cost (approximately \$1,000 vs \$10,000). In addition, the ceramic has a lower thermal conductivity (less conduction error) and is a good electrical insulator. For these reasons the ceramic was selected for the probe concept.

A review of the fabrication requirements of the conceptual designs shown in Figures 1 and 2 revealed the basic approaches are acceptable. Fabricating butt-welded thermocouple wire junctions with no weld beads had been demonstrated by P&WA in the wire sizes required. Recent P&WA experience in fabricating probes of similar design indicated that the method of attaching the small wires to the support wires should be based on using holes drilled in the support wires and the smaller wires threaded through these holes and then welded instead of wrapping the smaller wires around the support wires, which has proved to be difficult.

3. Transient Thermal Analysis

A thermal model (shown in Figure 3) of the thermocouple probe wires was generated to evaluate the effects of pulse heating, radiation losses, and end conduction losses. The physical thermocouple junction, the small wire, and the larger support wires were simulated by a finite difference model. The gas temperatures were assumed to be a mean gas temperature of 1400K (2520°R) with fluctuations of ±500K (±900°R). The more realistic* case defined in the data acquisition analysis, ±65K (±117°R), was also evaluated. These cases were evaluated at

*Engine test data from a 76 μm t/c analyzed in Task 6 exhibited random signal characteristics with measured overall time waveform amplitudes of about ±110K (±200°R) uncompensated and ±670K (±1200°R) compensated.

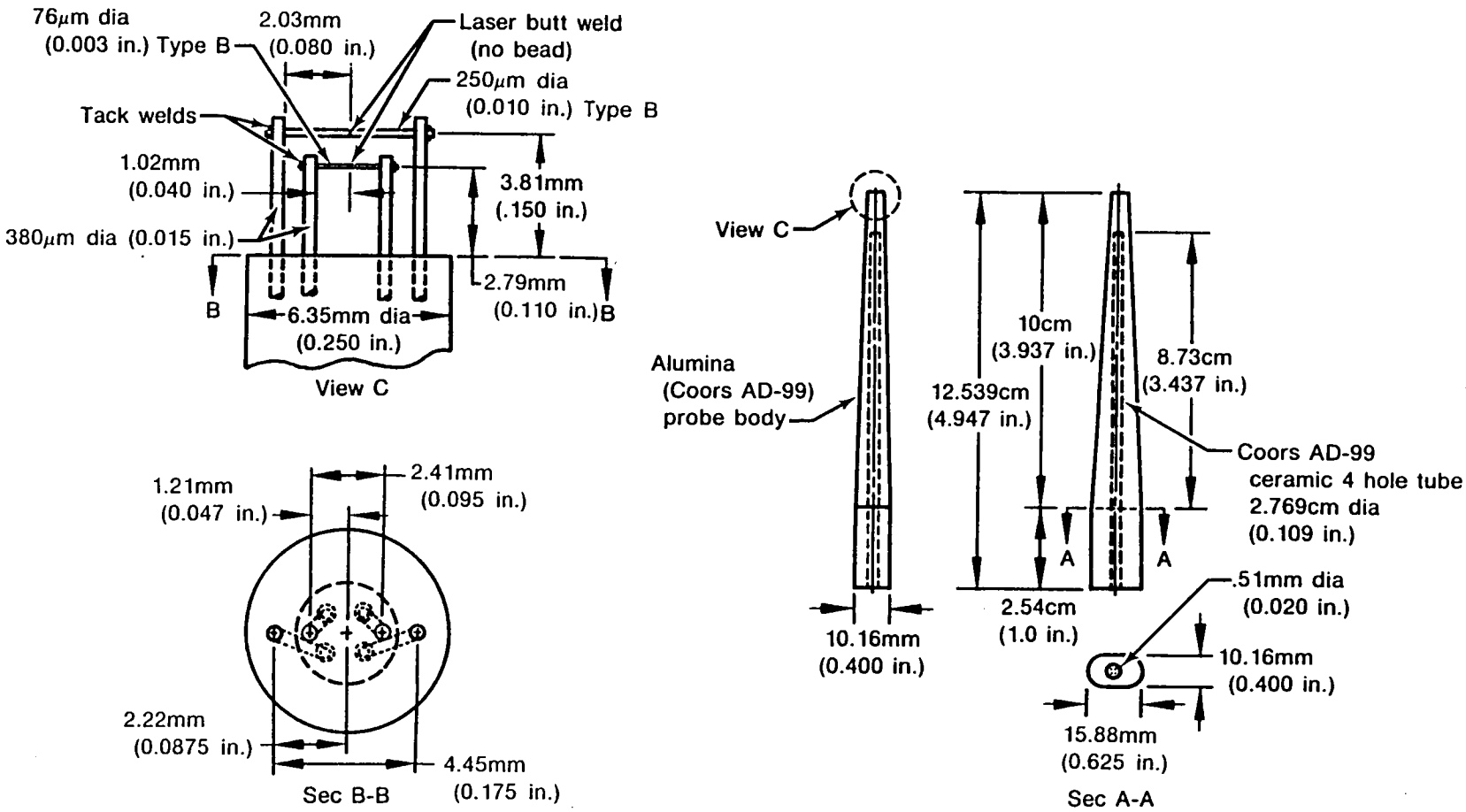

Figure 1. Dual Passive Thermocouple — Preliminary Design Concept

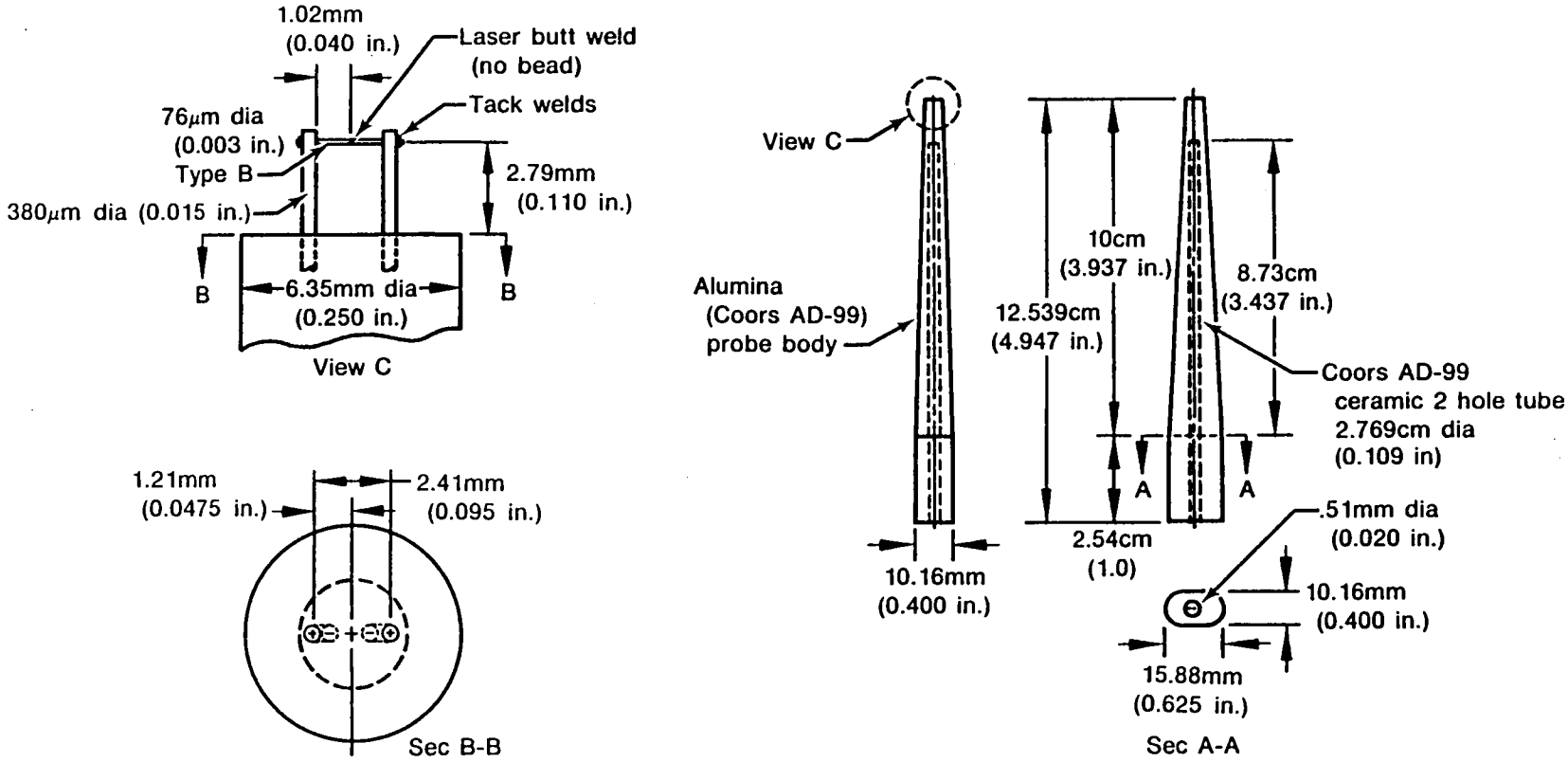

Figure 2. Single Pulse-Heated Thermocouple — Preliminary Design Concept

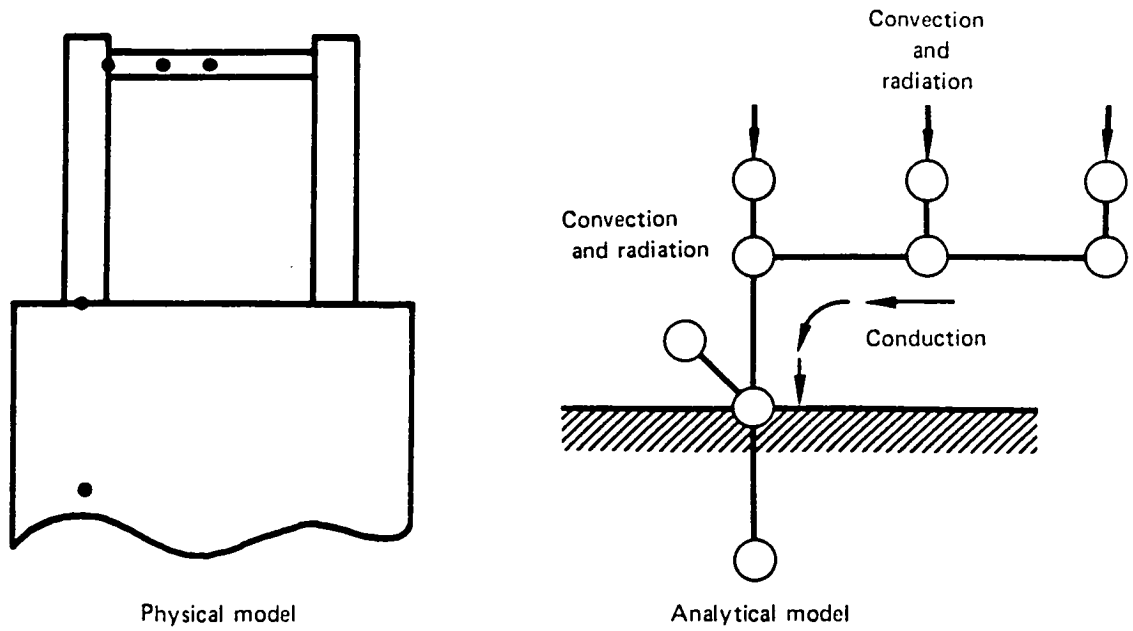

Figure 3. Model Employs Finite Difference Method — Physical Model Represented by Finite Difference Analytical Model

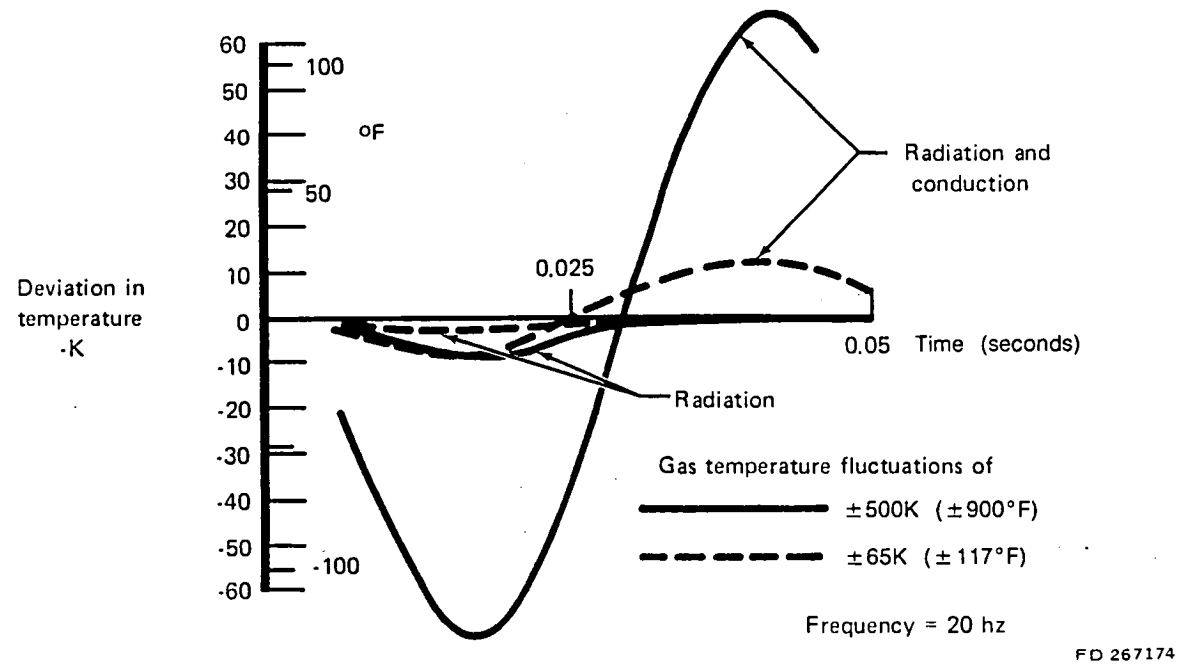

Figure 4. Predicted Thermal Response — Maximum Deviation in Predicted Junction Temperature from a 1st-Order System

frequencies of 20, 100, and 1000 Hz. The model was also used to simulate the calibration procedures for the pulse-heated thermocouple by simulating the electrical heating and thermal decay process.

Selected thermocouple configurations were modeled for the worst-case environmental conditions (maximum temperature oscillations and minimum frequency). Results of the transient simulations (shown in Figure 4) indicate that radiation heat losses are not significant (less than 10K), but the conduction losses are too large (maximum of 67K) to be ignored and, because of structural requirements previously discussed, cannot be reduced by making the wires longer.

This discovery required that analysis of the measured temperature data be performed with a second-order equation containing both conduction and convection terms, rather than the simplified first-order equation containing only convection terms. The second-order energy equation is a linear equation in time and space, whereas the first-order equation is only time dependent. This required a modification in the procedures for data processing originally proposed, since the form of the solutions of the second-order energy equation is quite different from the simpler first-order equation. The method developed for data reduction is described in Tasks 4 and 5.

4. Data Acquisition/Reduction System

The data acquisition and reduction systems required for the single pulse-heated and dual passive thermocouple concepts were refined and modeled to predict noise levels. The results of these analyses are discussed further in the following paragraphs.

a. Single Wire Pulse-Heated Concept

A conceptual design of the pulse heating system was made. The dc power supply was sized at 10 amperes and 200 vdc based on amperage requirement established during the thermal analysis modeling. The pulse repetition rate was chosen to be approximately 10 Hz (100 ms period) based on $2 \times 7.5\tau$ (τ is the time constant) for the lowest time constant anticipated for a 76 μm (0.003 in.) diameter thermocouple at the contract Statement of Work operating conditions and verified by the thermal analysis model.

The pulse heating system would require an electronic control unit which would limit the applied current based on the maximum instantaneous temperature reached by the thermocouple to prevent failure due to overtemperaturing. This would be done by sensing the maximum instantaneous temperature reached during any portion of the decay cycle (current OFF). It would also automatically control the heating current in incremental steps while sensing the peak instantaneous temperature reached during the initial portion of the decay cycle until the desired temperature increment is reached. It would be more desirable to monitor the temperature of the thermocouple during the heating cycle, but the thermocouple output cannot be monitored while the heating current is on. After the desired temperature increment is set, it would then automatically pulse the temperature for a preselected time. During the operation it would no longer *adjust* the current except to limit the current if the maximum instantaneous temperature exceeds the safe operating temperature of the material. Following the pulse heating, the data would be recorded for compensation by the time constant derived from the pulse heating.

The predicted time constants of the thermocouple proposed are smaller than the switching times of mechanical relays. This dictates the use of solid state relays (SSR). The SSR's have off-state leakage currents which are a function of the temperature of the SSR and are dependent on the current, voltage, and ambient temperature. These leakage currents would result in loss of the absolute calibration of the thermocouple channel which is required. The input to the first data acquisition system amplifier could be passively ac-coupled at some very low frequency (approximately 0.1 Hz), but the zero shift effects may still couple if they are dependent upon load current pulses during the incremental current changes to set the desired temperature increment (which occures at a 10-Hz rate). This is considered a major problem. Use of an ac SSR with an ac power supply, which would have to operate at approximately 1.5 kHz to permit filtering of off-state leakage current emf's from the signal, was considered. However, a suitable ac SSR capable of meeting this frequency requirement was not identified. Additionally, use of 1.5 kHz high-voltage power supplies could produce noise problems with other instrumentation channels on a test stand (instrumentation such as strain gages and kulites).

A computer noise model of the data acquistion and analysis system was generated and the system noise (μv rms/ $\sqrt{\text{Hz}}$) was determined with various amplifier gains chosen to optimize the signal-to-noise ratio (SNR) for selected dynamic temperature signals. These system noise levels were then used in determining data averaging requirements and accuracy. A suitable commercially available differential amplifier (Preston DX series) was identified. The SSR was found to be the major source of noise (perturbated through the system).

The ensemble averaging required to smooth the decay cycles for measurement of time constant was determined for 1000K (1800°R) peak-to-peak fluctuations at discrete frequencies of 1, 200, and 1000 Hz. At 1 Hz, where the 76 μm (0.003 in.) thermocouple *tracks* the 1000K fluctuation, approximately 91,000 averages (9,100 sec) are needed. At 1000 Hz, where the thermocouple would only indicate 23K (42°F) peak-to-peak fluctuations, 378 averages are required. It is more realistic to model the temperature fluctuations as 1000K peak-to-peak white noise, for which a 76 μm thermocouple would indicate approximately 139K peak-to-peak overall. This was determined by inputting a random noise signal of approximately 1 kHz bandwidth into an RC low-pass filter with a time constant equivalent to a 76 μm thermocouple and measuring the resultant output signal. For this case, about 2221 averages (222 sec) are needed for ensemble averaging.

The accuracy of the compensated frequency spectra was evaluated (neglecting conduction and radiation errors) for the above specific dynamic temperature cases for 76 μm and 130 μm diameter thermocouples with data system gains optimized for each specific case. For the 1000K peak-to-peak discrete signals at 1, 200, and 1000 Hz, the 76 μm thermocouple met the specifications at all frequencies. The 130 μm diameter thermocouple did not meet the specifications at 1000 Hz. For the more realistic case of 1000K peak-to-peak white noise, neither the 76 μm nor the 130 μm thermocouple met the specification. The 76 μm had 8.7% error at 1 Hz, 38% at 200 Hz, and 77% at 1000 Hz. The major contributions to these errors are the very poor SNR due to high noise levels of the SSR (after propagation through the high signal amplification) and, to some extent, the inability to employ bandpass filtering to improve the SNR (since the time constant is determined in the time domain). Based on predicted accuracy, the 130 μm thermocouple was judged as unsuitable for this application and the 76 μm thermocouple was selected for use in the single wire heated concept.

The difficulty in application of the pulse-heated concept was judged to be very high because of the apparent zeroing problems associated with the use of the SSR's, the complexity of the pulse heating system and to the very nature of the technique which requires raising the temperature of the thermocouple element.

b. Dual Wire Concept

The data acquisition and analysis systems originally proposed were reanalyzed for use in accuracy predictions. A computer noise model was generated and system noise (μv rms/ $\sqrt{\text{Hz}}$) predictions were made for an Astrodata Model 885 amplifier which has better noise characteristics than the Preston MX amplifier originally proposed. A suitable commercially available alternate amplifier was also identified. Noise predictions were made for various amplifier gain settings chosen to optimize the SNR for specific cases of temperature fluctuations.

The 76 μm (0.003 in.) and 250 μm (0.010 in.) diameter dual wire combination was selected over a 76 μm and 130 μm combination based on an evaluation of the governing equation (equation 1) with and without error in the measurement of a_1/a_2, as follows:

$$\tau_1 = \frac{1}{2\pi f} \sqrt{\frac{1 - (a_1/a_2)^2}{(a_1/a_2)^2 - (d_2/d_1)^3}} \qquad (1)$$

where
τ_1 = time constant of wire No. 1
f = frequency, Hz
a_1 = amplitude of wire No. 1
a_2 = amplitude of wire No. 2
d_1 = diameter of wire No. 1
d_2 = diameter of wire No. 2

The above equation was derived from the classical equation for the amplitude ratio of a first-order system responding to a sinusoidal input. Expressions were written for each thermocouple wire and then solved for the above expression using the additional relationship of $\tau_1/\tau_2 = (d_1/d_2)^{1.5}$. This relationship was derived from the definition of the thermocouple junction as a first-order system and assuming an expressionfor the heat transfer coefficient of a cylinder in cross flow.

Even without noise there was error in the computed value of the time constant τ for the 76 μm/130 μm combination. The higher the percentage that the value of $(a_1/a_2)^2$ is of the value of $(d_2/d_1)^3$, the more the error in the computation, regardless of the error present in the a_1/a_2 measurement.

The number of averages necessary to compute the time constant to within an error of $\pm 2.9\%$ (the accuracy necessary to meet the specifications for the compensated frequency spectrum) was computed. For the 1000K peak-to-peak discrete temperature fluctuations at any frequency, it will require 32 averages. For the 1000K peak-to-peak white noise case, it requires 256 averages (128 sec).

Various evaluations were made to predict the accuracy of the compensated frequency spectrum for the 1000K peak-to-peak temperature fluctuations at discrete frequencies of 10, 200, and 1000 Hz for the 76 μm/250 μm combination (compensation made to the 76 μm thermocouple). Additionally, the case of 1000K peak-to-peak white noise was evaluated at 20, 200, and 1000 Hz. The analysis was based on the perturbation of errors in a_1/a_2 and d_2/d_1 in equation 1. The measurement accuracy of the diameter of the two thermocouple wires was found to be the major driver in overall accuracy (after minimizing the error in a_1/a_2 by averaging). For the 1000K fluctuations at discrete frequencies (data system gains optimized at each frequency), the predicted errors were less than 5% at all frequencies. For the 1000K peak-to-peak fluctuation white noise case, the errors were 5.0% at 20 Hz, 5.6% at 200 Hz, and 8.9% at 1000 Hz.

A method of measuring time constant τ from the transfer function of the dual wires (a_1/a_2) without prior knowledge of the wire diameters was investigated in the laboratory utilizing two passive first-order low-pass RC filters. The filters had time constants approximating 76 μm and 250 μm thermocouples. This technique was first proposed by Strahle and Muthukrishnan in reference 1, p. 97. With this technique, the time constant corresponds to the frequency where the imaginary term passes through a maxima. Additionally, the real term approaches the limit $(d_2/d_1)^{1.5}$ as frequency increases. Results were similar to those reported by Strahle in which, due to the broad nature of the maxima, the time constant could be determined to only about 25 percent accuracy. Various schemes to measure $(d_2/d_1)^{1.5}$ from the real term offered no improvement in accuracy.

The dual wire technique was judged to be much superior to the single pulse-heated wire method in terms of ease of use. The requirement for two data channels, one for each thermocouple, does not increase the difficulty of the dual-wire concept application. The addition of bandpass filtering does add some complexity but would not be required to meet accuracy specifications based on 1000K peak-to-peak fluctuations at discrete frequencies. The ability to passively ac-couple the thermocouple signals eliminates zeroing problems and permits optimization of SNR's.

5. Evaluation/Selection

The results of the Task 2 analyses were used to rate the two concepts; the results are shown in Table III. Both concepts are acceptable in terms of suitability for use in the extreme environment; however, the single pulse-heated concept was rated lower in terms of temperature due to pulse heating near the melting temperature of the thermocouple material. Both concepts were also rated acceptable in terms of fabricability and cost. However, the dual passive concept was superior in terms of the data acquistion/reduction system requirements. Based on these results, the dual passive thermocouple concept was selected as the most promising technique and was recommended for use in Task 4.

TABLE III. — CONCEPT EVALUATION AND SELECTION

Criteria	*Dual Wire Passive*	*Single Wire Pulse-Heated*
Suitability for Extreme Environment		
High Temperature	2	1
High Pressure	2	2
Vibration	2	2
Corrosive Gases	2	2
Erosion	2	2
Size	2	2
Fabricability	2	2
Data Acquisition/Reduction		
Frequency Response	2	2
Amplitude Limits of Temperature Changes	2	1
Accuracy	3	2
Difficulty of Use	3	1
Cost	2	2
Amplitude Limits of Temperature Changes	2	1
Accuracy	3	2
Difficulty of Use	3	1
Cost	2	2

3 *Superior*
2 *Average*
1 *Below Average*
0 *Inferior*

C. TASK 4 — SYSTEM DESIGN AND TEST PLAN FORMULATION

1. Sensor Design

The dynamic gas temperature sensor design was based on the environmental conditions specified in Exhibit B of the contract Statement of Work (SOW) and the analyses conducted during Tasks 1 and 2, and was presented in the Task 3 review. However, based on the decision to conduct the full-scale testing in an F100 engine instead of a combustor rig, the sensor was reanalyzed and modified for these requirements. In addition, a modified sensor design was used in the subscale combustor burner tests due to the different test conditions. This design used longer thermocouple element lengths to take advantage of the lower stress levels due to lower combustor mass flows and thus minimized conduction effects.

The F100 sensor design was based on installation in the AP-5 borescope plug location which corresponds to a position between two 1st-stage turbine vanes aft of the combustor exit. The sensor installation is shown in Figure 5. The test conditions at this location vary from idle to intermediate power settings of the engine and correspond to the required test conditions; except, the Mach number 0.36 instead of 0.15-0.20, which is typical for the combustor exit.

The sensor assembly shown in Figure 5 is defined on drawing SSSG-3030 and SSSG-3031 (see Appendix D) and consists of a 0.478 cm (0.188 in.) diameter ceramic stick which has four 0.079 cm (0.031 in.) diameter through holes. The ceramic stick is a standard item of Coors Porcelain Co. Coors AD-99 ceramic was selected based on its superior strength and electrical

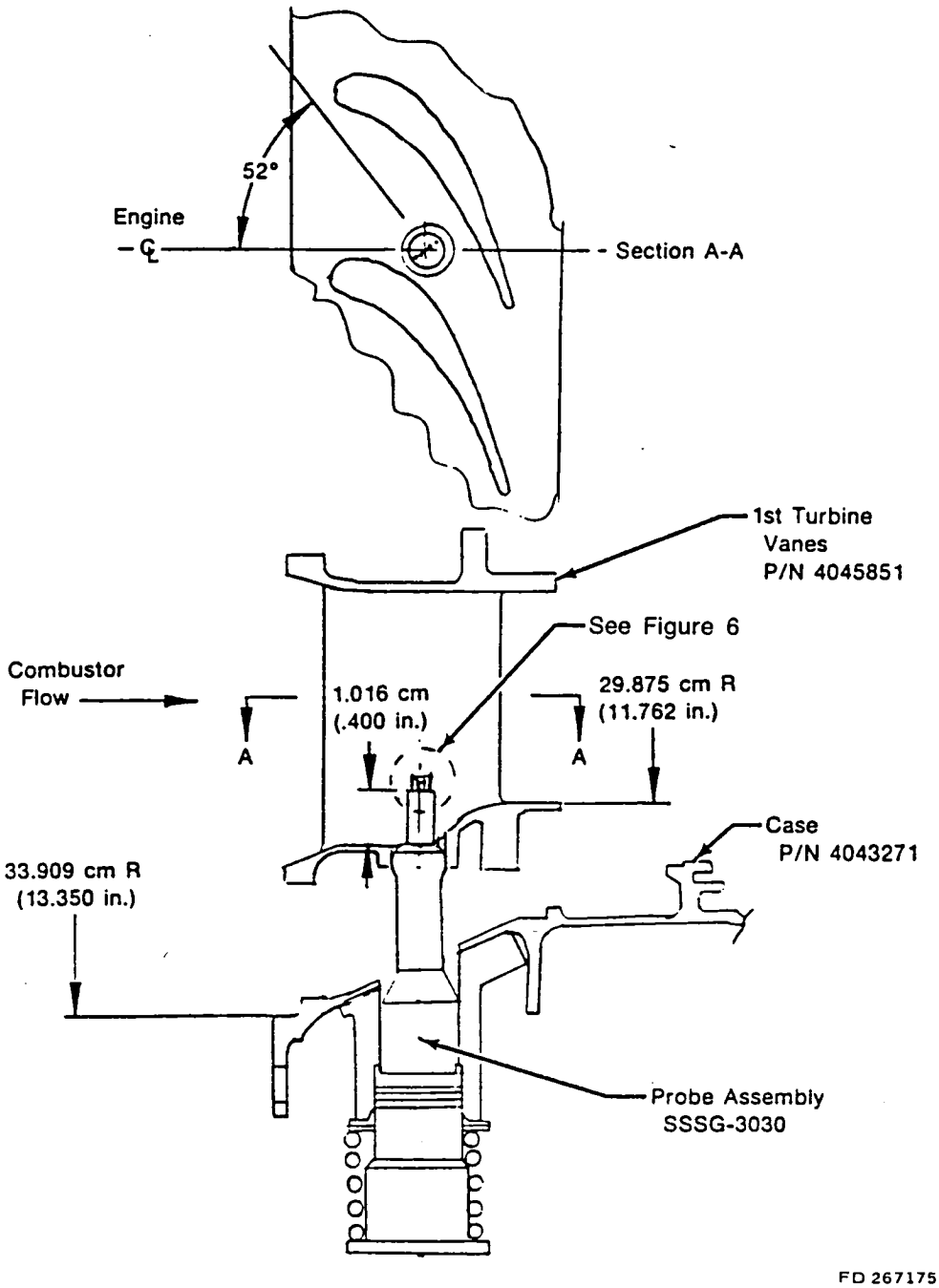

Figure 5. Dynamic Gas Temperature Probe Installation in F100 AP-5 Borescope Location

resistivity at high temperatures. The ceramic stick is installed in a 0.635 cm (0.250 in.) Inconel tube with 1.016 cm (0.400 in.) length of the exposed ceramic protruding into the flow stream. The thermocouple support wires (ANSI Type B) are installed in the four holes and the smaller laser butt-welded elements are installed as shown in Figure 6. The thremocouple wires are terminated at the other end of the probe using a standard six pin Bendix connector which is maintained at a temperature of 339K (150°F) or less so that it may be used as the reference temperature.

The stresses in the exposed ceramic, due to aerodynamic loading and vibration, were evaluated at the maximum flow conditions of the F100 engine which are:

T = 1682K (3028°R)
P = $2.01 \times 10^{+6}$ Newton/meter^2 (292 psia)
M = 0.36

A maximum stress of $5.97 \times 10^{+6}$ Newton/meter^2 (866 psi) was calculated based on:

$S_{max} = S_{vibration} + S_{air\ loading}$

$S_{max} = G_a S_v K + S_A$ where S_v = 1g vibrational stress and S_a = air loading stress

$S_{vibration} = 1.46 \times 10^{+6}$ Newton/meter^2 (212 psia)

$S_{air\ loading} = 4.51 \times 10^{+6}$ Newton/meter^2 (654 psia)

$S_{max} = 5.97 \times 10^{+6}$ Newton/meter^2 (866 psia)

A G_a of 500g's loading and a stress concentration factor of K = 1.0 were used to calculate the vibrational stress. These stresses are acceptable when compared to the flexural strength of $2.07 \times 10^{+8}$ Newton/meter^2 (30,000 psi) for Coors AD-99 ceramic at 1270K (2290°R).

The natural frequency of the ceramic body was also calculated and reviewed with respect to the frequencies that occur in the F100 engine and found not to present a problem. The natural frequency was calculated based on the following equation from "Formulas for Natural Frequency and Mode Shape," R. D. Blevins, Von Nostrand Reinfold Co., 1979:

$$f = \frac{\lambda_i^2}{2\pi L^2}\left(\frac{EI}{m}\right)^{1/2} = 6.14 \times 10^{+4}\ \text{Hz}$$

λ_1 = 1.875 (for cantilever beam)
E = Young's Modulus
I = Moment of inertia
L = Beam length
m = Mass/length.

This frequency of $6.14 \times 10^{+4}$ Hz is higher than the blade passing frequencies encountered in the engine due to the high and low rotor speeds which are a maximum $1.5 \times 10^{+4}$ Hz.

The thermal gradient through the ceramic along its axis was also calculated for the gas stream condition corresponding to the idle engine condition of

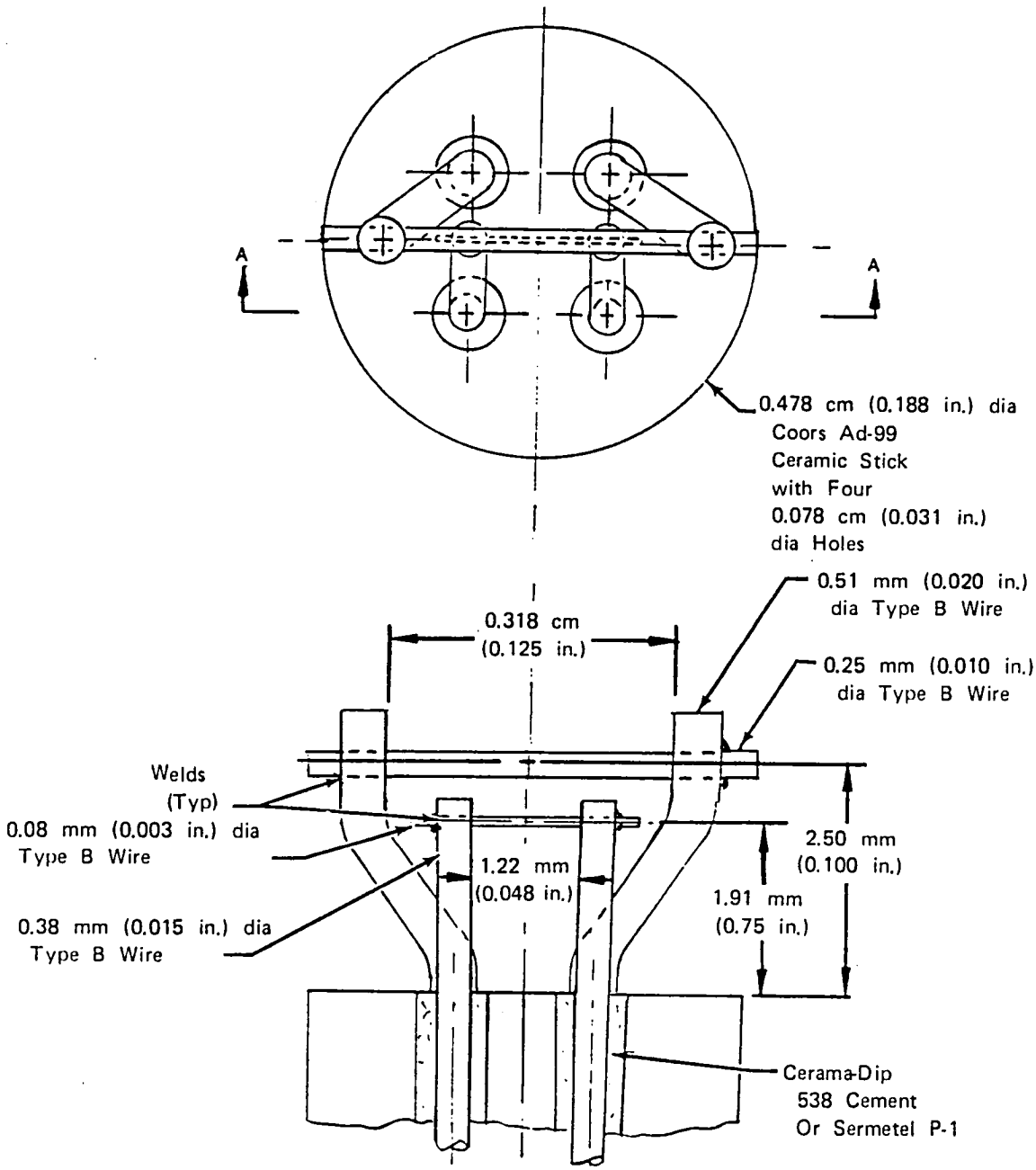

Figure 6. Sensor Tip Geometry

T_g = 956K (1720°R)
P = $2.81 \times 10^{+4}$ Newton/meter^2 (60 psia)
M = 0.36

These conditions along with a case or probe ceramic base temperature of only 644K (1160°R) would produce the largest variation of the probe ceramic tip temperature from the average gas stream temperature (largest conduction loss). Using these conditions and calculating the ceramic tip temperature (T_P) by analyzing the ceramic as a cylindrical fin in cross flow gives the following:

$$T_P = T_g - (T_g - T_B)\psi = 954K\ (1718°R)$$

where,

T_g = 956K (1720°R)

T_B = 644K (1160°R)

$$\psi = \frac{1}{\cosh\ [L\eta]}$$

L = ceramic height = 1.02 cm (0.400 inches)

$$\eta = \sqrt{\frac{4\ Nu\ k_g}{D^2\ k_c}}$$

Nu = Nusselt number = 114.7

k_g = thermal conductivity of the gas = 1.57×10^{-4} cal/sec-cm-K

k_c = thermal conductivity of the ceramic = 8.33×10^{-4} cal/sec-cm-K

D = ceramic diameter = 0.48 cm (0.188 inches)

These low conduction losses of 1.2K (2.1°R) indicate the probe tip will run at the average gas temperature conditions and thus not affect the thermocouple support wires and the final probe accuracy.

The thermocouple support wires and the smaller butt-welded elements were also analyzed for stresses for the same maximum gas conditions using the same type of analyses previously described for the ceramic stick. The support wire stresses were based on the assumption that the wires are a cantilever beam, and the smaller butt-welded element stresses are based on the assumption that the beam has both ends fixed. Assuming an allowable stress of $4.39 \times 10^{+7}$ Newton/meter^2 (6360 psi) for type B wire, the allowable length to diameter ratios (L/D) for the wires were calculated. The maximum L/D for the support wire is 6.5 and for the butt-welded elements is 15.5

The sensor tip geometry shown is Figure 6 was then determined by selecting support wire diameters of 0.38 mm (0.015 inch) and 0.51 mm (0.020 inch) and using the previously calculated L/D values. The smaller butt-welded elements lengths were also determined using their corresponding L/D values and nominal wire diameters.

The natural frequencies of the probe thermocouple elements and support wires were calculated using the same formula used in the analysis of the ceramic previously discussed. The 76 μm (0.003 in.) and 250 μm (0.010 in.) wires were analyzed as a beam supported on both ends (λ_i = 4.73 instead of 1.875) and the natural frequencies were $1.2 \times 10^{+5}$ Hz and $5.93 \times 10^{+4}$ Hz. The support wires of 510 μm (0.020 in.) and 380 μm (0.015 in.) were analyzed as a cantilever beam (λ_i = 1.875) and the natural frequencies were $2.4 \times 10^{+4}$ Hz and $3.7 \times 10^{+4}$ Hz, respectively. These frequencies are again higher and are removed from the maximum engine frequencies by more than 20% which is the normally used minimum criteria.

The sensor design of the probe used for the subscale combustor tests was based on the F100 probe design; however, the element lengths were increased to minimize the conductive loss effects to the junctions. This was possible due to the lower mass flow and subsequent aerodynamic loading existing at the subscale combustor test conditions. The final design of the subscale combustor sensor tip is shown in Figure 7.

2. Data Acquistion and Reduction System Design

The data acquisition and reduction system design discussed in the following sections is based on the results of the analyses performed in Task 2 and which were presented in Task 3. The design was based on acquiring and compensating the dynamic temperature data to the system accuracies specified and includes corrections for conduction losses in the probe elements. The following paragraphs present a detailed discussion of the system requirements, system description, and compensation methods. The requirements for the data acquisition and reduction system design are as follows:

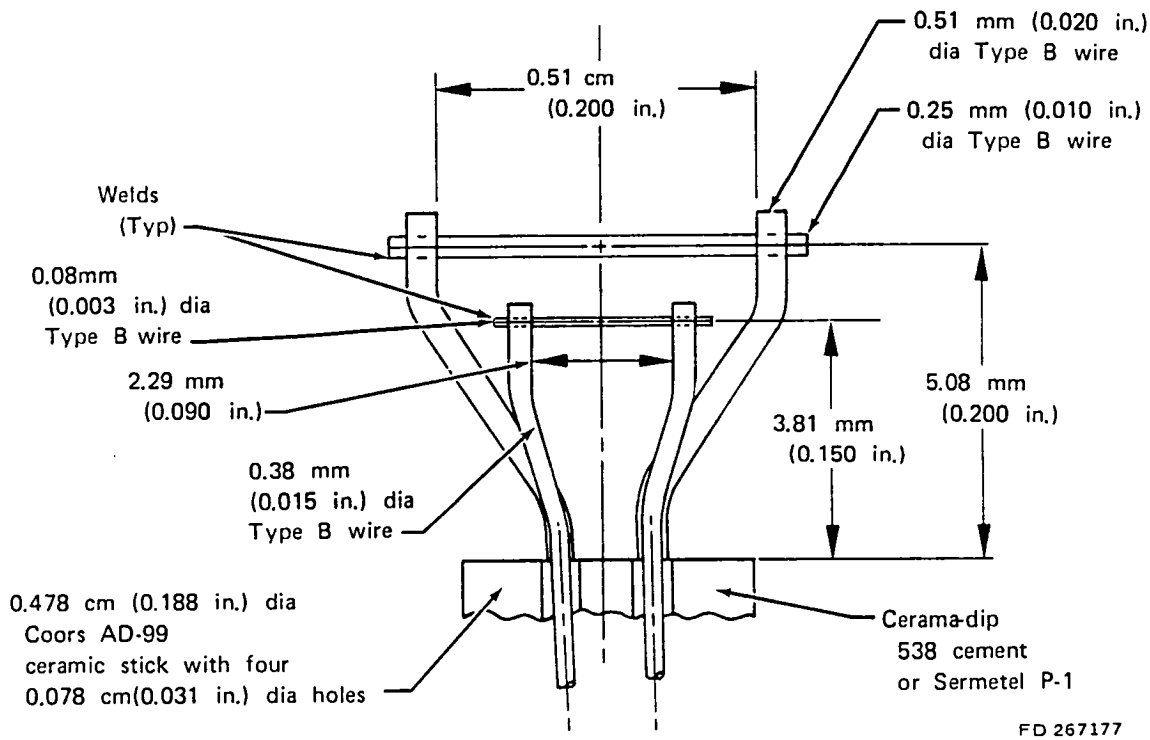

Figure 7. Sensor Tip Geometry — Subscale Combustor Tests

a. Requirements

- Optimized signal-to-noise ratio (dynamic signals, all system components)
- Data reduction on-line or off-line
- Digital compensation of data from $\approx$ 2 Hz to 1000 Hz (minimum).
- Three channel simultaneous (sample and hold) digitization of data into the data reduction computer system
  - (1) Minimum of 4 kHz sampling per channel
  - (2) Real time (i.e., no loss of data between data records) thruput of digitized data to mass storage (i.e., minimum thruput rate = 3 ch $\times$ 4 kHz/ch = 12 kHz)
  - (3) Minimum of 1024 time samples per data record (512 spectral lines per Fourier Transform)
  - (4) Minimum mass storage capacity of 64 records $\times$ 3 chs = 192 data records.
- Analog anti-aliasing filters with minimum of 48 db/octave roll-off characteristics.

b. System Description

The data acquisition and reduction system utilized are shown schematically in Figures 8, 9, and 10.

The thermocouple (t/c) signals were referenced to the ambient temperature at the thermocouple probe connector. For reference junction temperatures less than 339K (150°F) the output of the type B thermocouple is zero. The ambient temperature of the probe housing was monitored during all testing utilizing a chromel/alumel t/c which was tack welded to the probe housing and monitored on a temperature readout.

The 76 μm (3 mil) diameter and 250 μm (10 mil) t/c signals were ac coupled into the low noise high gain Preston DX-A3 differential amplifiers to permit optimization of the dynamic temperature signal to noise levels. The Preston Amplifiers for the ac coupled t/c signals were operated in the 10 kHz bandwidth mode (2 pole Bessel filter). To provide mean temperature data, the output of the 250 μm (10 mil) t/c was direct coupled to an additional Preston DX-A3 differential amplifier operating in the 1 Hz bandwidth mode.

The Preston DX-A3 dc amplifiers were selected based on side-by-side evaluations made on one of these amplifiers and an Astrodata 885 dc amplifier. The primary considerations in the selection of the Preston amplifier were its noise characteristics and availability from commercial sources. Based on the vendor specifications, the maximum common mode voltage is only 10 vdc and the input impedance at gains of less than five is only 100K ohms and 1500 pf (at all other gain settings the impedance is 100 meg ohms and 1500 pf). Neither of these marginal performance specifications were of any consequence in this application.

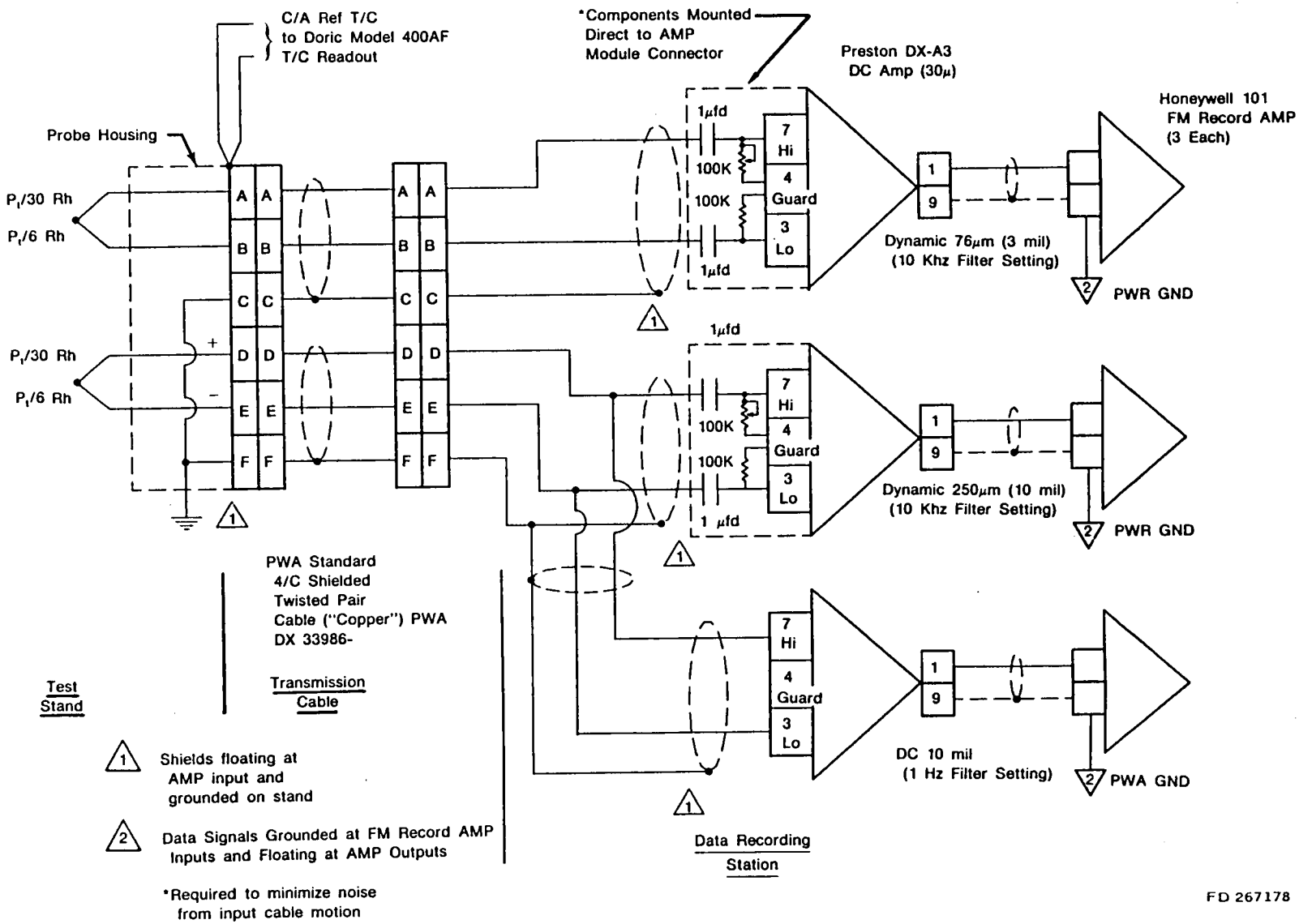

Figure 8. Dynamic Temperature Data Acquisition System

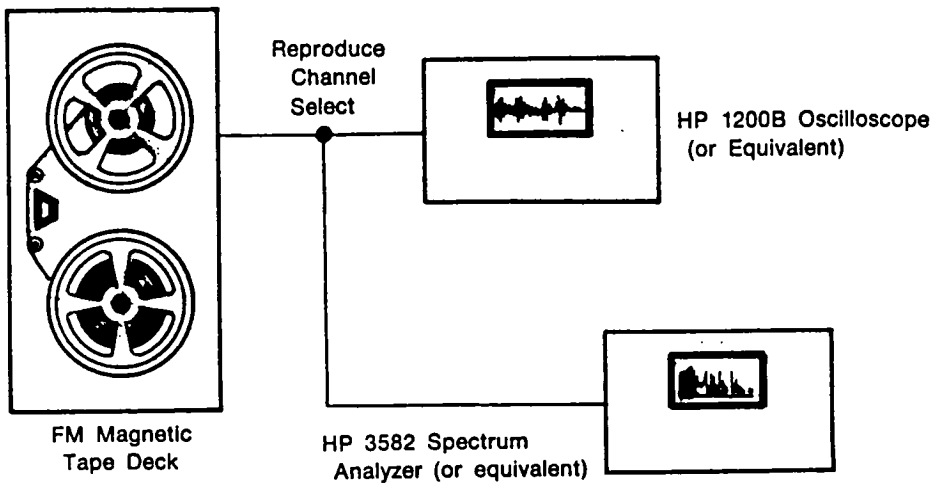

Figure 9. Data Monitoring During Acquisition

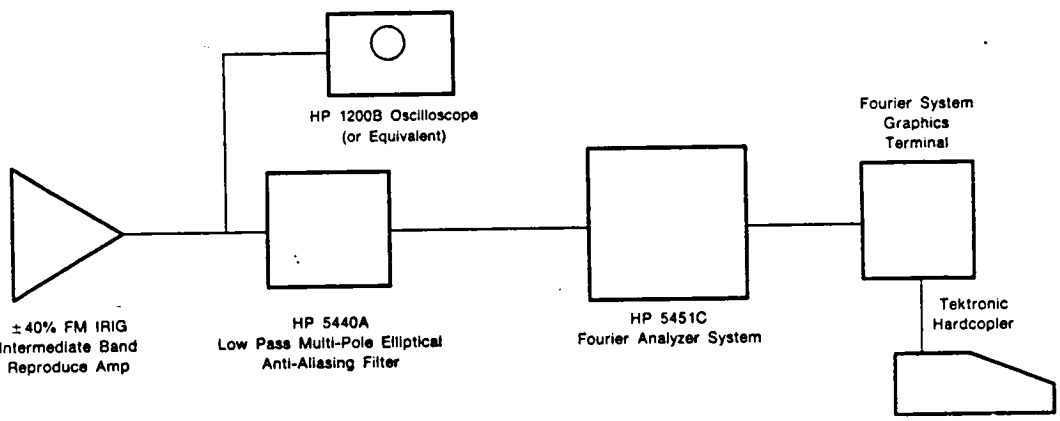

Note: (1)Standard equipment and set-up for analysis of dynamic data signals at PWA-GPD, grounding and wiring not shown.

HP 5451C Fourier Analyzer System Hardware:

HP 54451A Processor (HP21 MXE Computer With 128K Bytes)
HP 7970E 1600 cp: Digital Magnetic Tape
HP 7906A Disk Drive
HP 2648A Graphics Terminal
HP 5460B Channel, 12 bit, 100 Khz Sampling ADC
HP 5460A Display Unit
HP 5475A Control Unit
HP 5477A System Control

FD 267180

Figure 10. Dynamic Temperature Data Reduction System

A Honeywell model 101 magnetic tape recorder was used to record the amplified t/c signals during test stand operations. The tape was operated in an FM record mode, ±40% IRIG intermediate band dc to 10 kHz data bandwidth.

Data signals were double-recorded using ±0.707 volt and ±1.414 volt FM tape record levels. The amplifier gains, operated in the *fixed* mode, were adjusted at each engine rig test point to maintain optimum signal levels on the ±0.707 volt record channels. Gain settings were documented for each data point to maintain system calibration.

A general purpose oscilloscope was used online to monitor data signal levels. Additionally, a spectrum analyzer was used online to monitor the frequency content of the data signals.

The data reduction system consisted of a Honeywell model 96 tape deck with appropriate FM reproduce electronics (±40% IRIG intermediate band 10 kHz data bandwidth) and a Hewlett Packard model 5451C Fourier analyzer.

Data system calibration signals utilized for the 76 μm (3 mil) and 250 μm (10 mil) *dynamic* channels were:

(1) Short circuit (0mv) applied to the FM tape recorder input
(2) 400 mv rms ≈ 400 Hz applied at the FM tape recorder input.

Calibration signals for the 250 μm (10 mil) dc channel included (1) and (2) above plus the following, run with the amplifier gain set to the value utilized in acquiring the engine/rig data:

(3) Short (0 mv) applied to the dc amplifier input
(4) +10.00 mv dc applied to the dc amplifier input.

Approximately one minute long records of the above calibration signals were recorded on the FM tape. Calibration signals (1) and (2) were used to set up the FM tape playback reproduce system. Calibration signals (3) and (4) were used in establishing the overall system calibration. Typical gain settings used in acquiring engine/rig data were 1000 and 500 for the *dynamic* channels and 50 for the *dc* channel. Direct calibration of the *dynamic* channels (i.e., apply ac calibration signal to *dc* amplifier input with amplifier gain set the same as used during data acquisition) was attempted but was found to be too inaccurate in this application. AC calibration signal levels of about 500 μv rms could not be accurately set in the test stand with available equipment. The amplifiers were calibrated in the P&WA instrument laboratory to the manual specifications. The accuracy (±0.05%) of the fixed gain setting and linearity (±0.005% full scale) were judged satisfactory for use in establishing the overall data acquisition and reduction system calibration.

C. *Compensation Method — Dual Wire with Conduction and Convection Effects Included*

Approach

Historically the problem of compensating wire thermocouples for frequency response rests on accurate determination of the in-situ film heat transfer coefficient, h_g. For wire thermocouples, three simplifications allow this to be done easily: (1) the thermocouple junction is fabricated without a bead, allowing the wire to be analyzed as a cylinder in cross flow, (2) two wires of different diameters may be co-located on the probe tip, and ratioing the different responses allows one to measure time constants τ, which are proportional to h_g for large L/D values; and (3) the thermocouple and support wires can be made long enough to eliminate conduction effects, facilitating the ratio analysis in (2). As shown in preceding sections, however,

values; and (3) the thermocouple and support wires can be made long enough to eliminate conduction effects, facilitating the ratio analysis in (2). As shown in preceding sections, however, probe durability requirements allowed only moderate L/D values, and initial calculations revealed that conduction effects should be included to meet accuracy goals.

The compensation approach used to include conduction and convection effects simultaneously still involves ratioing signals of two different-diameter beadless thermocouples. Heat transfer coefficient h_g is determined, however, by comparing finite-element conduction-convection calculations with experimental data. The calculations are done using h_g as a parameter, and require matching calculated thermocouple signal amplitude ratios at several discrete frequencies from ~6 to ~40 Hz. Agreement between calculated and experimentally observed signal amplitude ratios determine h_g. For convenience, h_g is combined with other system parameters into an aerodynamic parameter, Γ. The measured values of Γ obtained at specific frequencies are arithmetically averaged and used in the thermal model to compute the compensation frequency spectrum (gain and phase) for the smaller diameter thermocouple. The smaller diameter thermocouple is selected for compensation since it has faster response and inherently better signal to noise characteristics at the higher frequency fluctuations. Compensation is performed digitally in the frequency domain by complex math division of the FFT spectrum of the thermocouple output by the compensation spectrum. The compensated time waveform is obtained by inverse Fourier transforming the compensated frequency spectrum.

Thermal Model

For the thermocouple probe modeled as a cylinder in cross-flow, the basic thermal equation is:

$$\text{Rate of Energy} = Q_{\text{convection}} + Q_{\text{conduction}} + Q_{\text{radiation}}$$

$$\frac{\partial T}{\partial t} = \frac{4h}{\rho_w C_{pw} D}(T_g - T) + \alpha \frac{\partial^2 T}{\partial X^2} + \frac{4\sigma\epsilon}{\rho_w C_{pw} D}(T_e^4 - T^4) \qquad (1)$$

In Task 2, thermal analysis of the thermocouple model showed that radiation effects could be neglected. In Task 5, it was shown that neglecting conduction errors would typically introduce a 25% error (GAIN) in the compensated data. In the analysis that follows, only the radiation term from equation (1) has been omitted.

The gas stream temperature can be expressed in terms of its mean and dynamic components as:

$$T_g = \bar{T}_g + \sum_{n=1}^{\infty} a_n \sin(\omega_n t - \phi_n) \qquad (2)$$

Substituting equation (2) written for a single frequency for T_g in equation (1) and normalizing, the transfer function between the temperature in the thermocouple wire and the gas stream temperature can be written as:

$$\frac{\partial \zeta}{\partial t} = \frac{4h}{\rho_\omega C_{pw} D}\left[a_n \sin(\omega_n t - \phi_n) - \zeta\right] + \alpha \frac{\partial^2 \zeta}{\partial x^2} \tag{3}$$

$$\text{where } \zeta = \frac{T_n - \overline{T}_g}{T_g - \overline{T}_g} = \frac{\theta_{1n}}{a_n} \tag{4}$$

The finite-difference solution for equation (3) is of the form:

$$\frac{\partial \zeta}{\partial t} \simeq \frac{\zeta_{j+1} - \zeta_j}{\Delta t} = \frac{\zeta'_x - \zeta_x}{\Delta t} \tag{5}$$

$$\frac{\partial^2 \zeta}{\partial x^2} \simeq \frac{\zeta_{x+1} + \zeta_{x-1} - 2\zeta_x}{\lambda^2} \tag{6}$$

Application of the finite diferences solution to equation (3) for the 9 node model of the thermocouple in Figure 11 yields equations (7) thru (16).

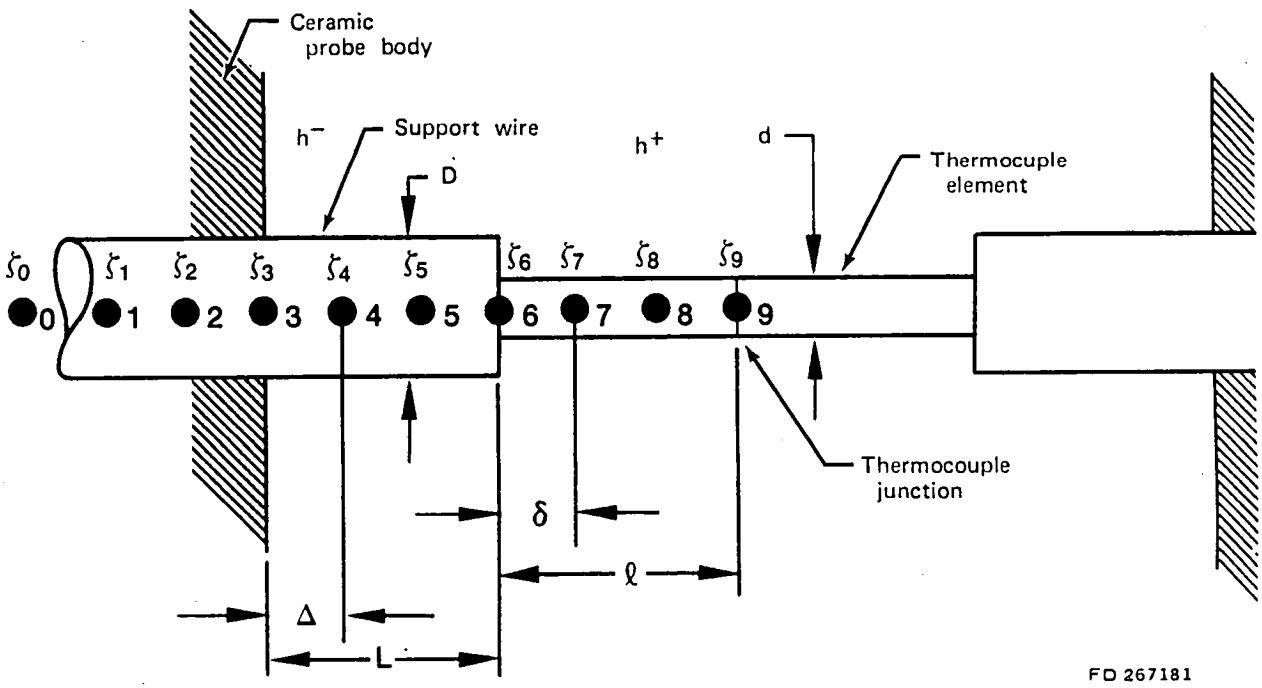

Figure 11. Finite Element Thermal Model — Used in Computer Compensation Program

$$\zeta_o = O \text{ (Assumed)} \tag{7}$$

$$\zeta_1' = \frac{C}{2A}[\zeta_o + \zeta_2 - 2\zeta_1] + \zeta_1 \tag{8}$$

$$\zeta_2' = \frac{C}{2A}[\zeta_1 + \zeta_3 - 2\zeta_2] + \zeta_2 \tag{9}$$

$$\zeta_3' = \frac{1}{2A}[C(\zeta_2 + \zeta_4 - 2\zeta_3) + F(\sin C_n t - \zeta_3)] + \zeta_3 \tag{10}$$

$$\zeta_4' = \frac{1}{2A}[C(\zeta_3 + \zeta_5 - 2\zeta_4) + 2F(\sin C_n t - \zeta_4)] + \zeta_4 \tag{11}$$

$$\zeta_5' = \frac{1}{2A}[C(\zeta_4 + \zeta_6 - 2\zeta_5) + 2F(\sin C_n t - \zeta_5)] + \zeta_5 \tag{12}$$

$$\zeta_6' = \frac{1}{(A + B)}[C(\zeta_5 + \zeta_6) + E(\zeta_7 - \zeta_6) + (F + G)(\sin C_n t - \zeta_6)] + \zeta_6 \tag{13}$$

$$\zeta_7' = \frac{1}{2B}[E(\zeta_6 + \zeta_8 - 2\zeta_7) + 2G(\sin C_n t - \zeta_7)] + \zeta_7 \tag{14}$$

$$\zeta_8' = \frac{1}{2B}[E(\zeta_7 + \zeta_9 - 2\zeta_8) + 2G(\sin C_n t - \zeta_8)] + \zeta_8 \tag{15}$$

$$\zeta_9' = \frac{1}{B}[E(\zeta_8 - \zeta_9) + G(\sin C_n t - \zeta_9)] + \zeta_9 \tag{16}$$

- Definition of the dynamic temperature components are as follows:

θ_{1n} = peak amplitude of smaller diameter thermocouple at frequency n

θ_1 (f) = θ_{1n} as a function of frequency

θ_{2n} = peak amplitude of larger diameter thermocouple at frequency n

θ_2 (f) = θ_{2n} as a function of frequency

a_n = peak amplitude of the dynamic component of the gas stream temperature at frequency n

a_n (f) = a_n as a function of frequency

ϕ_n = phase shift of the gas temperature with respect to arbitrary time t_o at frequency f_n

η_{1n} = phase shift of smaller diameter thermocouple with respect to gas temperature at frequency f_n

η_{1n} = phase shift of smaller diameter thermocouple with respect to gas temperature at frequency f_n

η_1 (f) = η_{1n} as a function of frequency

η_{2n} = phase shift of larger diameter thermocouple with respect to gas temperature at frequency f_n

η_2 (f) = η_{2n} as a function of frequency

j = time index

x = special index along length of thermocouple

T_n = instantaneous temperature of thermocouple wire at frequency n

$T_{1 \ldots 9n}$ = instantaneous temperature of thermocouple wire at spacial location at frequency n

$T_{x\ peak}$ = max peak in instantaneous temperature of thermocouple wire at spacial location x

T_g = instantaneous gas stream temperature

T_{gn} = instantaneous gas stream temperature at frequency n

h^+ = convective film coefficient of thermocouple element

h^- = convective film coefficient of thermocouple support wire

σ = Boltzmann constant

α = thermal diffusivity of the wire

$$\alpha = \frac{k_w}{\rho_w C_{pw}}$$

L = length of larger diameter thermocouple support wire

ℓ = one half of length of smaller diameter thermocouple wire

D = diameter of larger diameter support wire

d = diameter of smaller diameter thermocouple wire

ρ_w = density of thermocouple wire

k_w = thermal conductivity of thermocouple wire

C_{pw} = specific heat of the thermocouple wire

ρ_g = density of the gas stream

k_g = thermal conductivity of the gas stream

C_{pg} = specific heat of the gas stream

P_{rg} = Prandtl number of gas stream = $\frac{C_{pg}\,\mu_g}{K_g}$

U_g = velocity of the gas stream

μ_g = viscosity of the gas stream

γ_g = ratio of specific heats of gas stream

P = mean gas stream pressure

M_n = Mach number

$f_1 \rightarrow f_x$ = frequencies of f_n at which transfer functions will be evaluated

F/A = fuel air ratio

$A = \frac{D^2\,\Delta}{8\alpha(\Delta t)}$

$B = \frac{d^2\,\delta}{8\alpha(\Delta t)}$

$C = \frac{D^2}{4\Delta}$

$C_n = 2\pi f_n$

$\delta = \ell/3$

$E = \frac{d^2}{4\delta}$

$$F = \frac{h^- D\Delta}{2K_w} = \frac{\Gamma D^{1/2}}{2\alpha}$$

$$G = \frac{h^+ d\delta}{2K_w} = \frac{\Gamma d^{1/2}\delta}{2\alpha}$$

Δ = L/3 = space step

Δt = time step

$$\Gamma = \frac{0.48\ k_g\ P_{rg}^{1/3}\ U_g^{1/2}}{\left(\frac{\mu_g}{\rho_g}\right)^{1/2} \rho_w\ C_{pw}} = \text{Aerodynamic parameter} \qquad (17)$$

$H(f)$ = Measured transfer function (i.e., FFT frequency response function) of larger diameter t/c with respect to smaller diameter t/c

$G_{11}(f)$ = Measured FFT autospectral density function of smaller diameter thermocouple

$G_{12}(f)$ = Measured FFT cross-spectral density function between small t/c and large diameter t/c

$\gamma_{12}^2(f)$ = Measured FFT ordinary coherence function between larger diameter t/c and smaller diameter t/c

$S_1(f)$ = Measured FFT spectrum of smaller diameter t/c

Overview of Compensation Procedure

1. The theoretical transfer functions (frequency response function gain) between the 76 μm (3 mil) t/c and the gas stream (θ_{1n}/a_n) and the 250 μm (10 mil) t/c and the gas stream (θ_{2n}/a_n) are computed from the thermal finite difference solution using equations 7 through 16, for a range of values of the aerodynamic parameter (Γ) at a number of discrete frequencies falling between the corner frequencies of the two t/c's. These data are then used to compute the theoretical transfer function between the 250 μm (10 mil) t/c and the 76 μm (3 mil) t/c (θ_{2n}/θ_{1n}) for the corresponding values of Γ and frequency. These curves will be used to determine the insitu value of Γ from the measured transfer function of θ_{2n}/θ_{1n}. The process is as follows:

   a. The following parameters are input or already stored in the computer. For type B thermocouple wire — L, ℓ, D, d, ρ_w, k_w, Cp_w, and α_w. For the gas stream — ρ_g, k_g, Cp_g, γ_g,

μ_g and P_{rg}. The wire and gas property parameters are curve fits of the curves shown in Appendices B and C.

b. The average or mean conditions for the test data for the following variables are entered into the computer.

T	= mean gas temperature
P	= mean gas pressure
F/A	= fuel air ratio
$f_1 \rightarrow f_x$	= frequencies of f_n at which transfer functions will be evaluated
Mn	= Mach No.

c. The program computes an estimated value of Γ based on the estimated run conditions using equation 17.

d. The program then computes ζ_9', the transfer function between the wire thermocouple and the gas stream, for the 76 μm (0.003 in.) and the 250 μm (0.010 in.) thermocouple via equations 7 through 16 from 0.5 Γ to 1.5 Γ in steps of 0.1 Γ at frequencies f_1, ..., f_x which are user selected to fall in between estimated values of the corner frequencies of the two t/c's (Figure 12). The equations are evaluated until steady state conditions are reached. The criteria for steady state is that the positive maximum peak of θ_{xn}/a_n be within 0.1% of the absolute values of the negative maximum peak within the same period. The computer code determines the sampling interval for each frequency evaluated to ensure mathematical stability of the finite element model and minimize computation time. The normalized ratio of the magnitude of the temperature fluctuation in the wire to the temperature fluctuation of the gas stream ($\zeta_9' = \theta_n/a_n$) at frequency f_n is determined by locating the maximum peak amplitude (Figure 13) after the model has iterated to steady-state conditions. The phase shift (η_x) of the temperature fluctuation in the wire is determined by locating the time at which ζ_9' crossed zero going positive at the beginning of the period in which the model reached steady-state conditions (Figure 13).

e. The data from (d) are then used to compute the theoretical transfer function θ_{2n}/θ_{1n} from 0.5 Γ to 1.5 Γ (Figure 14) at frequencies of f_1 through f_x.

2. Thermocouple test data are digitized into the Fourier system computer, typically 32 to 120 records each of the 76 μm t/c *dynamic* signal and the 250 μm t/c dynamic and dc signals. Each record contains 2048 samples of the data. These data are then converted from millivolts to temperature utilizing NBS calibration curve coefficients for type B thermocouples. The 250 μm dc channel is utilized as the mean for both dynamic data channels

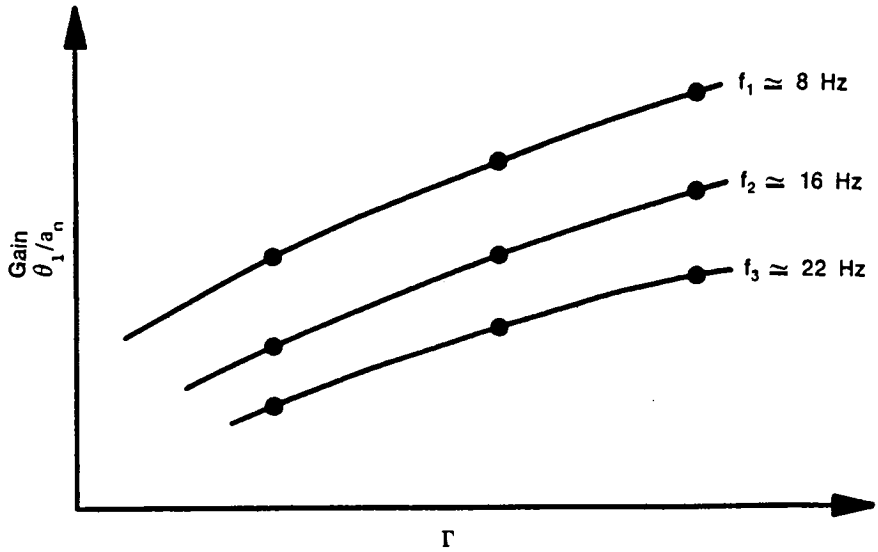

(a) Gain of 76μm Thermocouple vs Aerodynamic Parameter

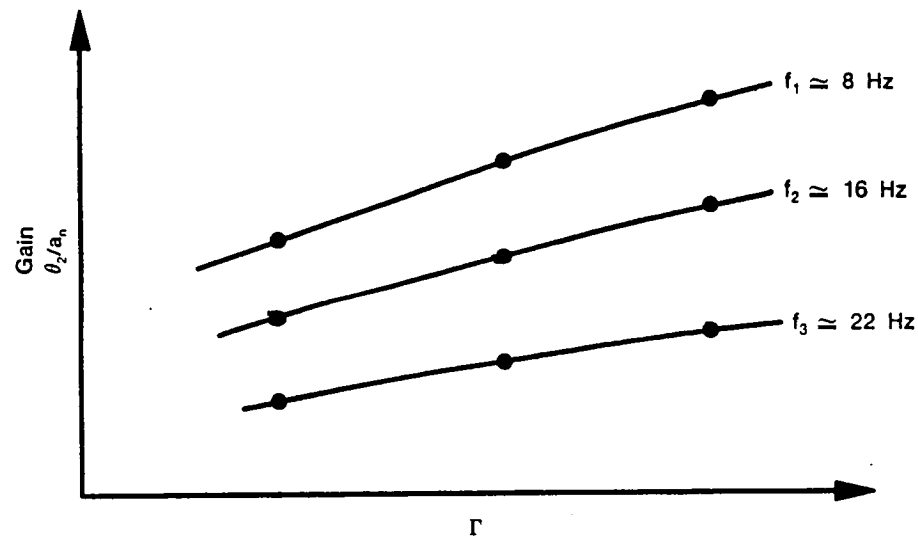

(b) Gain of 250μm Thermocouple vs Aerodynamic Parameter

FD 267182

Figure 12. Theoretical Curves of ζ_9 for 76 μm and 250 μm Thermocouples

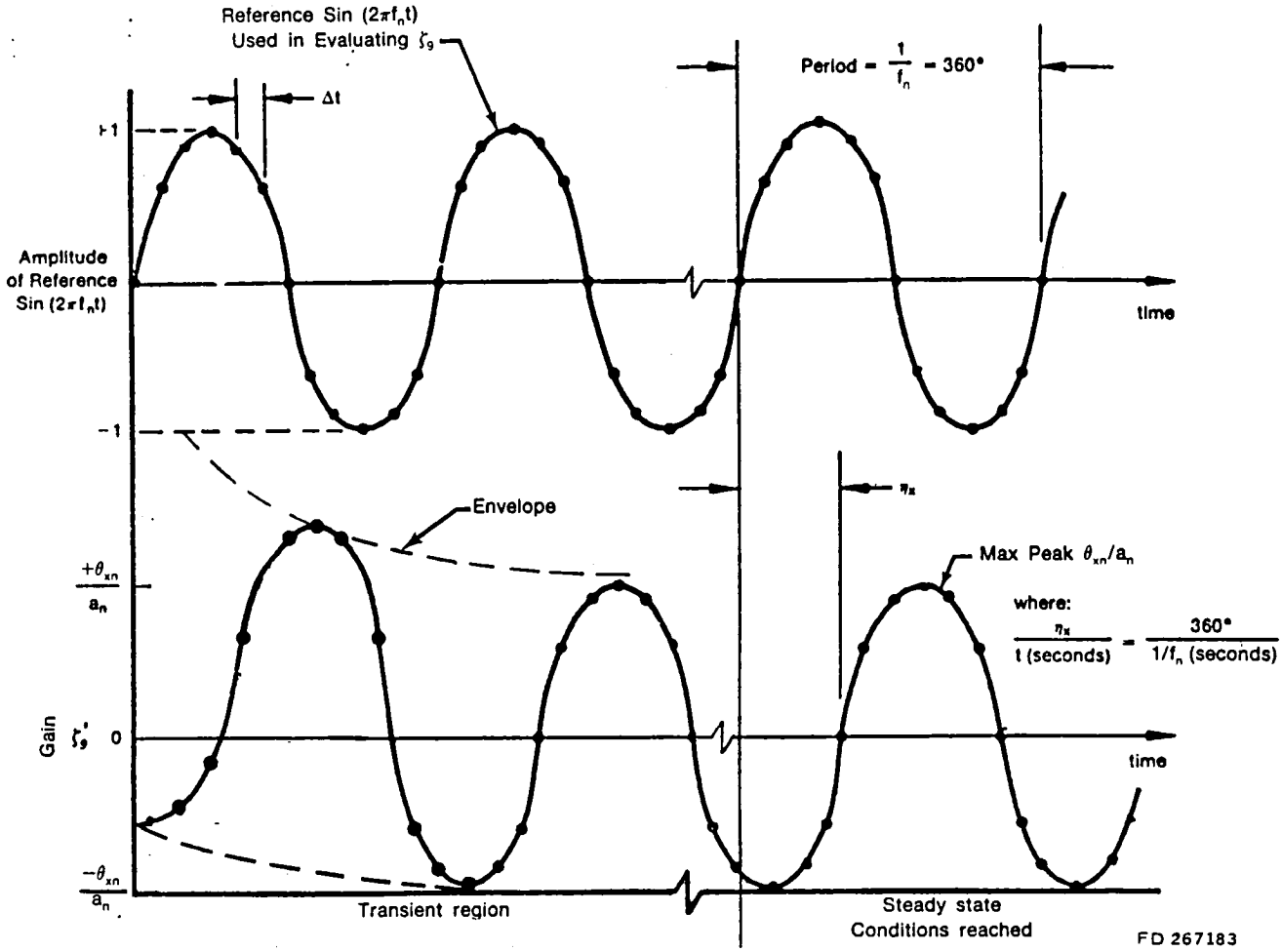

Figure 13. Transfer Function of Thermocouple With Respect to Gas Temperature

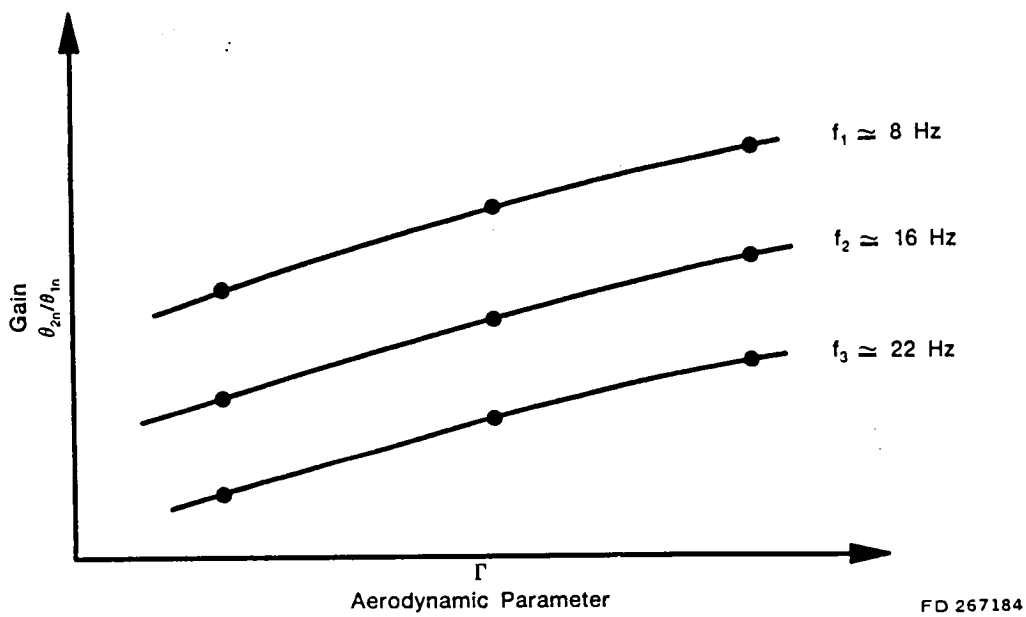

Figure 14. Theoretical Curves of ζ_9 for the 250 μm Thermocouple Divided by ζ_9 of the 76 μm Thermocouple

in converting the nonlinear t/c mv signals to linearized temperature. These data records are then saved for recall for additional processing or plotting.

3. An ensemble averaged FFT (Fast Fourier Transform) transfer function (frequency response) analysis is then performed on x number of time records of the *dynamic* data to yield the measured value of θ_{2n}/θ_{1n} (i.e., H(f)) as a function of frequency. The transfer function is computed as the FFT cross-spectral density function between the 76 μm thermocouple and the 250 μm thermocouple divided by the FFT autospectral density function of the 76 μm signal:

$$H(f) = \frac{G_{12}(f)}{G_{11}(f)}$$

In conjunction with the computation of the measured transfer function, the coherence function $\gamma^2_{12}(f)$ is computed and utilized to assess the quality of the measurement. For the 2048 time sample data record lengths utilized, 1024 line FFT's are produced. For the typical sampling rate of 4096 Hz (certain other sampling rates are permitted), the FFT analyses yield spectral information from dc to 2048 Hz in 2 Hz intervals. A standard Hewlett Packard windowing function (P301) is utilized prior to computation of the FFT's. This window is characterized by excellent spectral amplitude accuracy ($< \pm 0.1\%$). Side lobe suppression is > -70 db at $\pm$ 4 spectral lines and the effective noise bandwidth is 3.4 spectral lines.

4. Each measured value of H(f) at frequencies $f_n = f_1 \rightarrow f_x$ are used in conjunction with the theoretical values of θ_{2n}/θ_{1n} vs Γ at the corresponding frequencies to determine a measured value of Γ (the program interpolates between the 0.1 Γ increments computed in (1) above). The arithmetic average of Γ obtained for each frequency is taken as the insitu measured value.

5. Using the measured insitu average value of Γ obtained in (4), ζ_9, the normalized transfer function (gain θ_{1n}/a_n and phase η_{1n}) of the 76 μm thermocouple with respect to the gas stream temperature is then computed at all frequencies from the 1st spectral line of the FFT spectrum to the Nyquist frequency of the FFT for each discrete frequency contained in the FFT (Figure 15). This is typically from 2 Hz to 2048 Hz in 2 Hz increments. This is the compensation spectrum $\theta_1(f)/a_n(f) \underline{/\eta_1(f)}$ which is then used to compensate the 76 μm t/c data as follows:

6. To compute the compensated ensemble averaged power spectral density function (PSD), the measured ensemble averaged autospectral density function of the 76 μm (3 mil) t/c obtained in (3) above is divided by the autospectral density function of its compensation spectrum:

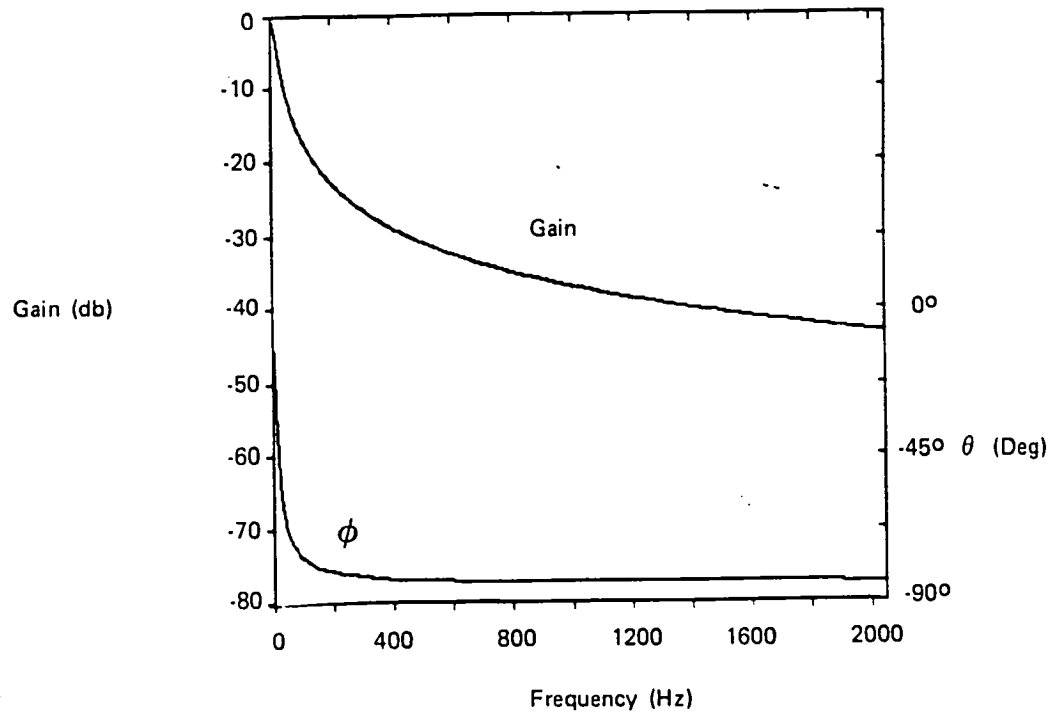

Figure 15. Compensation Spectrum for 76 μm (3 mil) Thermocouple Output for Test Point No. 10 (Subscale Combustor Rig)

$$\frac{G_{11}(f)}{\left(\frac{\theta_1(f)}{a_n(f)}\right)^* \left(\frac{\theta_1(f)}{a_n(f)}\right)} \approx \frac{\theta_1(f) * \theta_1(f)}{\left(\frac{\theta_1(f)}{a_n(f)}\right)^* \left(\frac{\theta_1(f)}{a_n(f)}\right)} \rightarrow a_n^2(f)$$

where * = complex conjugate multiplication

Scaling factors for effective noise bandwidth and FFT Fourier symmetry are applied.

7. To compute the compensated instantaneous time waveform, an FFT spectrum ($S_1(f)$) is made on a specific time record yielding amplitude and phase terms for each spectral component. This spectrum expressed in rectangular frequency coordinates is then divided (complex math) by the compensation spectrum. The compensated instantaneous spectrum is then inverse Fourier transformed to yield the compensated instantaneous time waveform. The software contains information on specific techniques employed to prevent time waveform distortions associated with the inverse Fourier transform. A threshold, in relative db, is applied to the frequency spectrum of the data signal prior to division by the compensation spectrum to prevent errors where the signal to noise ratio is too low:

$$\frac{S_1(f)\,\angle\lambda_1(f)}{\left(\frac{\theta_1(f)}{a_n(f)}\right)\angle\eta_1(f)} \simeq \frac{\theta_1(f)\,\angle\eta_1(f)+\phi(f)}{\left(\frac{\theta_1(f)}{a_n(f)}\right)\angle\eta_1(f)} \rightarrow a_n(f)\,\angle\phi(f)$$

which is the compensated instantaneous frequency spectrum

and $F^{-1}\, a_n(f)\ \angle\phi(f)$

the compensated time wave form where F^{-1} is the inverse Fourier Transform.

the compensated instantaneous frequency spectrum.

3. Test Plan

a. Summary

The test plan presented in the following section was formulated during Task 4 efforts and is based on three test series consisting of (1) System Shakedown and Compensation Verification Lab Tests, (2) Laboratory Burner Tests, and (3) Full-Scale F100 Engine Tests. These tests allowed for a step-by-step checkout and optimization of the various components of the system while allowing for the experimental evaluation and substantiation of the criteria specified in Exhibit B of the contract SOW. All of the criteria of Exhibit B were tested directly. The test plan matrix shown in Table IV summarizes how the criteria of Exhibit B were evaluated in the three test series.

Each of the planned tests are discussed in the following paragraphs. The actual testing was conducted in Task 5 and some modifications to the plan were necessary. The final testing and results are discussed in detail in Task 5.

TABLE IV. TEST PLAN SUMMARY

Criteria	*System Shakedown and Compensation Verification*	*Lab Burner Rig*	*Full-Scale F100 Tests*
Temperature (1900K peak; ±500K fluctuations)			X
Frequency response (1000 Hz compensated)	X	X	X
Pressure (1.01×10^6 to 2.02×10^6 Newton/meter^2)			X
Flow (200 m/s with ±50 m/s fluctuations)			X
Gas Composition (Products of combustion and air)		X	X
Sensor Lifetime (5 hr minimum)		X	X
Accuracy	X		
Vibration (10g loading up to 500 Hz)			X

The first test consisted of a laboratory bench-top system shakedown test using an electrically heated air blower as a fluctuating temperature source. A heat gun was used to supply a low velocity, turbulent air stream at a maximum temperature of 550K. Both the probe and heat gun were mounted on a bench top in the instrumentation laboratory near the Fourier Analyzer. The data was acquired, recorded, and finally processed.

The second test served to evaluate the accuracy of the computer FFT compensation techniques. An electrical analogy of the measurement was constructed. First order low pass filter networks were fabricated with time constants to correspond with the maximum condition case values of the 76 μm (0.003 in.) and 250 μm (0.010 in.) thermocouples, respectively. The frequency response functions of the filters were measured via the *transfer function* analysis in the Fourier Analyzer System using an existing P&WA processing program. The measured transfer functions of the list order filters were substituted in the data processing program in place of the compensation spectrum that would normally be computed. This permitted evaluation and refinement of the computer FFT compensation techniques independent of errors in the compensation spectrum.

The filter(s) were substituted for the thermocouple(s) of the probe sensor. Various types of generator signal waveforms with output levels similar to predicted thermocouple signal levels were input to the filter(s) and an additional ADC channel on the Fourier Analyzer. This provided a measurement input representing true *gas stream* temperature acquired simultaneously with the *simulated thermocouple* signals. The data processing program was run and the compensation performed (using the correctly known compensation spectrum). The measured input representing the true gas temperature was then compared to the compensated spectrum to determine the accuracy of the computer FFT compensation techniques. Note that for this specific test, it wasn't necessary to use a complex analog model of the t/c because the test was not designed to evaluate the accuracy with which the compensation spectrum could be measured but rather to evaluate and refine the computer FFT compensation techniques.

The 3rd test was designed to evaluate and verify the validity of the duel t/c data processing program using 9 node analog models of the t/c's. In these tests, comparison of the compensation spectrum of the simulated 76 μm t/c produced by the data processing program (using the measured transfer function between the outputs of the 76 μm and 250 μm analog circuits) with its known frequency response function was the primary objective along with comparison of the compensated output signals with the input signals.

For these tests, the data processing program input parameters for wire diameters, length, and gas properties were based on the matching condtions used in designing the electrical analog circuits. The input signal representing the true gas stream fluctuations was digitized simultaneously with the output signals of the 76 μm and 250 μm analog circuits. The known frequency response functions for the 9 node analog circuits were measured via the transfer function analysis in the Fourier Analyzer System using an existing P&WA processing program.

c. Subscale Combustor Tests

The second system test performed used a laboratory burner rig test using a high temperature flame. The flame was characterized by fluctuating high temperature (1500K maximum) and fluctuating velocity (305 meters/sec maximum) at a constant ambient pressure of 1 atmosphere.

This test allowed evaluation of the sensor and measurement system in an elevated temperature combustion environment, and also allowed evaluation of the effects of gas composition, corrosion, and erosion on the sensor wires.

The test plan for these tests was based on setting the maximum exhaust velocity obtainable with 11.2 cm (3 in.) diameter nozzle on the subscale combustor at each temperature setting. The average flame temperature increased in steps of 56K (100°F) beginning at 811K (1000°F) and going to a maximum temperature of approximately 1644K (2500°F) which was determined by the limits of the subscale combustor air and fuel flows. A minimum of 2 data points were taken at each rig condition with signals recorded for off-line processing using the data acquisition and reduction system previously discussed.

d. Full-Scale F100 Engine Tests

The third system test was performed in an F100 engine instead of the originally proposed test in a combustor rig. Full-scale testing in an F100 engine, as opposed to testing in the available combustor rigs, was found to coincide more fully with the program objectives, in terms of the required schedules and test conditions.

Dynamic temperature sensor data were taken during the initial F100 engine tests where steady-state power settings from idle to intermediate power (see Table V) were made. These power settings could provide combustor exit temperatures of 811K (1000°F) to 1867K (2600°F) in increments of 56K (100°F). Each engine run condition was maintained for approximately 5 min duration.

TABLE V. F100 TURBINE INLET GAS CONDITION RANGES

		Power Setting	
		Idle	*Max*
Average Total Temperature	K (°R)	950 (1700)	1680 (3020)
Average Total Pressure	N/m^2 (psia)	$4.13 \times 10^{\pm 5}$ (60)	2.02×10^{6} (292)
Average Mach No. at Combustor Exit			0.15-0.20
Mach No. at AP-5 Borescope Location			0.35

D. TASK 5 — FABRICATION AND TESTS

Three probe assemblies based on the final designs generated and approved in Task 4 were fabricated. Two subscale combustor probes and one F100 probe were completed. The fabricated sensors were then inspected prior to testing. The testing, consisting of the: (1) System Shakedown and Compensation Verification Tests; (2) Subscale Combustor Tests; and the Full-Scale F100 Engine Tests, were conducted as planned in Task 4. All test objectives or environmental guidelines were met except for the 5 hr life requirement. A post-test inspection of the probe sensor was also conducted.

1. Sensor Fabrication

Two subscale combustor probes were fabricated based on the design shown in Task 4 . Figure 16 shows the completed sensor trip geometry of the probe that was fabricated and later tested in the subscale combustor. One full-scale F100 probe assembly was fabricated and is shown in Figure 17.

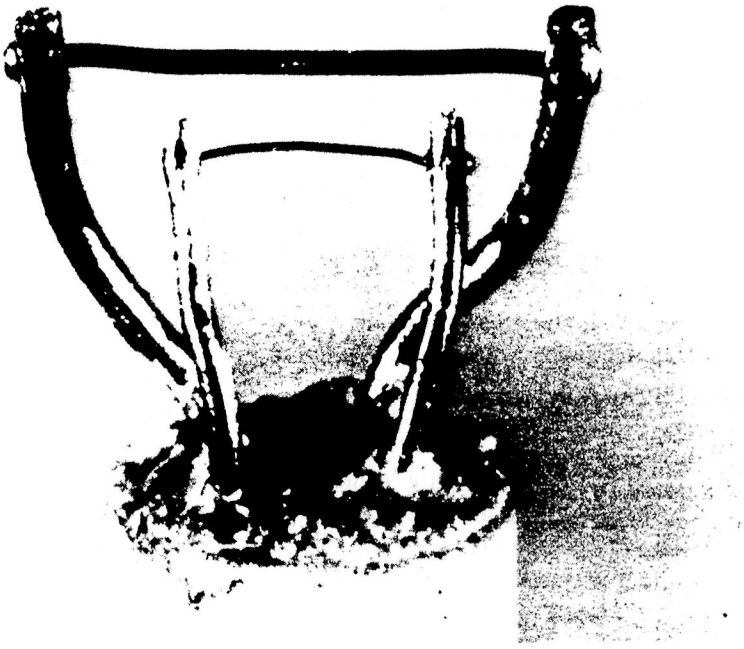

FD 267186

Figure 16. Subscale Combustor Probe — As Fabricated

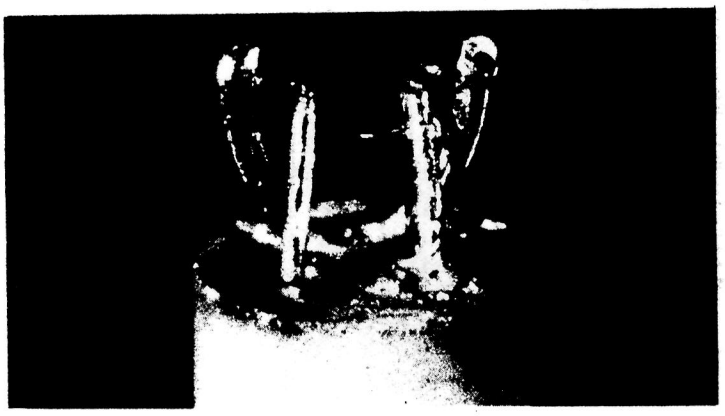

FD 267187

Figure 17. Full Scale F100 Probe — As Fabricated

2. Sensor Pre-Test Inspection

The subscale combustor probe element junctions were inspected to determine the junction's actual dimensions and weld uniformity. Each thermocouple junction was inspected under a Nikon Metaphot microscope at 100X or 200X magnification. Photomicrographs of each junction and a graduated scale were made to measure the junction diameter and uniformity of the wire cross section. Two angular orientations of each wire were photographed 90 deg apart. A number of different readings of each photograph were obtained to define the mean value and precision of each sample. Measurement uncertainty of this technique is ± 1.3 μm or 5×10^{-5} in. for the 76 μm elements and ± 2.5 μm or 1×10^{-4} in. for the 250 μm elements. Effects of these uncertainties on temperature uncertainty were later determined in Task 6 sensitivity analyses using the completed data reduction method.

The results of these element inspections for the subscale combustor are shown in Figure 18. Other important probe element dimensions were also determined by measuring photomicrographs of the completed sensor and the final results along with the print dimensions are presented in Table VI. Table VI shows that the final element diameters are slightly undersized from the nominal wire values, however, all of the dimensions presented no problems structurally or operationally.

The full-scale F100 probe element junctions were also inspected and the results are shown in Figure 19. A summary of the sensor tip dimensions for the probe is presented on Table VII and shows the elements are slightly oversized. A review of these dimensions shows that the minor variations listed in the dimensions should not affect the probe's operation.

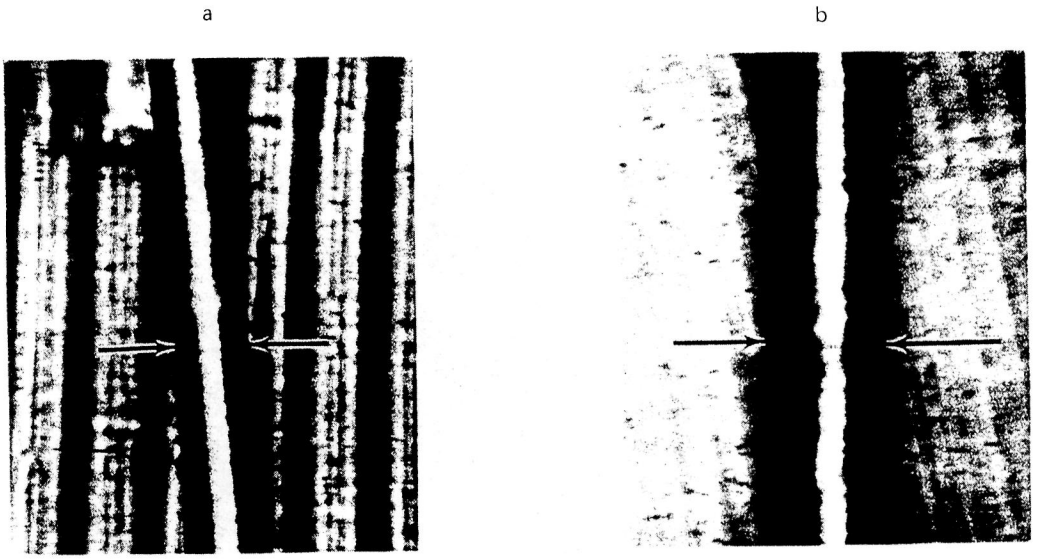

Figure 18. Subscale Combustor Probe Pre-Test Inspection — Microscopic Inspection of Junctions

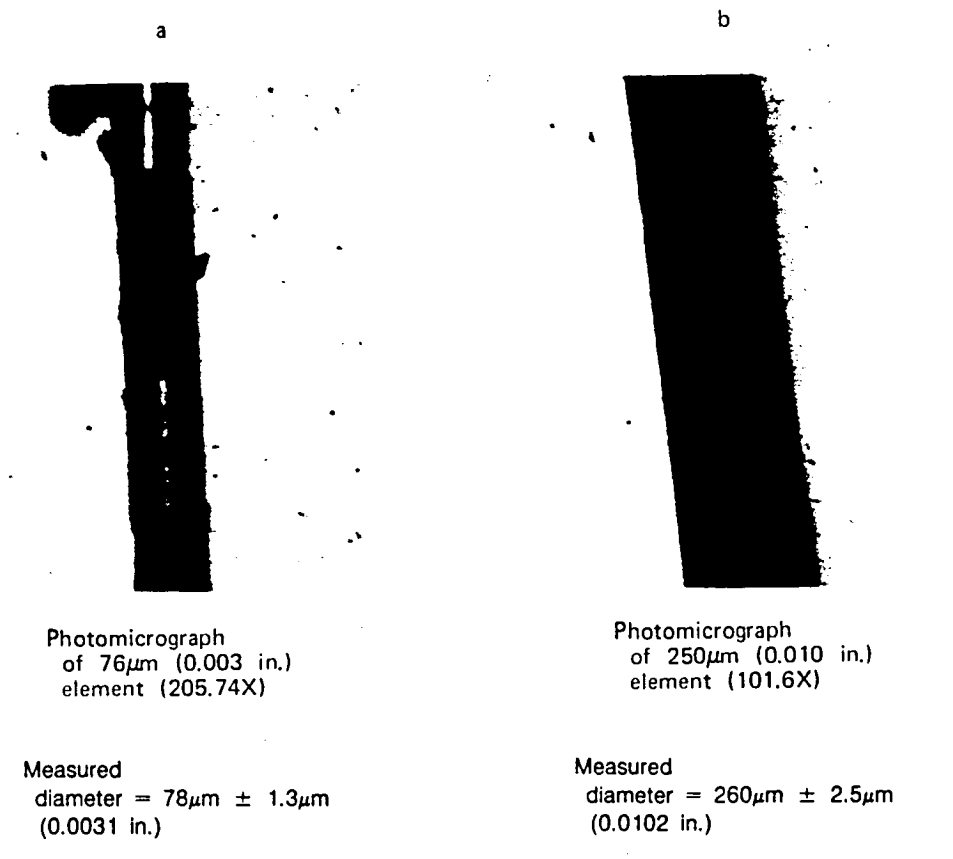

Figure 19. F100 Probe Pre-Test Inspection — Microscopic Inspection of Junctions

TABLE VI. SUBSCALE COMBUSTOR PROBE PRE-TEST INSPECTION SUMMARY

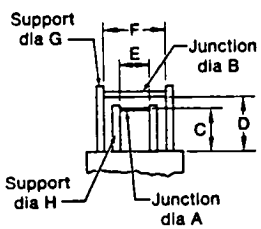

Dim	*Print μm (in.)*	*Measured μm (in.)*
A	76 (0.003)	74 (0.0029)
B	250 (0.010)	251 (0.0099)
C	3810 (0.150)	3810 (0.150)
D	5080 (0.200)	4570 (0.180)
E	2290 (0.090)	2670 (0.105)
F	5080 (0.200)	5590 (0.220)
G	510 (0.020)	510 (0.020)
H	380 (0.015)	380 (0.015)

TABLE VII. F100 PROBE PRE-TEST INSPECTION SUMMARY

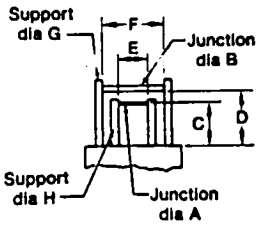

Dim	Print μm (in.)	Measured μm (in.)
A	76 (0.003)	78 (0.0031)
B	250 (0.010)	260 (0.0102)
C	1910 (0.075)	2080 (0.082)
D	2540 (0.100)	2260 (0.089)
E	1220 (0.048)	1270 (0.050)
F	3180 (0.125)	2810 (0.111)
G	510 (0.020)	510 (0.020)
H	380 (0.015)	380 (0.015)

3. Computer Software Development

a. Introduction

The data processing software for the Dynamic Gas Temperature Measurement System (DGTMS) was developed on a Hewlett Packard (HP) model 5451C Fourier Analyzer System with Signature Analysis Option. Software programs were written in HP Fortran IV and HP Keyboard (a high level language). Extensive use was made of the HP Signature Analysis package software to edit, acquire, store, transfer, Fourier transform and plot data. Overall program execution is controlled via keyboard programs. The finite difference model equations, NBS calibration curve coefficients, curve fit coefficients for various gas stream and t/c wire properties and the subroutine to determine the in-situ value of Γ from the measured transfer function were written in HP Fortran IV. The software listings and operating procedure are contained in Volume II.

The maximum number of time records the system can acquire is 120 (i.e., 120 records each of the 76 μm (3 mil) dynamic signal, the 250 μm (10 mil) dynamic signal, and the 250 μm dc signal sampled simultaneously). Each record is 2048 samples in length. The program as written, permits sampling rates of 409.6 Hz (spectral line $\Delta F = 0.2$ Hz), 1024 Hz ($\Delta F = 0.5$ Hz), 2048 Hz ($\Delta F = 1$ Hz), and 4096 Hz ($\Delta F = 2$ Hz). The lower sampling rate capability was included to permit utilization of the data compensation technique with larger diameter t/c's with inherently lower frequency response (i.e., data would be compensated over a lower frequency range).

b. Program Output Formats

The program outputs the processing results in plot format. Digital printouts of the plotted data can be output with simple HP Fourier operating system keyboard commands by the operator. Plots and printouts can be hardcopied. Data can be presented over a partial or the full range of the analysis in the frequency or time domains (single record basis).

Specific outputs available are:

1. Instantaneous temperature vs time for the compensated or uncompensated dynamic signal from the smaller (Note 1) diameter t/c and the

uncompensated dynamic signal from the larger diameter t/c — any user specified record out of a 120 records (maximum).

2. Instantaneous temperature vs time for the uncompensated dc signal from the larger diameter t/c — any user specified record out of a 120 records (maximum).

3. Ensemble averaged (1 to 120 averages) frequency spectra of compensated or uncompensated small diameter t/c or uncompensated (Note 1) larger diameter t/c — data can be presented in any of the following forms (user select):

Function	*Dimensions*	*Engineering Units*	
• Power Spectral Density (PSD)	Mean Square / Hz	°F² / Hz	K² / Hz
• Log Power Spectral Density •• 10 $\log_{10}$ PSD	Mean Square / Hz	db ref 1°F² / Hz	.309K² / Hz
• Linear Power Spectral Density •• Positive Square Root of Power Spectral Density function	rms / Hz	°F / Hz	.556K / Hz
• Narrowband Frequency Spectrum •• Positive square root of the autospectral density (autopower) function with narrowband signal correction for FFT windowing function applied and no normalization to per unit bandwidth.	rms	°F (K)	

4. Instantaneous frequency spectra of the time domain waveforms in (1) above using the presentations from (3). Use of the prefix "Instantaneous" in conjunction with the analyses in (3) denotes that the spectrum was made directly from the specified singular time record.

c. Program Structure

The basic steps in the program execution are as follows:

1. Operator enters program variables for t/c geometry, operating conditions, and data acquisition.

Note 1: Compensated spectra of the 250 μm (10 mil) t/c can be obtained by operator manipulation of the data storage locations utilizing simple HP Fourier System Keyboard Commands.

2. Program computes the theoretical gain ratio θ_{2n}/θ_{1n} vs a range of values of aerodynamic parameter Γ at frequencies $f_1 \rightarrow f_x$. The range of Γ is based on a nominal value of Γ corresponding to the variables entered in (1) above.

3. Operator keys program to acquire t/c test data (typically one to two minutes in length)

   - dynamic signals from the smaller and larger t/c's
   - dc signal from either the larger or smaller t/c

4. Program converts digitized t/c data from millivolts to temperature (°F) using NBS calibration curve coefficients for type B t/c.

5. Program determines H(f) the measured value of the transfer function (frequency response) between the larger and smaller diameter t/c's and the corresponding coherence function ($\gamma^2_{12}(f)$).

6. Program determines the insitu value of Γ using the measured transfer function (H(f)) from (5) in conjunction with the theoretical values of θ_{2n}/θ_{1n} vs Γ obtained in (2) above.

7. Program computes the compensation spectrum using the measured value of Γ.

8. Operator selects specific record(s) to be compensated and plotted.

4. System Shakedown and Compensation Verification Lab Tests

Laboratory tests were run to evaluate the effectiveness of the compensation technique and provide a system shakedown prior to acquisition of the rig and engine test data. Evaluation of the DGTMS software was accomplished in two test series. The first test series used a simple first-order RC network which simulated the 76 μm thermocouple. The purpose of this series was to refine and evaluate the Fast Fourier Transform technique, and culminated in definition of the error introduced through numerical manipulation of the data. In the second test series, a laboratory evaluation was performed on an analog simulation of the dual thermocouples (RC network equivalents of the 9 node finite models of the 76 μm and 250 μm t/c's). Using these analog circuits it was possible to make direct comparisons of DGTMS results with known input signals and known compensation spectra.

a. Evaluations of Computer FFT Compensation Technique and Associated Errors

Even if the compensation spectrum for the thermocouple could be measured without error, there could be significant errors in the DGTMS compensated results (particularly in the time waveform) due to the FFT techniques utilized in the compensation procedure.

During development of the FFT compensation procedures, a known correct compensation spectrum (i.e., a conventionally measured frequency response function) for a simple 1st order RC analog circuit with a frequency response function similar to a 76 μm t/c was used for initial evaluation and refinement of the software. Note that these particular tests do not evaluate the accuracy with which the DGTMS technique determines the compensation spectrum.

The test procedure consisted of first measuring the frequency response of the RC network using conventional Fast Fourier Transform (FFT) techniques and storing the measured

response in the computer (frequency domain). Various types of signals including wideband random, singular sinusoidal frequencies, and step inputs were then input to the RC network and both the input and output signals digitized into the Fourier System simultaneously. The output signal was compensated in the frequency domain using the previously measured frequency response function and then transformed to the time domain. The compensated output (frequency and time domain) was then compared with the measured input signal.

To minimize errors in the compensated time waveform generated by inverse FFT of the compensated frequency spectrum, the following procedure was developed and incorporated into the DGTMS software:

1. Multiply the uncompensated time waveform by the FFT Hanning window.

2. FFT the windowed signal to yield the instantaneous frequency spectrum.

3. At every frequency in the spectrum where the amplitude is less than a user specified threshold, set amplitude and phase to zero.

4. Divide the modified instantaneous spectrum by the compensation spectrum (complex math) accounting for both amplitude and phase terms.

5. Inverse FFT the compensated instantaneous spectrum to obtain the compensated time waveform.

6. Divide the compensated time waveform by the FFT Hanning window.

7. Set 1st and last quarter of compensated time waveform to zero.

8. Repeat steps 1 thru 7 on a new uncompensated time record composed by overlapping portions of the original uncompensated time record and the next contiguous time record to yield a composite compensated time waveform beginning one quarter of the time into the first time record and extending thru the first quarter of the next contiguous time record. Note that there must be no loss of sampled data between the contiguous time records (i.e., the data acquisition must be in real time). If only one time record is available, the compensated time waveform will be zero for the first and last quarter of the record.

The data analysis program contains a user variable threshold (relative db) which is applied when the compensated time waveform is generated ((3) above). The software determines the highest amplitude in the uncompensated instantaneous frequency spectrum and then sets to 0 the amplitude and phase of any spectral component whose amplitude is less than the specified value of db below the highest amplitude. This is to minimize errors in the compensated time waveform due to applying high gain corrections at spectral lines which are predominantly noise. The threshold is not applied to the compensated ensemble averaged frequency spectrum. Selection of the threshold should be made based on inspection of the instantaneous frequency spectrum (uncompensated) of the time record to be compensated and the ensemble averaged frequency spectrum of the ambient background noise. Additionally, the ensemble averaged noise frequency spectrum (uncompensated) can be utilized to select a threshold. As can be seen from Figure 20 (ensemble averaged frequency spectrum of the output, input, and compensated output of a 76 μm t/c), a threshold of about -35 db could be required to prevent errors in the compensated time waveform for the signal levels in this specific case. A noise floor (probably in the anti-aliasing filter) has been reached at about -43 db (relative) in the uncompensated spectrum. The threshold would be selected somewhat above this level.

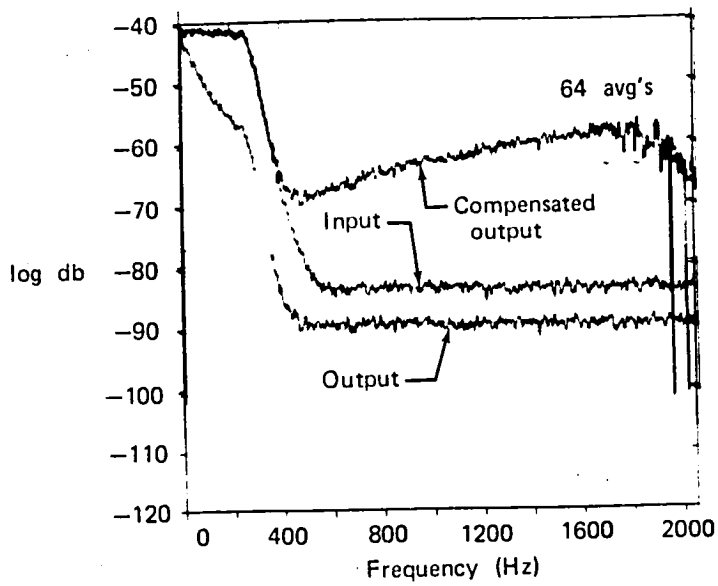

FD 267190

Figure 20. Evaluation of FFT Compensation Technique — Power Spectral Density PLOTS of 76 μm (3 mil) Analog Circuit Compensated Output, Measured Input and Measured Output Using 250 Hz Bandwidth Random Noise . . . . . .

The program also permits the repeated (user specified) application of a simple smoothing algorithm on time domain data:

$$d_n = 0.25\, d_{n-1} + 0.5\, d_n + 0.25\, d_{n+1}.$$

The routine was incorporated to permit smoothing of step function data which contain fluctuations in amplitudes thought to be associated with truncations in the compensated instantaneous frequency spectrum (Figures 21 through 23). In general, it appears that an erroneous fluctuation occurs in the envelope for the compensated time waveform at the frequency at which the compensated spectrum is truncated (prior to inverse FFT transforming to the time domain). In other words, if sufficient dynamic range existed in the compensated spectrum such that truncation occurred at the Nyquist frequency (the limit of the analysis) an amplitude fluctuation of Nyquist frequency would be present in the compensated step function time waveform. Based on the lab evaluations performed, application of this smoothing algorithm is not recommended for any wave shape other than a step and it should only be applied judiciously to step data. Smoothing was not applied to the data presented in this report.

The final evaluations of the software compensation techniques were made utilizing the 76 μm (3 mil) nine node analog model of Figure 24. These tests were used to establish the accuracy with which a signal could be compensated assuming that the correct compensation spectrum has been measured. The conventionally measured (256 average) frequency response for the 76 μm (3 mil) circuit was used as the compensation spectrum. The accuracy was determined by comparing the compensated output signal with the actual input signal which had been digitized simultaneously with the output signal. Comparisons were made on the data presented in both the time and frequency domains. The accuracy comparisons were made

utilizing digital printouts of the data (rather than scaling values from data presented in plot format). Evaluations were made for the following signals:

- 20 Hz sinusoid
  200 Hz sinusoid
  1000 Hz sinusoid
- 250 Hz BW random
  1250 Hz BW random
- STEP input.

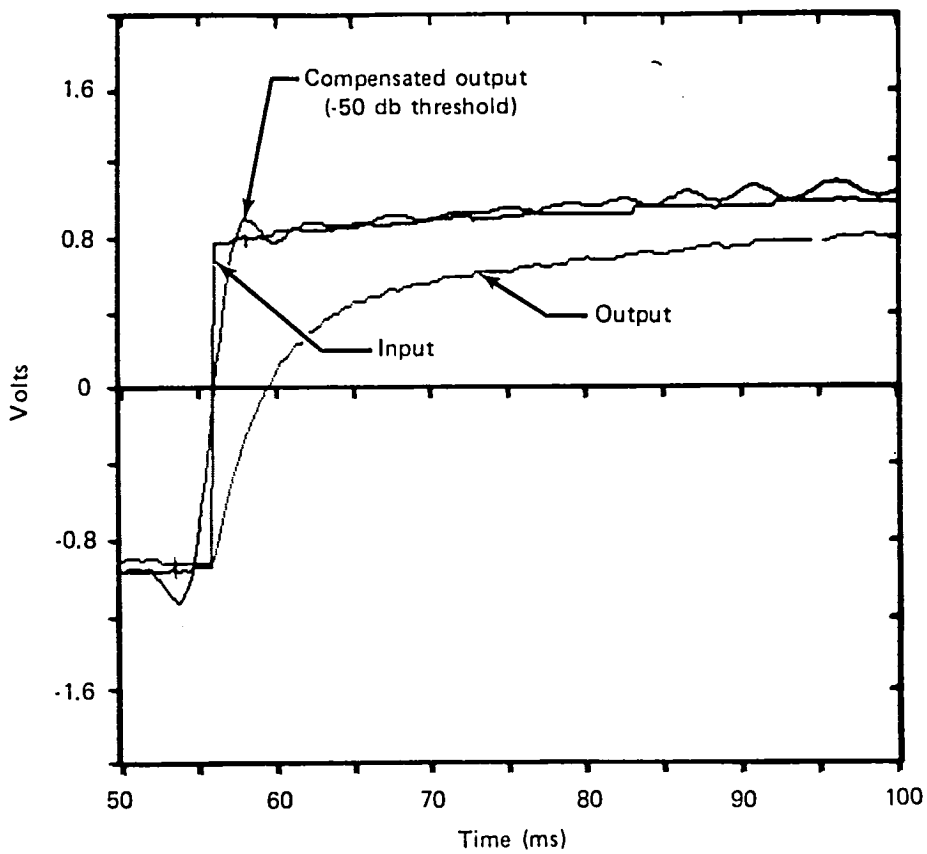

Figure 21. Evaluation of FFT Compensation Technique — Instantaneous Voltage vs Time: Compensated Output of 76 μm (3 mil) Analog Circuit Measured Input and Measured Output (−50db Threshold, Step Input)

Figures 20 thru 23, 25, and 30 thru 39 are plots of the measured output, compensated output, and the measured input in the time and frequency domains for the various types of signals evaluated (sine, random, step). For these evaluations the sampling frequency was 4096 Hz which yields a frequency spectrum range of 2048 Hz with 2 Hz spectral line separation. Each record was 500 ms in length.

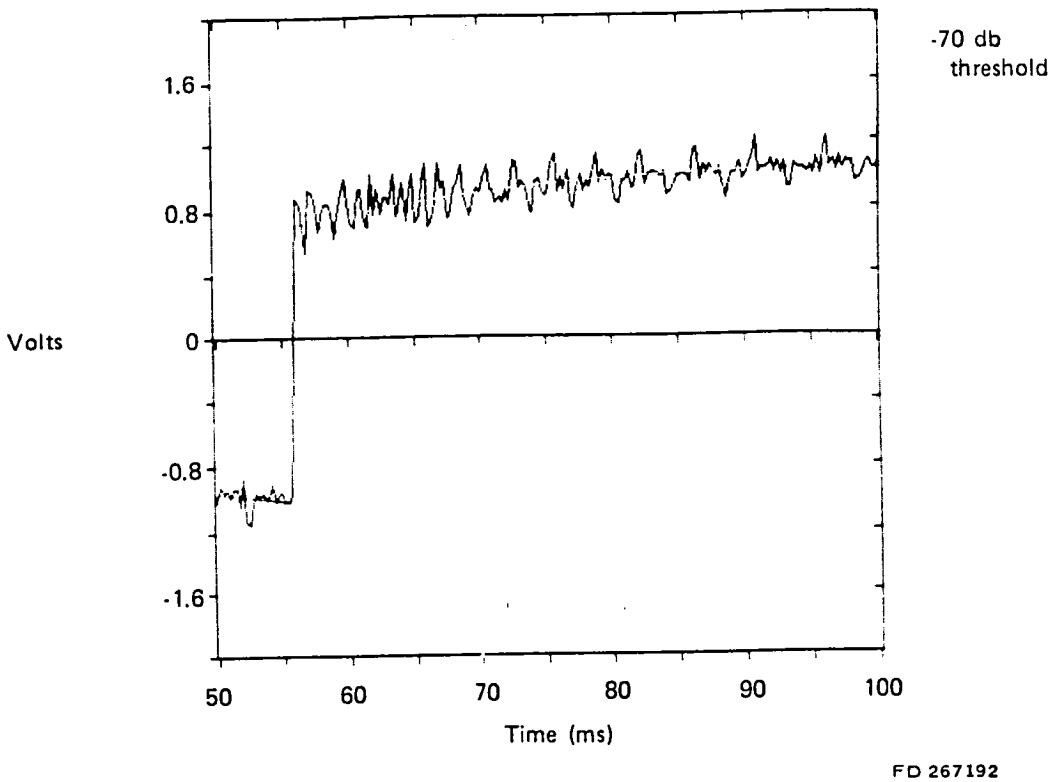

Figure 22. Evaluation of FFT Compensation Technique — Instantaneous Voltage vs Time: Compensated Output of 76 μm (3 mil) Analog Circuit (−70db Threshold, STEP Input)

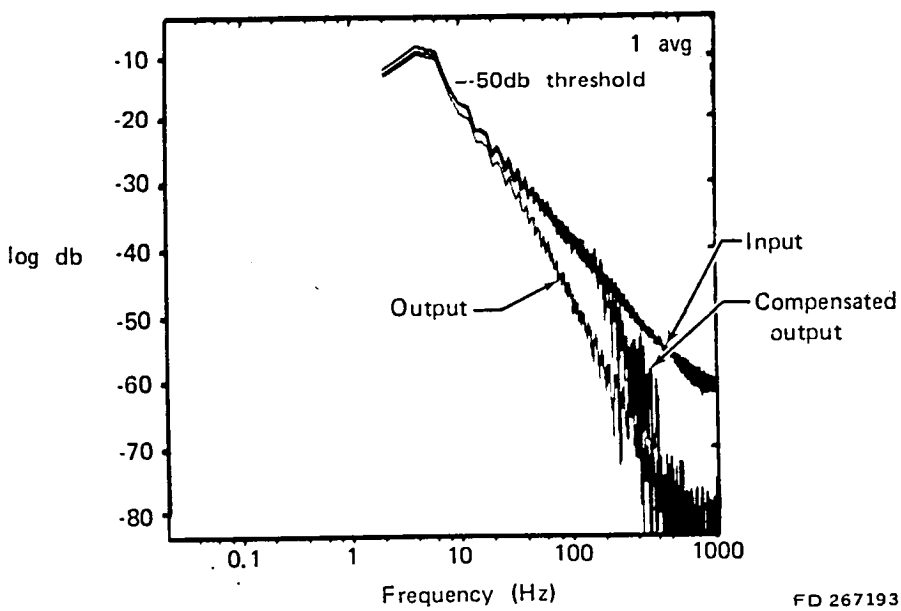

Figure 23. Evaluation of FFT Compensation Technique — Instantaneous Power Spectral Density Plots of Compensated Output of 76 μm (3 mil) Analog Circuit, Measured Input and Measured Output (−50 db Threshold, STEP Input

From digital printouts of the data presented in Figures 20 thru 23, and 30 thru 39, the accuracy of the FFT compensation technique was evaluated. Errors in the compensated functions were computed as follows and do not include errors associated with determination of the compensation spectrum:

a. Ensemble averaged frequency spectrum

$$\text{Gain Error (f)} = \left(\sqrt{\frac{\text{Compensated output power spectral density function}}{\text{Input power spectral density function}}} - 1 \right) \times 100\%$$

b. Instantaneous frequency spectrum of compensated time waveform:

$$\text{Gain Error (f)} = \left(\frac{\text{Polar Magnitude (compensated output)}}{\text{Polar Magnitude (input)}} - 1 \right) \times 100\%$$

Phase Error (f) = Input phase − Compensated output phase

Gain and phase errors were actually computed by complex division with respective frequency spectra expressed in rectangular coordinate form (real and imaginary) and then converted to polar coordinate form. The DGTMS software computes the instantaneous frequency spectrum as the square root of the power spectrum and does not contain phase information. The phase errors were evaluated during the lab tests to provide a measurement of the phase errors associated with the compensated time waveform.

c. Instantaneous time waveform (3 methods)

1. $$\left(\frac{\text{RMS compensated output}}{\text{RMS input}} - 1 \right) \times 100\%$$

2. $$\left(\frac{\text{RMS residue*}}{\text{RMS input}} \right) \times 100\%$$

3. $$\left(\frac{\text{Max instantaneous Peak Residue*}}{\text{Max instantaneous Peak input}} \right) \times 100\%$$

*Residue — input minus compensated output

The rms of the time waveforms were computed using operator keyboard functions provided in the Hewlet Packard (HP) Fourier System operating system.

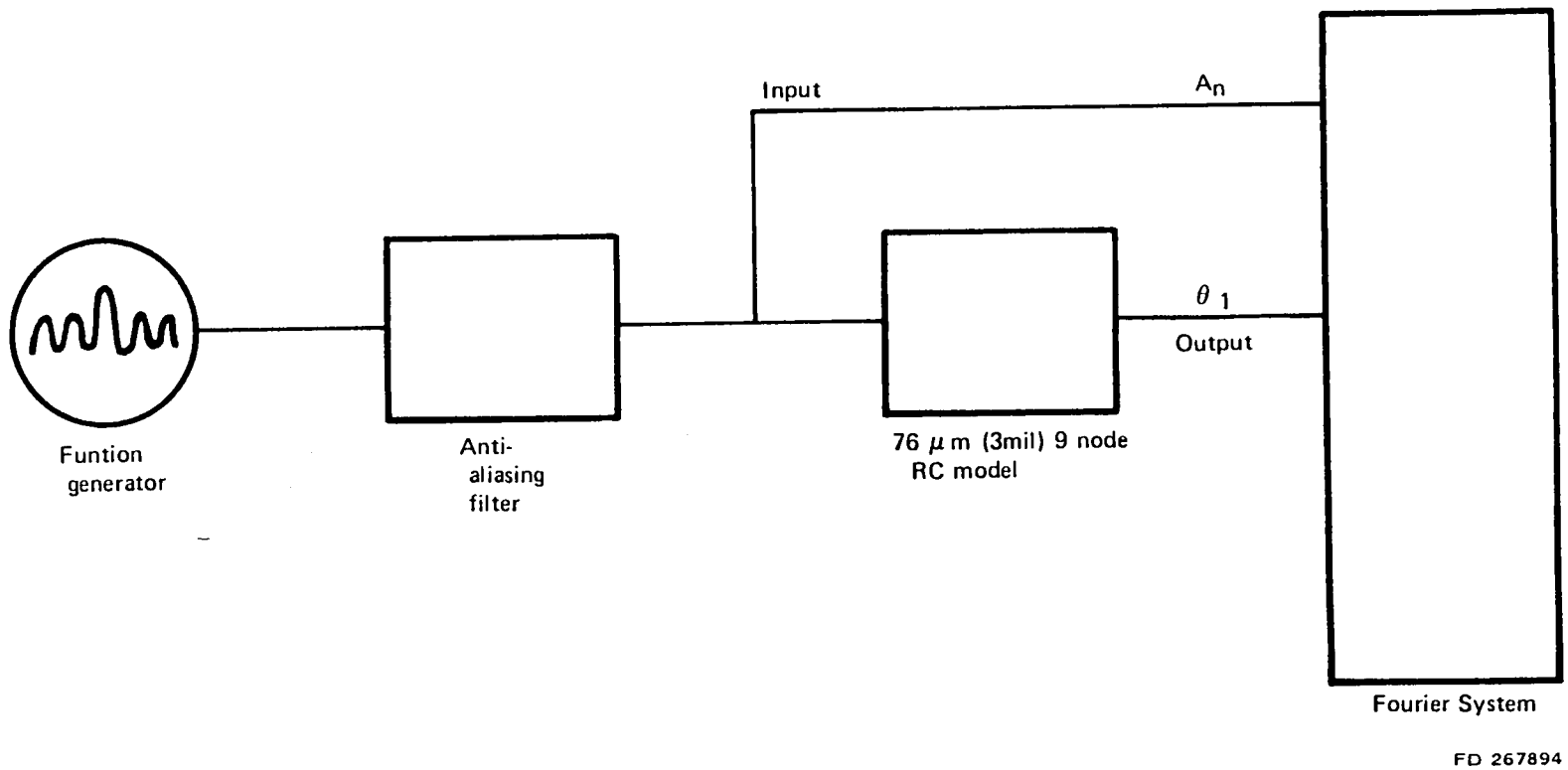

Figure 24. Evaluation of FFT Compensation Technique — Lab Setup

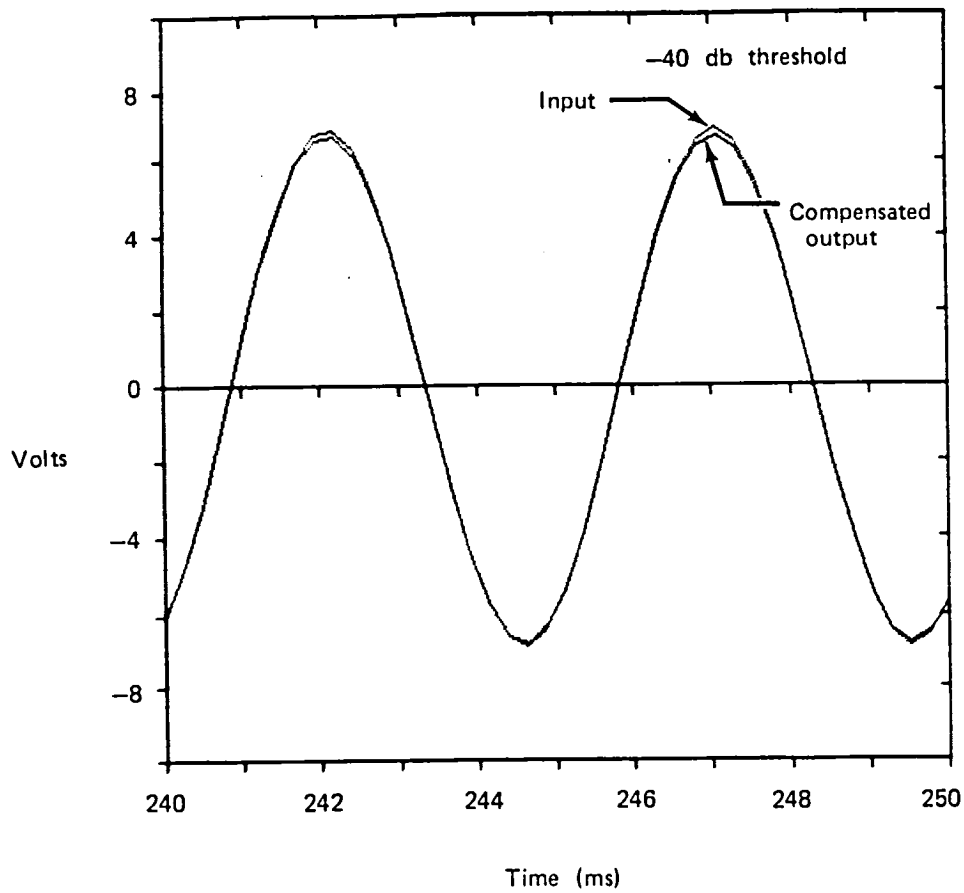

Figure 25. Evaluation of FFT Compensation Technique — Instantaneous Voltage vs Time: Measured Input to 76 μm (3 mil) Analog Circuit Compared With Compensated Output (≈ 1 KHz Sinewave)

$$\text{RMS} = \sqrt{\frac{\Sigma_0^{2047} (f(t))(f(t))}{2048}}$$

where:

2048 = the number of data points in the data record, and f(t) is the digitized time waveform of 2048 data points.

Tables VIII, IX, and X summarize the results. For time domain data, the error defined by RMS residue/RMS input is considered the most applicable because it includes error due to improper phasing.

TABLE VIII. AMPLITUDE ERROR IN COMPENSATED ENSEMBLE AVERAGED FREQUENCY SPECTRUM DUE TO COMPUTER FFT COMPENSATION TECHNIQUE

	4 Hz-200 Hz	*200 Hz-1000 Hz*
250 Hz BW random 64 avg's	PP−1.2%/+0.2%	—
1250 Hz BW random 64 avg's	−3.1%/+1.1%	−1.9%/+1.1%
20 Hz Sinewave 64 avg	−0.1%	—
200 Hz Sinewave 1 avg	−1.1%	—
1000 Hz Sinewave 1 avg	—	−2%

TABLE IX. AMPLITUDE AND PHASE ERRORS IN COMPENSATED INSTANTANEOUS* FREQUENCY SPECTRUM DUE TO COMPUTER FFT COMPENSATION TECHNIQUE

	4 Hz-200 Hz		*1 avg 200 Hz-1000 Hz*	
	Gain	*ϕ*	*Gain*	*ϕ*
250 Hz BW random −35 db	−5.7%/4.5%	−1.9°/2.1°	—	—
1250 Hz BW random −60 db	−8.6%/1%	−2.6°/3.0°	−19%/20%	−2.6°/3.0°
20 Hz Sinewave −40 db	0.4%	−0.4°	—	—
200 Hz Sinewave −40 db	−1.1%	−0.1°	—	—
1000 Hz Sinewave −40 db	—	—	−2%	0.1°

Large uncertainties in the random signals are due to very low signal levels at various frequencies within bandwidth

*Spectrum of compensated time waveform

TABLE X. AMPLITUDE ERROR IN COMPENSATED INSTANTANEOUS TIME WAVEFORM DUE TO COMPUTER COMPENSATION TECHNIQUE

	RMS Comp. / RMS Input	*RMS of Residue* / RMS Input*	*Max pk Residue / Max pk Input*
250 Hz BW Random −35 db	0.6%	4.4%	3.3%
1250 Hz BW Random −60 db	0.3%	10.6%	—
20 Hz Sinewave −40 db	0.3%	2.0%	3.6%
200 Hz Sinewave −40 db	1.0%	1.6%	2.8%
1000 Hz Sinewave −40 db	2.0%	2.5%	4.0%

Step input −50 db threshold: +10.5% overshoot with 2 ms lead and 2 ms lag

*Residue = input minus compensated output

Results in both the time and frequency domains for the discrete sinusoids are quite good as follows: <2.5% gain error and <0.4 deg phase error from 4 Hz to 1000 Hz.

Errors for the random signals are higher as would be expected due to the inherently poorer signal-to-noise ratio and, in the case of the time waveform, the accumulative nature of the gain and phase errors (i.e., the instantaneous waveform is the net summation of the amplitudes and phasing of all of its frequency components). The ensemble averaged frequency spectra of the random signals have less than ±3.1% gain error (4 Hz to 1000 Hz). The instantaneous time waveform error (RMS Residue/RMS input) was ±4.4% for the 250 Hz bandwidth and ±10.6% for the 1250 Hz bandwidth. Errors in the compensated time waveforms evaluated using the gain and phase errors in its instantaneous frequency spectrum ranged between −5.7% and +4.5% gain error and −1.9 deg to 2.1 deg phase error in the 250 Hz bandwidth and −19% to +20% gain error and −2.6 deg to +3.0 deg phase over the 1250 Hz bandwidth. The larger band of errors are due to the very poor signal to noise ratios at various frequencies within the instantaneous frequency spectrum (reference Figure 38).

The errors in the step function were predominately erroneous amplitude fluctuations thought to be associated with truncation of the frequency spectrum during the compensation process. With a −50 db threshold, there was a 10.5 percent overshoot in amplitude and a ±2 ms lead and lag time response. When the waveform was compensated over a higher frquency band (i.e., −70 db), the time response error decreased significantly. However, the amplitude of the erroneous oscillations increased. When a smooth curve is hand fit through the steady-state portion of the data (Figure 22), the results are significantly improved.

b. Evaluation of Errors in the Compensation Spectrum

To evaluate the error due to the measurement accuracy of the t/c element diameters, the theoretical transfer function between the large and small t/c's at $\Gamma = 1.0$ computed for the baseline conditions was used as the measured transfer function. Baseline conditions were the F100 probe with 76 μm (3.00 mil) and 250 μm (10.00 mil) t/c elements operating at:

T_T = 1200K (1700°F)
P_T = 2.0 x 10^6 N/m^2 (290 psia)
M_n = 0.23
F/A = 0.02

The compensation spectrum was computed for the baseline conditions ($\Gamma = 1.0$) and used as the correct spectrum. The finite model dimensions for the smaller wire were decreased by 1.7 ± 0.1% and the larger wire increased by 0.5%. Using the baseline measured transfer function, the in-situ value of Γ for the newly dimensioned model was obtained and the compensation spectrum computed. This spectrum was then compared to the baseline correct spectrum as above to yield the gain and phase errors. In the 4 Hz to 200 Hz frequency range, the maximum gain error was ±4.9% and the maximum phase error was ±1.3 deg. In the 200 Hz to 1K Hz range the maximum gain error was ±5.2% and ±0.8 deg.

Error in the measurement of the transfer function (H(f)) between the outputs of the two thermocouples will also influence the overall accuracy. The error in the transfer function measurement is described in terms of the coherence (measured in conjunction with the transfer function) and the number of averages taken as follows:

$$\epsilon_{Error} = \frac{(1 - \gamma^2)^{1/2}}{\gamma \sqrt{2N}}$$

where

γ^2 = coherence function
N = No. of ensemble averages.

For the F100 engine data processed under this contract, the measured coherence (γ^2) ranged from 0.9613 to 0.9767. The number of ensemble averages was 120. This yields a maximum error of ±1.3% in the measured transfer function. To assess the effect of an error in the measured transfer function, the compensation spectrum was determined with a +1.5% error introduced in the measured transfer function. The values of the "measured" baseline transfer function for the same F100 baseline model above were simply multiplied by 1.015. Using this modified data, the measured value of the Γ was determined and the corresponding compensation spectrum was generated and compared to the *correct* spectrum in the same manner as the other cases above. In the 4 Hz to 200 Hz range, the error was 3.3%. In the 200 Hz to 1000 Hz band the error was 3.5%.

To evaluate the error in the compensation spectrum when conduction effects are not included (i.e., if the t/c's were only modeled as first order), the F100 baseline model was run with the support wire diameters of the 76 μm (3 mil) and the 250 μm (10 mil) dimensioned the same as their element diameters (76 μm (3 mil) and 250 μm (10 mil), respectively). Again, the theoretical transfer function at Γ = 1.0 for the baseline F100 model was used as the measured transfer function and the in-situ value of Γ for the dimensionally modified case was determined and the corresponding compensation spectrum was generated. Figure 40 shows the gain error (using the baseline F100 probe model as reference) as a function of frequency. The errors are typically +20 to +25% over the entire bandwidth (1000 Hz).

c. Overall Accuracy

The overall accuracy was determined by root sum squaring (RSS) the errors associated with the computer FFT compensation technique, T/C element diameter measurement, measurement of the transfer function between the large and small diameter t/c (H(f)), and the data acquisition/reproduce system noise. The contract accuracy goal was ±5% in the 4 Hz to 200 Hz bandwidth and ±10% in the 200 Hz to 1000 Hz bandwidth (for 1000K p-p sinewave).

Table XI shows the errors associated with the compensated average frequency spectrum and Table XII the compensated instantaneous time waveform. The most accurate results are obtained for the compensated averaged frequency spectrum. This is because averaging reduces errors associated with poor SNR. Additionally, the gain and phase errors associated with each frequency component are accumulative in the time waveform but are not in the frequency spectrum.

TABLE XI. OVERALL ERROR — AVERAGED FREQUENCY SPECTRUM

	Error Due to Data System SNR	*Error Due to FFT Compensation Technique*	* *Error (DIA'S)*	** *Error (H(f))*	*Total Error (RSS)*
1000K (1800°F) p-p at 200 Hz	<0.1%	1.1%	4.9%	3.3%	6.0%
1000K (1800°F) p-p at 1000 Hz	<0.1%	2.0%	5.2%	3.5%	6.6%
≃ 15K (27°F) p-p/ $\sqrt{\text{Hz}}$ 4 Hz to 200 Hz	0.7%	1.2%	4.9%	3.3%	6.1%
≃ 15K (27°F) p-p/ $\sqrt{\text{Hz}}$ 200 Hz to 1000 Hz	3.8%	1.9%	5.2%	3.5%	7.6%
≃ 6.7K (12°F) p-p/spectral line at 200 Hz	2.2%	1.2%	4.9%	3.3%	6.4%
≃ 6.7K (12°F) p-p/spectral line at 1000 Hz	10.0%	1.9%	5.2%	3.5%	12.0%

* Error due to perturbation of measurement error in t/c diameters
** Error due to perturbation of measurement error in H(f)

TABLE XII. OVERALL ERROR — INSTANTANEOUS TIME WAVEFORM

	Error Due to Data System SNR	**Error Due to FFT Compensation Technique*	** *Error (DIA'S)*	*** *Error (H(f))*	*Total Error (RSS)*
1000K (1800°F) p-p at 200 Hz	<0.1%	1.6%	4.9%	3.3%	6.1%
1000K (1800°F) p-p at 1000 Hz	<0.1%	2.5%	5.2%	3.5%	6.7%
≃ 15K (27°F) p-p/ $\sqrt{\text{Hz}}$ 4 Hz to 200 Hz	0.7%	4.4%	4.9%	3.3%	7.4%
≃ 15K (27°F) p-p/ $\sqrt{\text{Hz}}$ 200 Hz to 1000 Hz	3.8%	10.6%	5.2%	3.5%	12.9%
≃ 6.7K (12°F) p-p/spectral line 4 Hz to 200 Hz	2.2%	4.4%	4.9%	3.3%	7.7%
≃ 6.7K (12°F) p-p/spectral line 200 Hz to 1000 Hz	10.0%	10.6%	5.2%	3.5%	15.9%

* $\dfrac{\text{RMS residule}}{\text{RMS input}} \times 100\%$

** Error due to perturbation of measurement error in t/c diameters
*** Error due to perturbation of measurement error in H(f)

For the averaged frequency spectrum, the error of 1000K (1800°F) p-p sinusoids in the 4 Hz to 200 Hz bandwidth was ±6.0% and ±6.6% in the 200 Hz to 1000 Hz bandwidth. For ≈15K (27°F) p-p/ $\sqrt{\text{Hz}}$ random noise with a bandwidth of 4 Hz to 200 Hz, the error was ±6.1% and in the 200 Hz to 1000 Hz bandwidth it was ±7.6%.

For the instantaneous time waveform, the overall error was ±6.1% for 1000K (1800°F) p-p sinusoids in the 4 Hz to 200 Hz bandwidth and ±6.7% in the 200 Hz to 1000 Hz bandwidth. The error for a 15K (27°F) p-p/ $\sqrt{\text{Hz}}$ random signal was ±7.4% for a 4 Hz to 250 Hz bandwidth and ±12.9% for a 250 Hz to 1000 Hz bandwidth.

d. Analog Simulation of Dual Wire Thermocouples

Equations were derived (Appendix E) for the electrical analog equivalent, passive RC network of the nine node finite element thermocouple model for use in lab evaluations of the dual t/c approach. Two breadboard nine node RC element network models, one for the 76 μm (3 mil) and one for the 250 μm (10 mil) thermocouple were fabricated. The circuits were modeled for the F100 probe geometry operating at the following conditions:

T_T = 1200K (1700°F)
P_T = 2.0 x 10^6 N/m^2 (290 psia)
M_n = 0.22
F/A = 0.02.

Design values of resistance and capacitance for these simulators are shown in Figure 26. Potentiometers were used for the resistive components and values were set by measurement with a digital ohmmeter ($\approx \pm 1\%$). Values of capacitive components were combinations of standard value capacitors ($\pm 10\%$) and were not measured. Schedule constraints precluded obtaining more precise capacitance values.

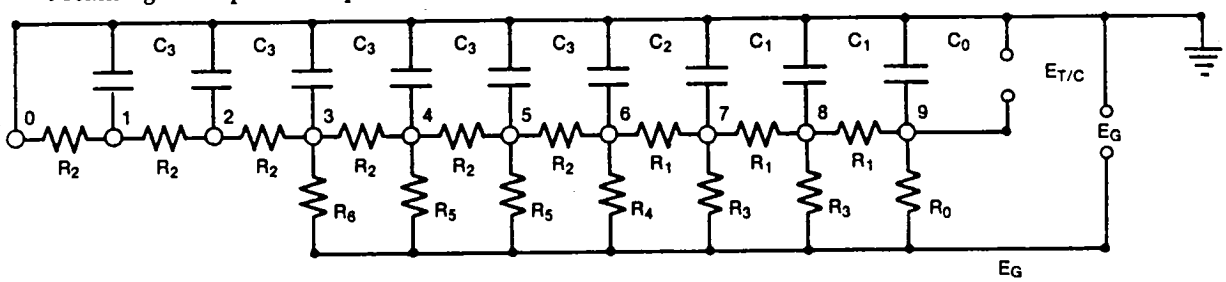

Thermocouple element diameter

Where:	76μm	254μm
R_0	7592 Ω	46.2 KΩ
R_1	1739 Ω	11.8 KΩ
R_2	217.4 Ω	5.66 KΩ
R_3	3796 Ω	23.11 KΩ
R_4	1049 Ω	12.447 KΩ
R_5	543.5 Ω	8.515 KΩ
R_6	1087 Ω	17.031 KΩ
C_0	0.5 μfd	0.5 μfd
C_1	1.0 μfd	1.0 μfd
C_2	2.45 μfd	4.34 μfd
C_3	78 μfd	7.67 μfd

Note: Values listed Correspond to F100 Probe operating at:
T_T = 1200K (1700°F)
P_T = 2.0 × 10^6N/m^2 (290 psia)
M_N = 0.22
F/A = 0.02

FD 267195

Figure 26. RC Analog Network Simulation — Full-Scale Test Conditions

The purpose of this test was to determine the compensation spectrum (gain and phase as a function of frequency) of the 76 μm (3 mil) analog circuit (and the 250 μm analog circuit) from the measured transfer function taken between the outputs of the analog circuits of the 76 μm (3 mil) t/c and the 250 μm (10 mil) circuit (Figure 27) utilizing the DGTMS software and compare it with the known frequency response spectrum (measured single input — single output using conventional FFT techniques). Wideband (1250 Hz BW) random noise was utilized in these measurements. Because of the lack of precision in the analog circuit components, thermocouple length and diameter values input to the HOST program compensation software were varied until best agreement between the DGTMS program results and the known compensation spectra were obtained. The conventionally measured spectra were generated by

measuring the transfer function between the input and output of the analog circuit using a 256 ensemble averaged FFT transfer function:

$$H(f) = \text{Gain} \angle \text{phase}\ (f) = \frac{G_{12}(f)}{G_{11}}$$

Note that the obvious errors in the conventional measurement above ≃1400 Hz (Figure 28) are due to poor signal-to-noise ratio intentionally introduced to prevent aliasing via an anti-aliasing filter.

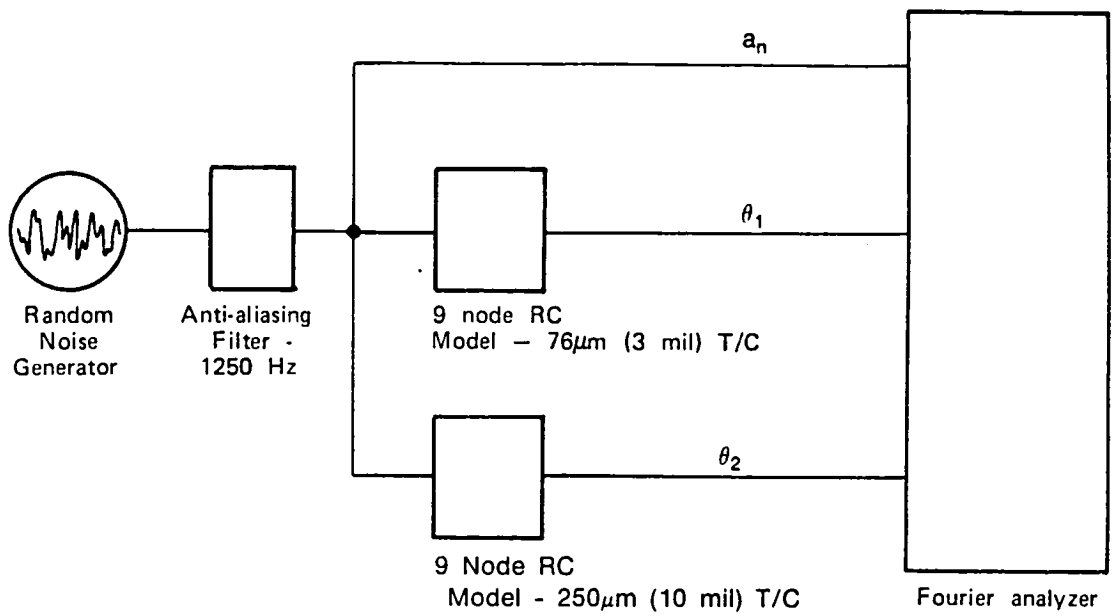

- RC networks model'd as F100 probe
  1200K (1700°F)
  $2.0 \times 10^6 N/m^2$ ATMS (290 PSIA)
  Mn 0.22
  F/A 0.02
- Resistive Components ≃ ± 1% (measured)
- Capacitive Components ≃ ± 10% (not measured)

FD 267196

Figure 27. Simulation of Dual Wire Thermocouples — Lab Setup

The best match for the 76 μm (3 mil) t/c was obtained when it was modeled with an element diameter of 75 μm (2.9 mils) and an element length of 711 μm (28.0 mils). The analog circuits were designed to model the t/c as 76 μm (3.00 mils) diameter with a length of 610 μm (24.0 mils). Gain match was within ±15% and phase match within +4.2 to −0.8 deg over the frequency range of 4 Hz to 1000 Hz (Figure 29).

Similarly, for the 250 μm (0.010 in.) thermocouple case, the following parameters produced the best match of compensation spectra: the diameter was 260 μm (10.3 mils) and the length was 1588 μm (62.5 mils) as opposed to design values of diameter equal to 250 μm (10 mils) and length equal to 1588 μm (62.5 mils). Gain disagreement for this case was less than ±5% out to 100 Hz (Figure 28). The compensation program developed under this contract uses the 250 μm (10 mil) data only out to about 40 Hz. The agreement between the two methods is satisfactory, despite lack of precision in the capacitance values in the analog model.

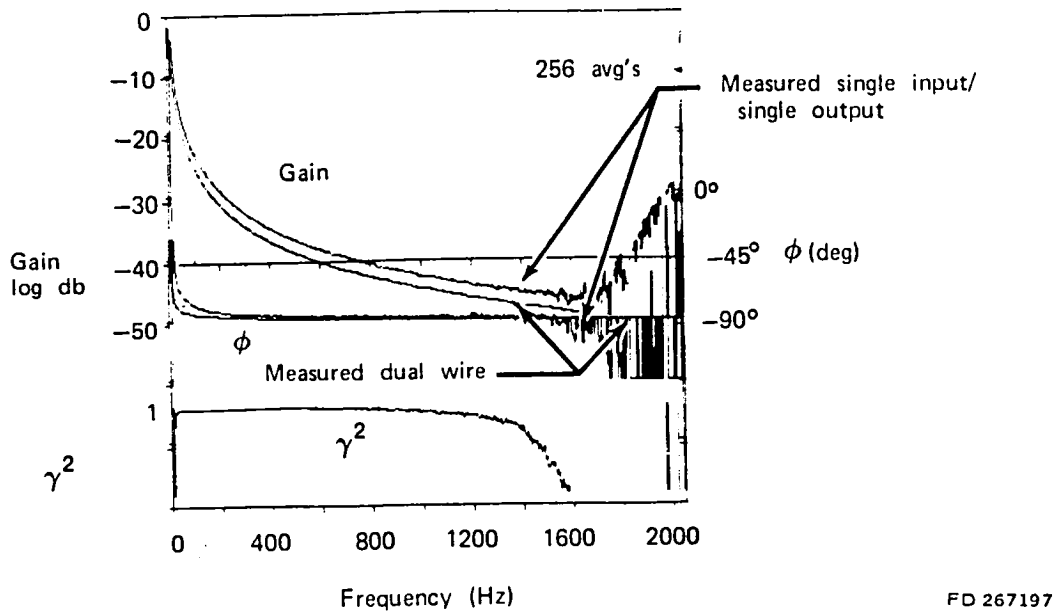

Figure 28. Comparison of 250 μm (10 mil) Experimentally Derived Compensation Spectrum With Measured Single Input/Single Output Compensation Spectrum

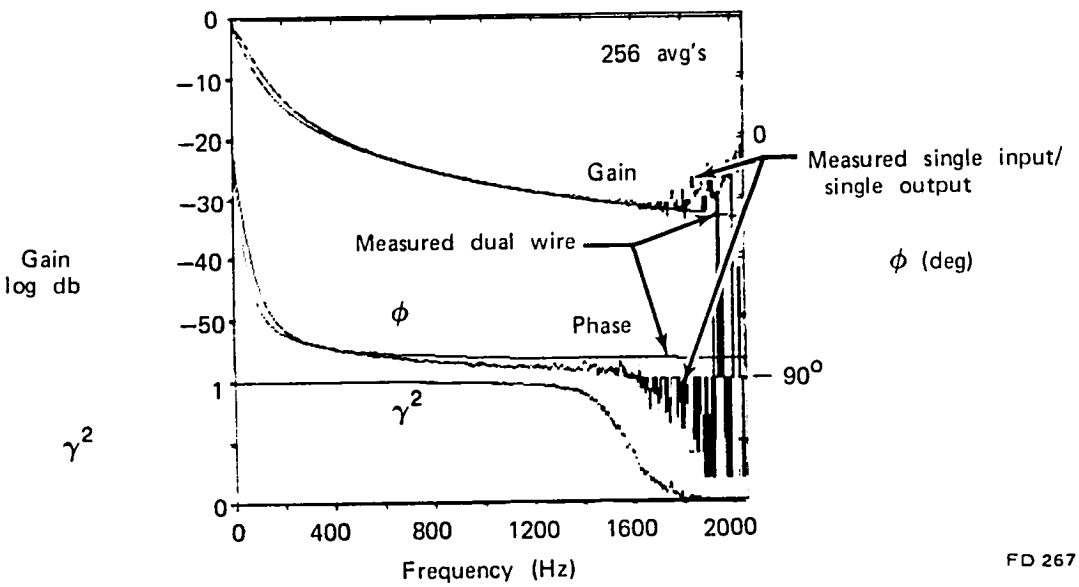

Figure 29. Comparison of 76 μm (3 mil) Experimentally Derived Compensation Spectrum With Measured Single Input/Single Output Compensation Spectrum

Experiments performed with the analog circuits verified that the finite-element models of the thermocouples work as required. Minor discrepancies, due to lack of precision in electrical component values, could easily be corrected, given adequate time and resources.

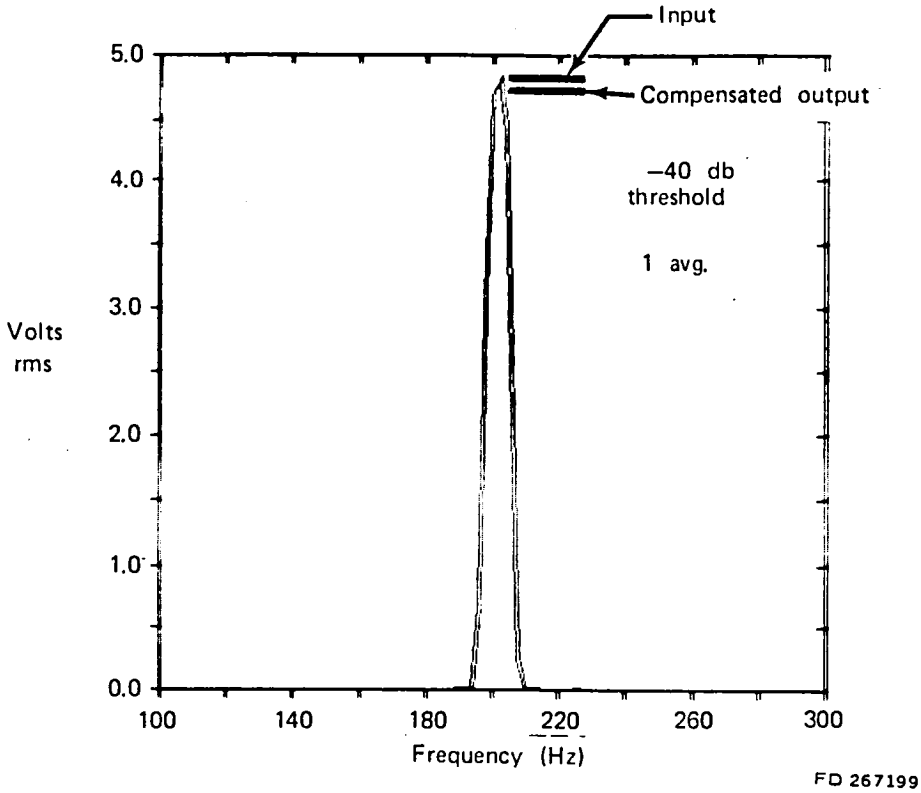

Figure 30. Evaluation of FFT Compensation Technique — Narrowband Frequency Spectra: Measured Input to 76 μm (3 mil) Analog Circuit with Compensated Output (≈ 200 Hz Sinewave)

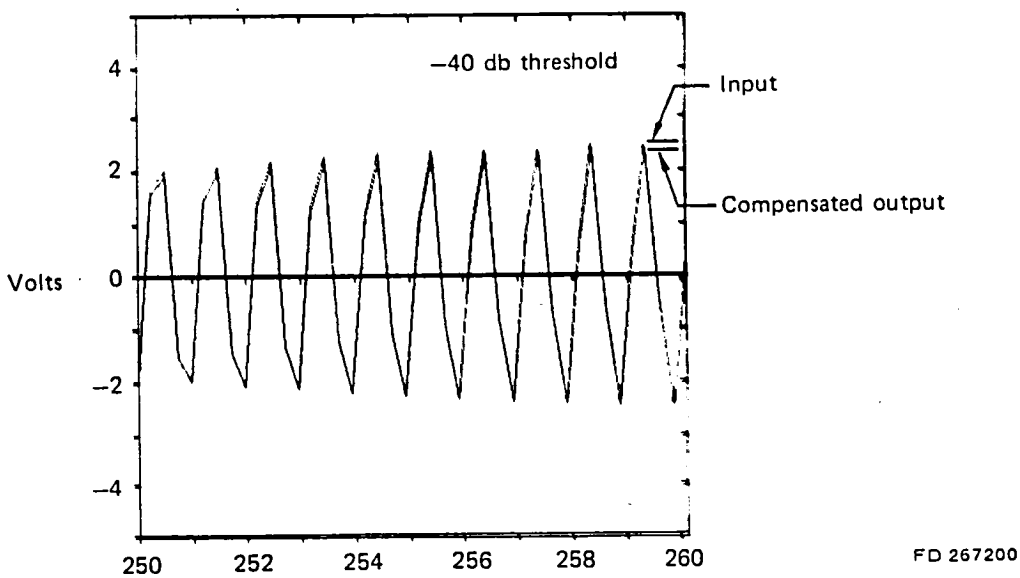

Figure 31. Evaluation of FFT Compensation Technique — Instantaneous Voltage vs Time: Measured Input to 76 μm (3 mil) Analog Circuit Compared with Compensated Output (≈1 K Hz Sinewave)

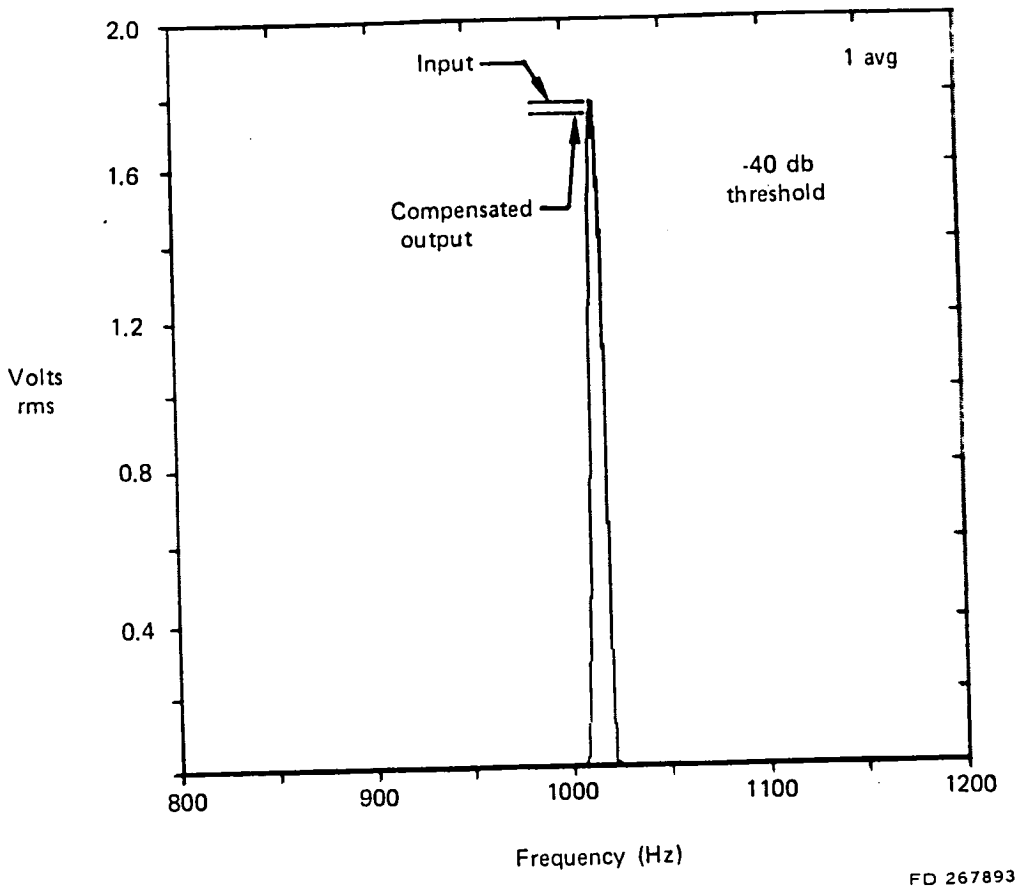

Figure 32. Evaluation of FFT Compensation Technique — Narrowband Frequency Spectra: Measured Input to 76 μm (3 mil) Analog Circuit Compared with Compensated Output (≈1 K Hz Sinewave)

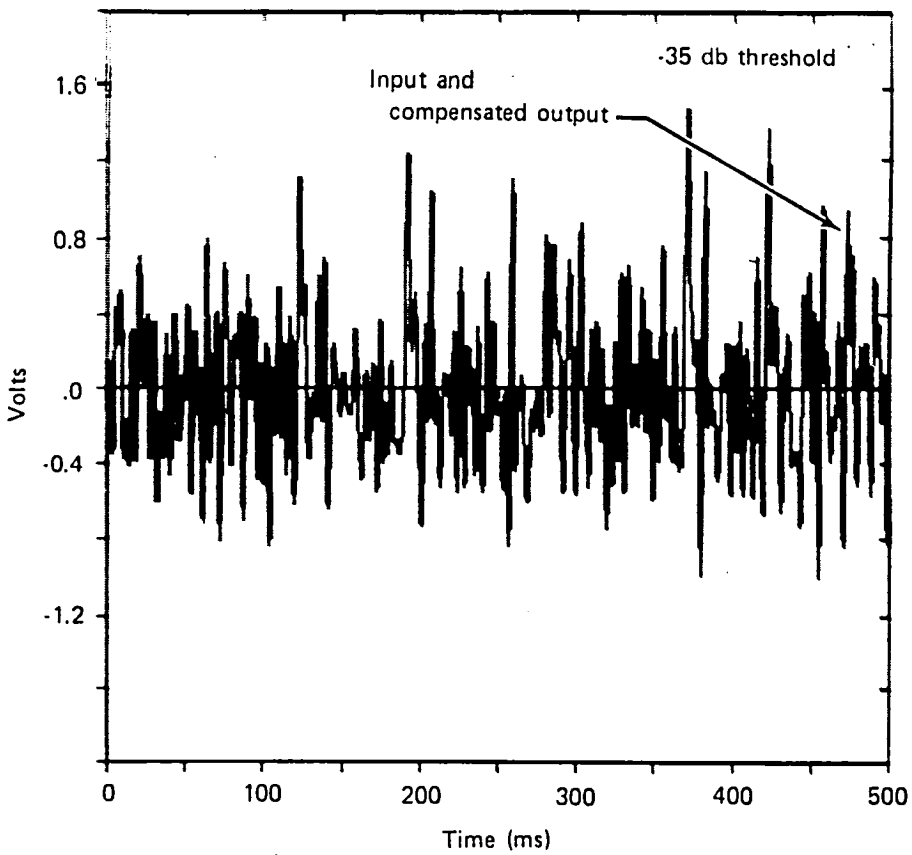

Figure 33. Evaluation of FFT Compensation Technique — Instantaneous Voltage vs Time: Measured Input to 76 μm (3 mil) Analog Circuit Compared with Compensated Output (250 Hz Bandwidth Random Noise)

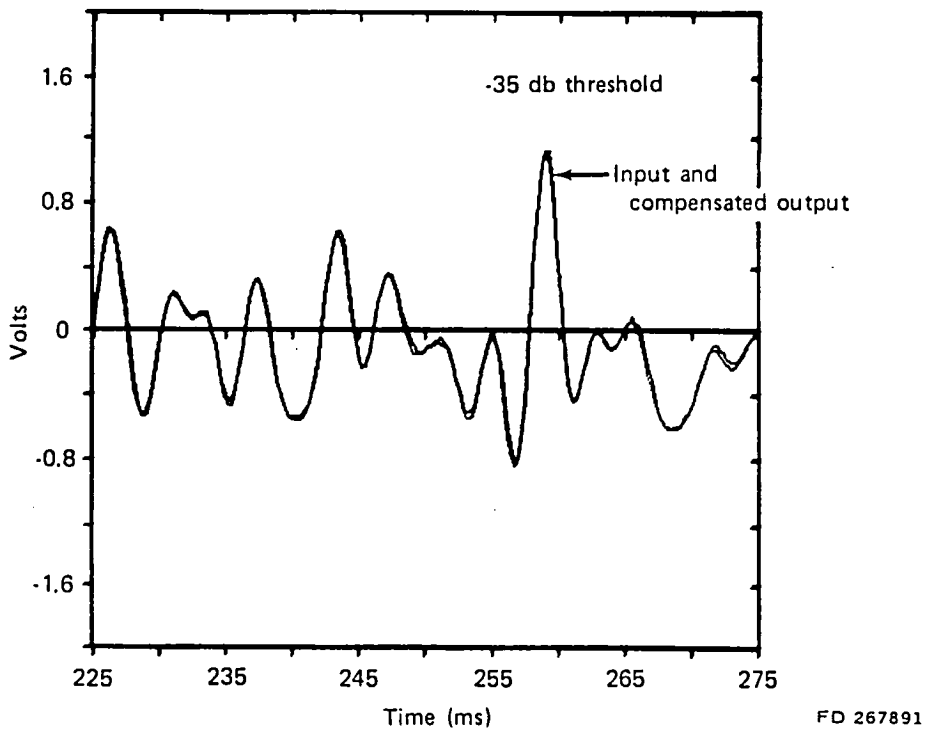

Figure 34. Evaluation of FFT Compensation Technique — Expanded Time Segment From Figure No. 33.

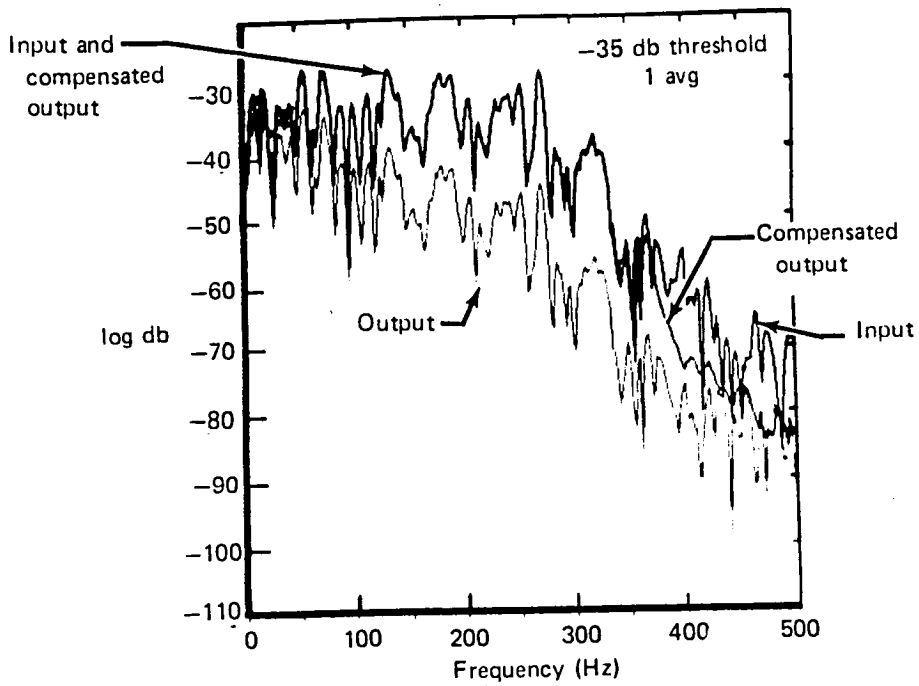

Figure 35. Evaluation of FFT Compensation Technique — Instantaneous Power Spectral Density Plots of 76 μm (3 mil) Analog Circuit Compensated Output, Measured Input and Measured Output (250 Hz Bandwidth Random Noise)

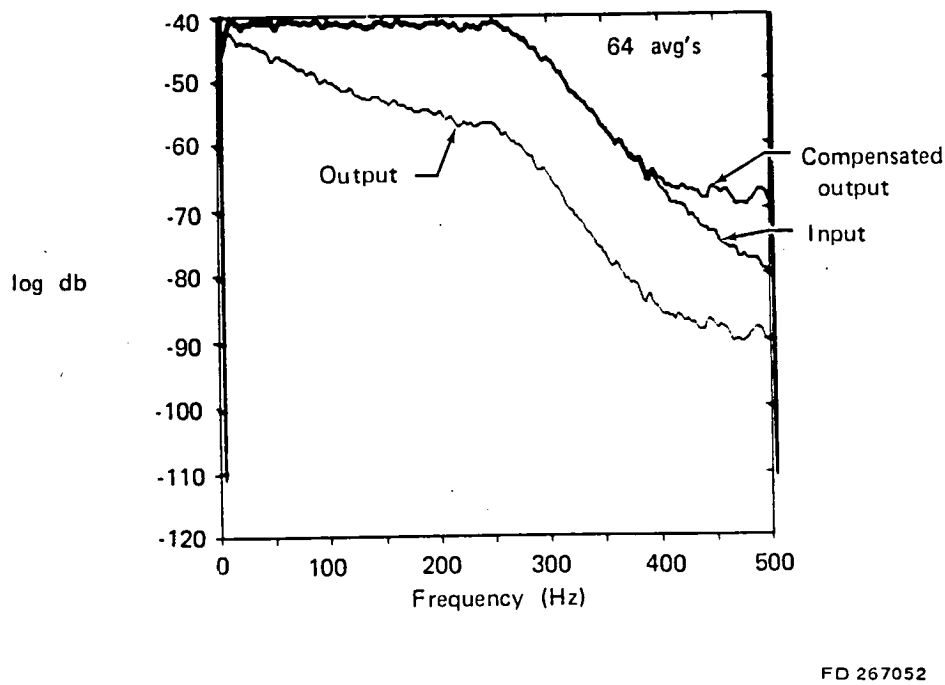

Figure 36. Evaluation of FFT Compensation Technique — Power Spectral Density Plots of 76 μm (3 mil) Analog Circuit Compensated Output, Measured Input and Measured Output (250 Hz Bandwidth Random Noise)

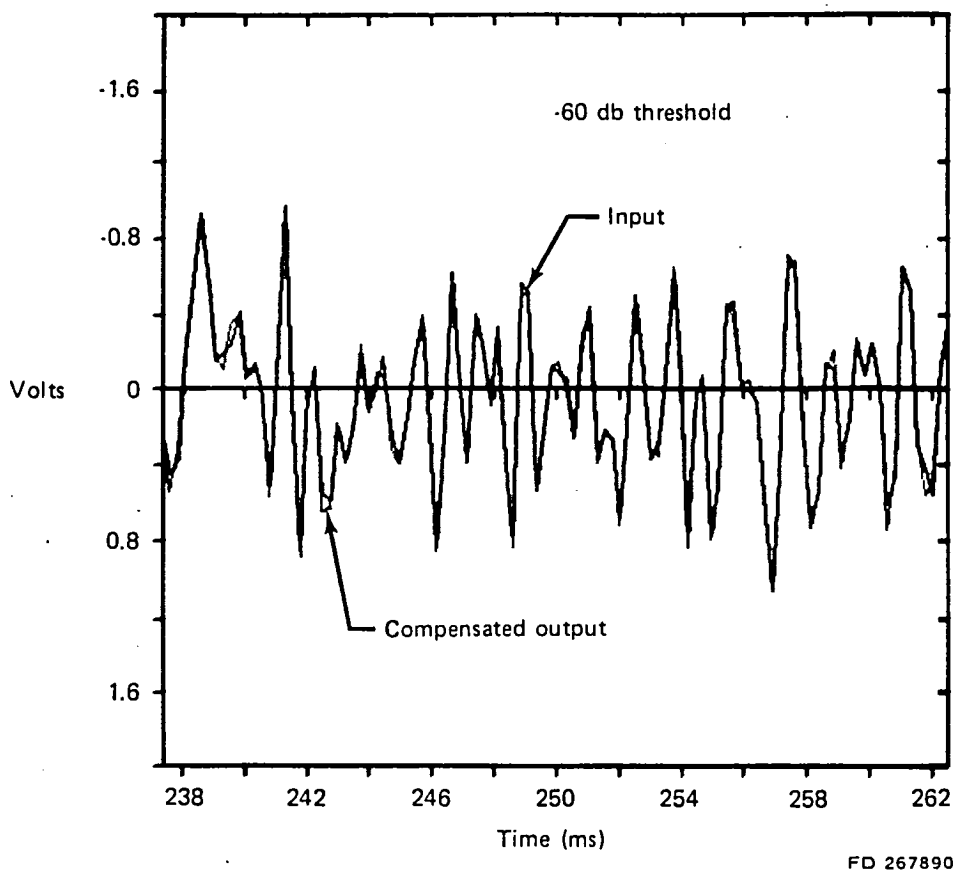

Figure 37. Evaluation of FFT Compensation Techniaue — Instantaneous Voltage vs Time: Measured Input to 76 μm (3 mil) Analog Circuit Compared with Compensated Output (1250 Hz Bandwidth Random Noise)

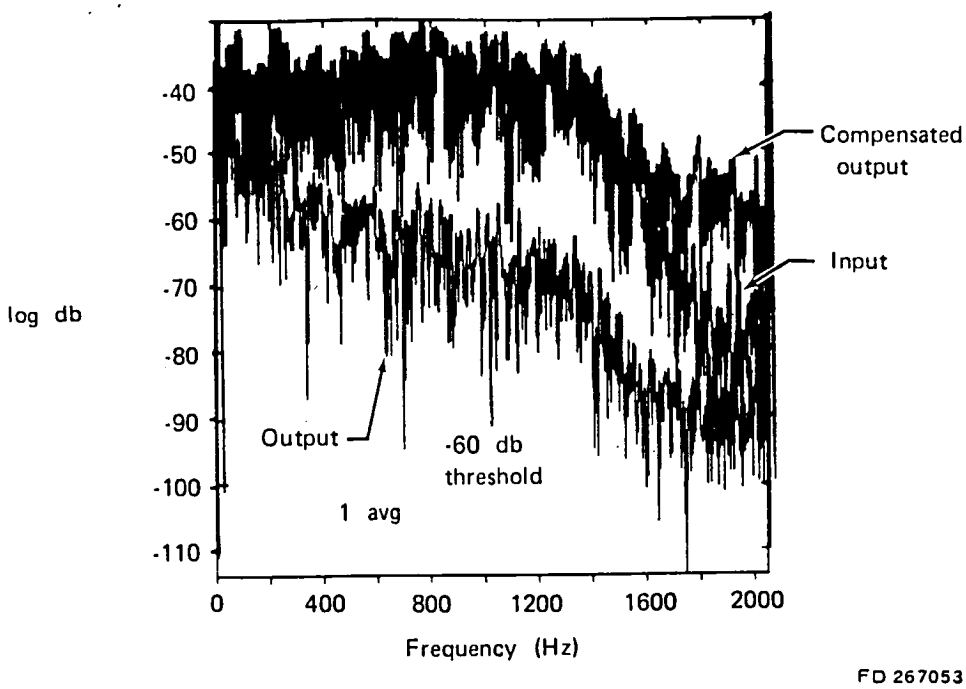

Figure 38. Evaluation of FFT Compensation Technique — Instantaneous Power Spectral Density Plots of 76 μm (3 mil) Analog Circuit Compensated Output, Measured Input and Measured Output (1250 Hz Bandwidth Random Noise)

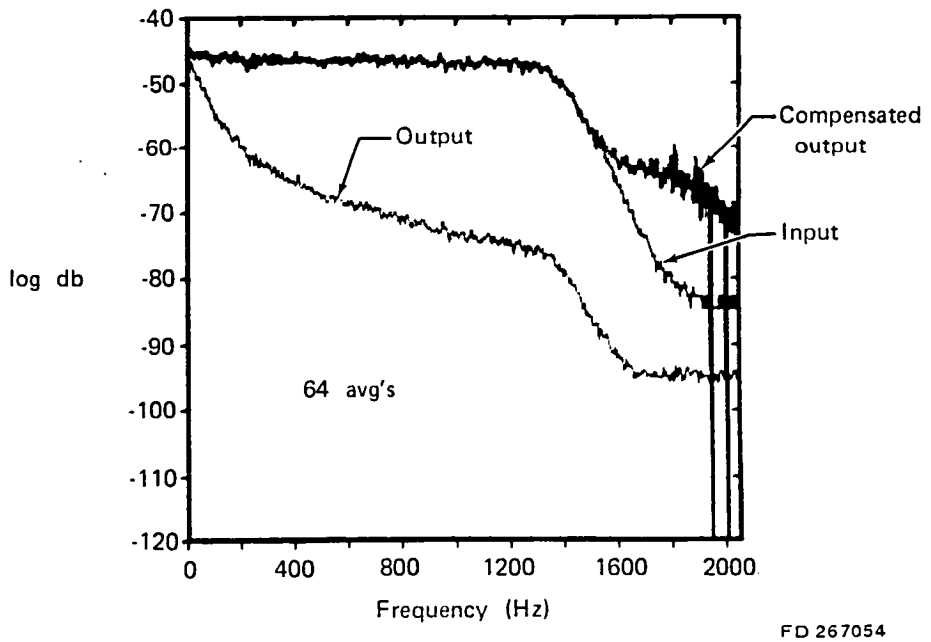

Figure 39. Evaluation of FFT Compensation Technique — Power Spectral Density Plots of 76 μm (3 mil) Analog Circuit Compensated Output, Measured Input and Measured Output (1250 Hz Bandwidth Random Noise)

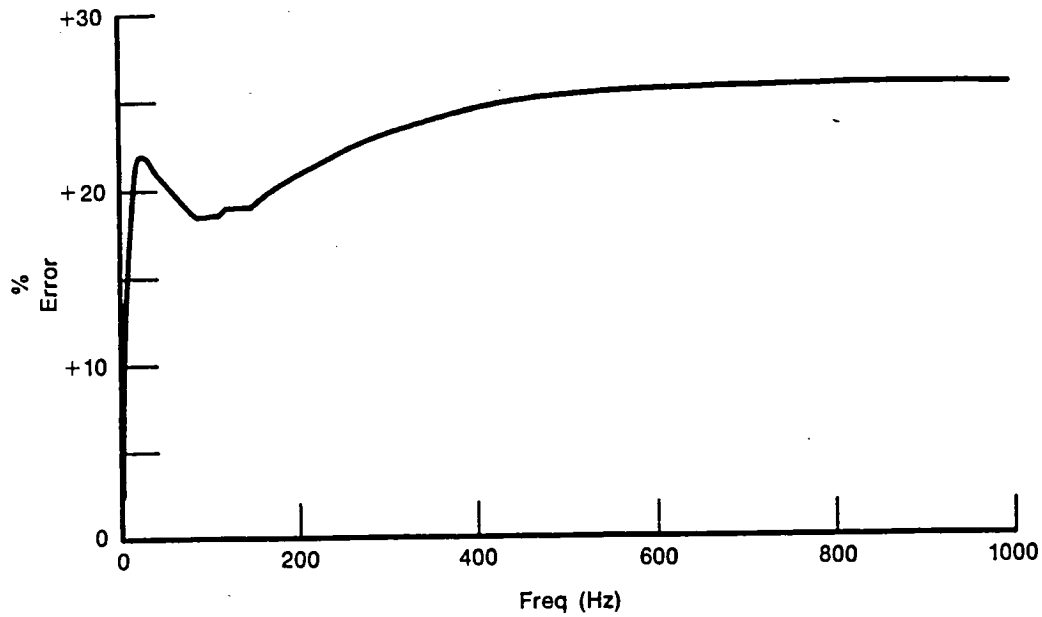

Figure 40. Gain Error in Compensation Spectrum Due to Neglect of Conduction Effects (F100 Engine Probe)

e. System Shakedown

For the system shakedown, an F100 probe was used with an on-line data acquisition and analysis system setup configuration. The setup was made as shown in Figures 8 through 10. However, the FM tape recorder/reproducer was not used. A Cadillac model 1000B flameless torch was used to heat the thermocouples. This test was used primarily to checkout the data acquisition portions of the system. The flameless torch only produced measurable temperature fluctuations to about 30 Hz. The system successfully acquired the data and computed the measured transfer function between the outputs of the two thermocouples.

In the shakedown configuration, the amplifier output signals were found to have excessive (200 to 300 MV p-p at X1000 gain) 60 Hz noise. Additionally, any motion of the cabling between the AC coupler output and the amplifier input was found to generate excessive noise. The noise levels were reduced to acceptable levels (approximately 25 MV p-p at 60 Hz with a gain of 1000) by increasing the value of the coupling capacitors from 0.018 μ farad to 1.0 μ farad and lowering the input impedance of the amplifiers to approximately 100K ohms. The lower input impedance was obtained by connecting 100K ohm resistors between input high and guard, and input low and guard. Additionally, the coupling capacitors were mounted directly on the amplifier input connectors to minimize noise generated by the input cable. The final configuration is shown in Figure 8.

5. Subscale Combustor Tests

The subscale combustor tests were conducted without incident and the test data were obtained with one probe.

The probe was installed and tested (see Figure 41) in the subscale combustor rig as discussed on Task 4. The probe and a platinum tube used for measuring gas stream total pressure were mounted downstream of the combustor exit plane. The mounting system was retractable so the probe was not in the gas stream except when data was recorded.

TABLE XIII. SUBSCALE COMBUSTOR TEST CONDITIONS

Test Point	P_s/P_t	*Mach No.*	*Velocity M/S (Ft/s)*	T_{TOTAL}* *K(°R)*
1	0.968	0.22	104 (340)	1050 (1890)
2	0.965	0.23	113 (370)	1160 (2090)
3	0.966	0.23	116 (380)	1220 (2200)
4	0.965	0.23	119 (390)	1280 (2310)
5	0.965	0.23	122 (400)	1330 (2400)
6	0.965	0.23	122 (400)	1390 (2500)
7	0.966	0.23	125 (410)	1450 (2610)
8	0.966	0.23	128 (420)	1510 (2720)
9	0.969	0.22	125 (410)	1570 (2820)
10	0.967	0.23	131 (430)	1800 (3240)

$P_{AMB} = 1.014 \times 10^{+5}$ N/M^2 (1.001 ATMS)
*Estimated

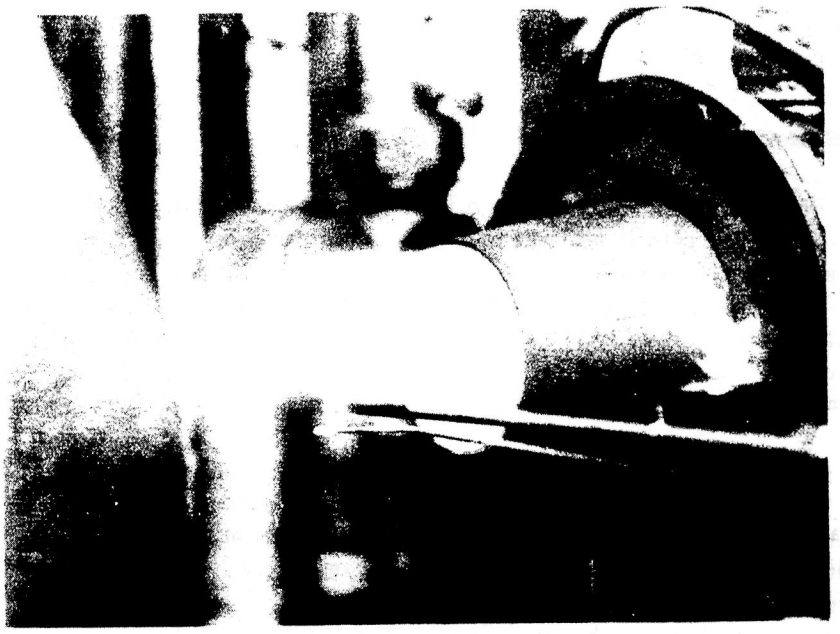

FD 267056

Figure 41. Subscale Combustor Tests — Probe Installed in MMT Burner

Dynamic temperature data and ambient temperature data were recorded on FM tape per the data acquisition system discussed in Task 4. The output of each amplifier was *double recorded* on the FM tape recorder (0.5V rms and 1.0V rms full-scale record level channels). The signal levels were monitored on an oscilloscope and the *fixed* gain setting(s) of the amplifier(s) were set as necessary to maintain optimum signal levels on the 0.5V rms record channel. Gain settings were correlated with test points to maintain calibration. The 1.0V rms channels were recorded precautionary in case the 0.5V rms channels were overdriven. Data was recorded at ten steady-state combustor test conditions ranging from the minimum to maximum conditions obtainable with the combustor facility. The final combustor and probe test conditions are summarized in Table XIII. Average gas temperatures varied from 1050K (1890°R) to 1800K (3240°R). The gas stream Mach number and total pressure was relatively constant at 0.23 and 1.0 atms, respectively.

6. Full-Scale F100 Engine Tests

The full-scale tests were conducted as planned in an F100 jet engine which was undergoing testing at P&WA's Government Products Division (GPD) test facility. Dynamic temperature data were recorded at 15 engine test conditions shown in Table XIV. Two element data were recorded at the first six test points; at this point, the small element failed. Data were recorded for the larger element on the remaining test conditions.

TABLE XIV. F100 TEST CONDITIONS

Test Point	*FTIT K(°F)*	P_{T4} *N/M² × 10⁵ (psia)*	T_{T4} *(PRED) K(°F)*	T_{PROBE} *K(°F)*
1	770 (920)	84.1 (83)	1080 (1490)	970 (1290)
2	820 (1020)	112 (110)	1130 (1580)	1060 (1450)
3	860 (1080)	128 (126)	1190 (1690)	1110 (1530)
4	890 (1140)	145 (143)	1230 (1760)	1170 (1640)
5	930 (1210)	160 (158)	1280 (1850)	1230 (1750)
6*	960 (1260)	175 (173)	1320 (1920)	1270 (1830)
7	990 (1330)	196 (193)	1380 (2030)	1310 (1900)
—	—	—	—	—
—	—	—	—	—
—	—	—	—	—
—	—	—	—	—
15	1220 (1740)	313 (309)	1710 (2620)	1570 (2370)

Probe $M_m \approx 0.36 \rightarrow$ Vel = 160 M/S (510 ft/sec)

*76 μm (0.003 in.) element failed

The F100 type probe was installed, as previously detailed in Figure 5 of Task 4. The test program was completed with dynamic temperature data being recorded on FM taper per the data acquisition system discussed in Task 4. Fifteen steady-state engine conditions or power settings (see Table XIV) from idle to intermediate power were run and recorded. Ambient (engine not running) data were also recorded to establish the system noise characteristics.

Dynamic temperature data for the probe's two elements were recorded on the first six test conditions, at this point the smaller 76 μm (0.003 in.) element failed. The test condition at this time corresponded to an average gas temperature of 1270K (1830°F) and a pressure of 11.77 atms (173 psia). Dynamic temperature data were then recorded on the remaining larger

250 μm (0.010 in.) element to the maximum gas temperature of 1570K (2370°F) and pressure of 21.03 atms (309 psia).

Post-test inspection of the probe elements later confirmed that the smaller 76 μm (0.003 in.) element had failed and this was attributed to bombardment from solid particles in the gas stream.

7. Post-Test Inspection

Microscopic inspections were made on the subscale and F100 probes that were tested. Photomicrographs were made and used to measure the probe element dimensions. The results of these inspections revealed a very small amount of erosion on both probes and confirmed that the 76 μm (0.003 in.) element on the F100 probe had failed and was missing.

Figure 42 shows a magnified view of the subscale combustor probe after testing. The surface of the elements shown corresponds to the side presented to the gas flow and shows an increased surface roughness. Closer inspection revealed this was a very thin buildup layer only on the upstream gas side of the probe. This buildup layer did not affect the element dimensions.

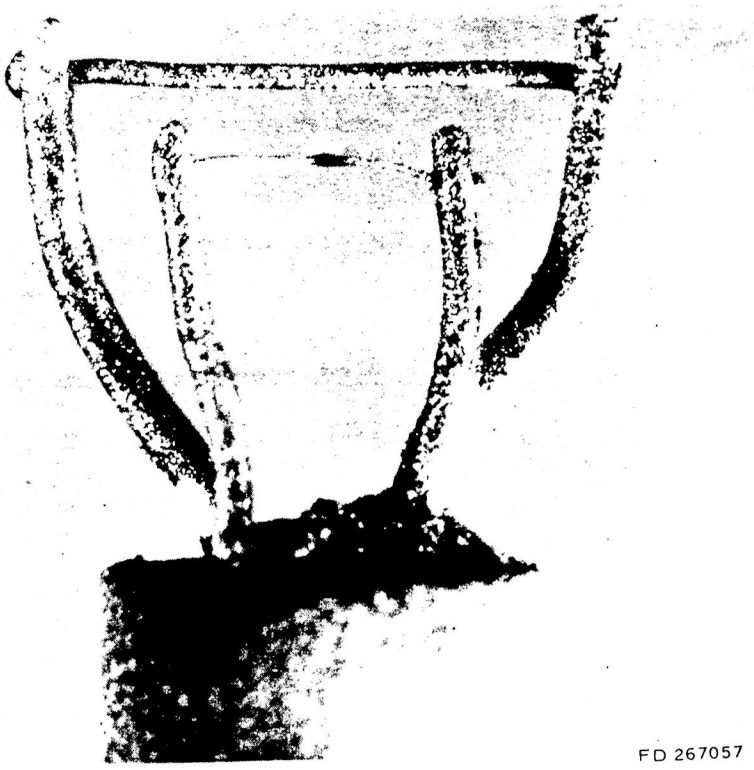

Figure 42. Subscale Combustor Probe — Post-Test Inspection

Figures 43 through 46 show various magnified views of the F100 probe after testing. Inspections of the photographs shows that the 76 μm (0.003 in.) element is missing. It broke at each support wire and it is assumed this was due to bombardment from solid particles in the gas stream or excessive aerodynamic loading. Failure of the 76 μm (0.003 in.) element occurred at the intersection of the support wires and the element which corresponds to the maximum stress location. Additionally, the support wires have been bent in the direction of the flow. This is attributed to excessive bending stresses from aerodynamic loading and the longer length of the

support wires caused by the erosion of the ceramic cement used to pot around the support wires and the holes in the ceramic stick (shown in Figure 46). The 250 μm (0.010 in. element) was also bent due to the additional loading from the 76 μm (0.003 in.) element support wires.

The probe dimensions were determined by measuring the photomicrographs taken of the various probe structures. Table XV summarizes the pre-and post-test dimensions of both probes. The dimensions of the 76 μm (0.003 in.) and 250 μm (0.010 in.) elements reveal that there was a slight indication of a reduction 0.5 μm (0.00002 in.) after testing. However, this amount of reduction is within the measurement accuracy and is therefore questionable.

FD 267058

Figure 43. F100 Probe Post-Test Inspection — Front View

TABLE XV. PRE- AND POST-TEST PROBE INSPECTION SUMMARY

	Diameter, μm (Inches)			
	Subscale Combustor Probe		*F100 Probe*	
Item	*Pre*	*Post*	*Pre*	*Post*
76 μm Junction (0.003 in.)	74 (0.0029)	74 (0.0029)	78 (0.0030)	— (—)
250 μm Junction (0.010 in.)	250 (0.0099)	250 (0.0098)	260 (0.0102)	250 (0.0100)
380 μm Support (0.015 in.)	380 (0.0150)	380 (0.0150)	380 (0.0150)	380 (0.0148)
510 μm Support (0.020 in.)	510 (0.0200)	510 (0.0200)	510 (0.0200)	510 (0.0200)

FD 267059

Figure 44. F100 Probe Post-Test Inspection — 3/4 View

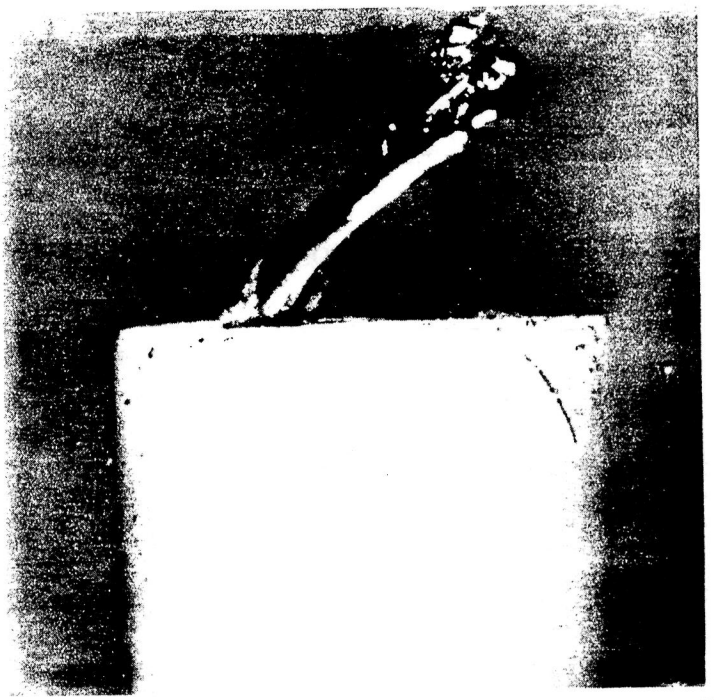

FD 267060

Figure 45. F100 Probe Post-Test Inspection — Side View

FD 267062

Figure 46. F100 Probe Post-Test Inspection — Top View

E. TASK 6 — ANALYSIS OF RESULTS

1. General

Test data were obtained for probes installed in a subscale combustor rig and an F100 engine. Two events were processed from each: an ambient point to establish the background noise and the test point. All test data were recorded on FM tape. The data point processed from the subscale combustor rig was the point of maximum operating temperature. The F100 data point was the highest temperature point prior to failure of the 76 μm (3 mil) thermocouple element. The as built dimensions of the probe elements were measured utilizing an optical microscope and these dimensions were used with the program software.

One hundred and twenty data records were ensemble averaged to compute the measured transfer function between the outputs of the 76 μm and 250 μm t/c for both the subscale combustor rig and F100 engine data test points. At the sampling rate (4096 Hz) and record length (2048 points/record) used, each record was 500 ms long and the total time over which the data were averaged was 60 sec. The Fourier system anti-aliasing filters were set to 1250 Hz (−3 db point). Note that the amplitude of data presented at frequencies above 1000 Hz will be erroneous due to the *roll-off* of the filter. The measured transfer function data at frequencies 8, 10 ... 28, 30 Hz were used in determining the in-situ value of Γ used to generate the compensation spectra. In this frequency band, the measured coherence function γ^2 (computed in conjunction with the measured transfer function) ranged from about 0.96 to 0.98 indicating excellent quality in the measured transfer function (frequency response function).

The ambient events which were recorded to establish background system noise levels were run with the amplifier gains set the same as during the test data. Gains were typically X500 for the 76 μm t/c and X1000 for the 250 μm t/c. For the subscale combustor, the ambient was established with the combustor on and the t/c probe mounted, but retracted from the gas path. For the F100 engine, the probe was installed in the engine but the engine was not running.

Additionally, the compensation spectrum measured at each test point was applied to the ambient event to establish the signal-to-noise ratio of the compensated data.

2. Subscale Combustor Tests

The data point processed was test point No. 10. Test conditions were as follows:

- Pressure 1.04 atms (15.20 psia)
- Mean Temperature 1840 K(2780°F)
- Fuel/Air Ratio 0.025
- Probe Mn 0.23

Figure 47 shows the uncompensated instantaneous time domain outputs of the 76 μm (3 mil) t/c and the 250 μm (10 mil) t/c. Both t/c's clearly indicate the presence of the same periodic components but of widely differing amplitudes due to the difference in the t/c dynamic responses. The 76 μm t/c was indicating about 222K (400°F) p-p fluctuations with an rms of 36K (64°F). The 250 μm t/c read about 44K (80°F) p-p with an rms of 12K (21°F). The background noise for the 76 μm t/c was about 1.6K (2.8°F) rms (Figure 48) and was predominately at power line frequency (60 Hz). This indicates an overall time domain signal-to-noise ratio (SNR) for the 76 μm data of about 27 db based on the rms signal levels. Figure 49 is the Power Spectral Density (PSD) plot of the 76 μm t/c output for test point No. 10 and ambient. With the exception of harmonics of power line frequency, the SNR was >20 db up to 500 Hz, >12 db up to 1000 Hz and >10 db out to 2000 Hz.

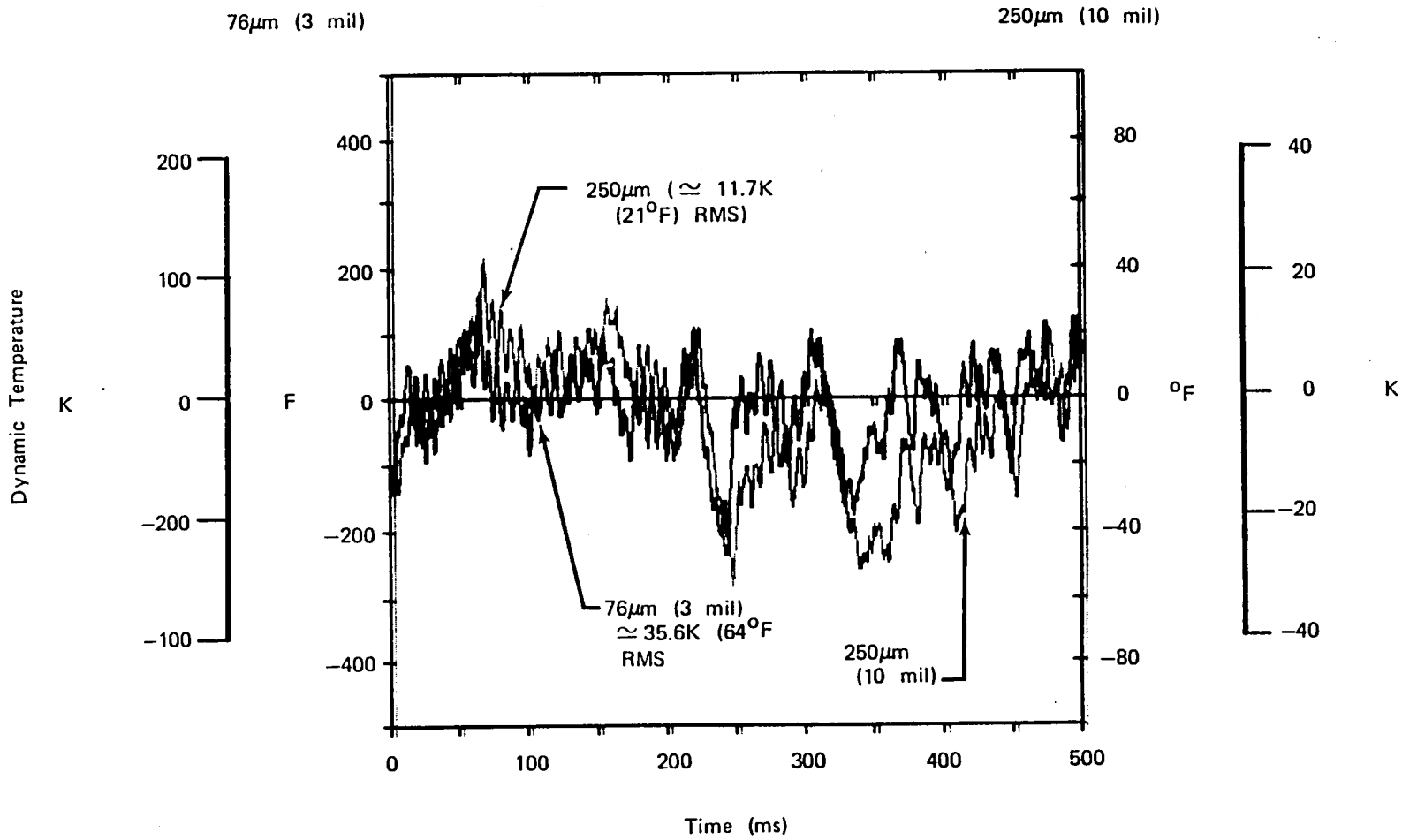

Figure 47. Instantaneous Temperature vs Time: Comparison of Uncompensated 76 μm (3 mil) and 250 μm (10 mil) Thermocouple Outputs — Subscale Combustor Rig Test Point No. 10

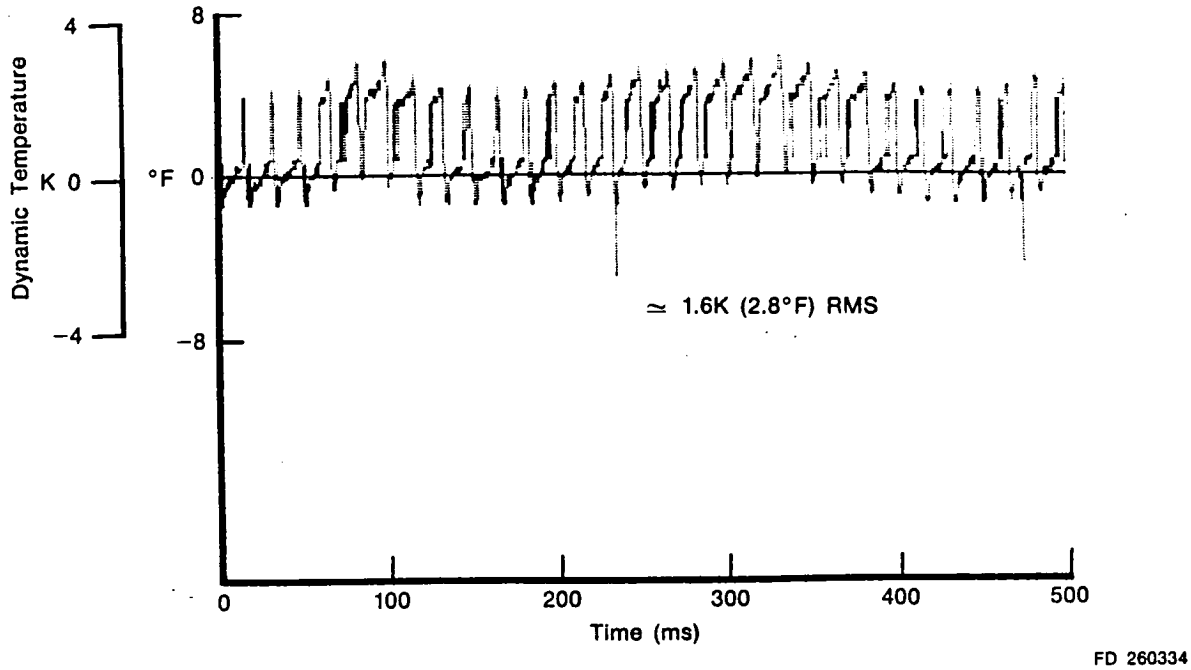

Figure 48. Instantaneous Temperature vs Time: Uncompensated Background Noise Measurement for 76 μm (3 mil) Thermocouple (Subscale Combustor Rig)

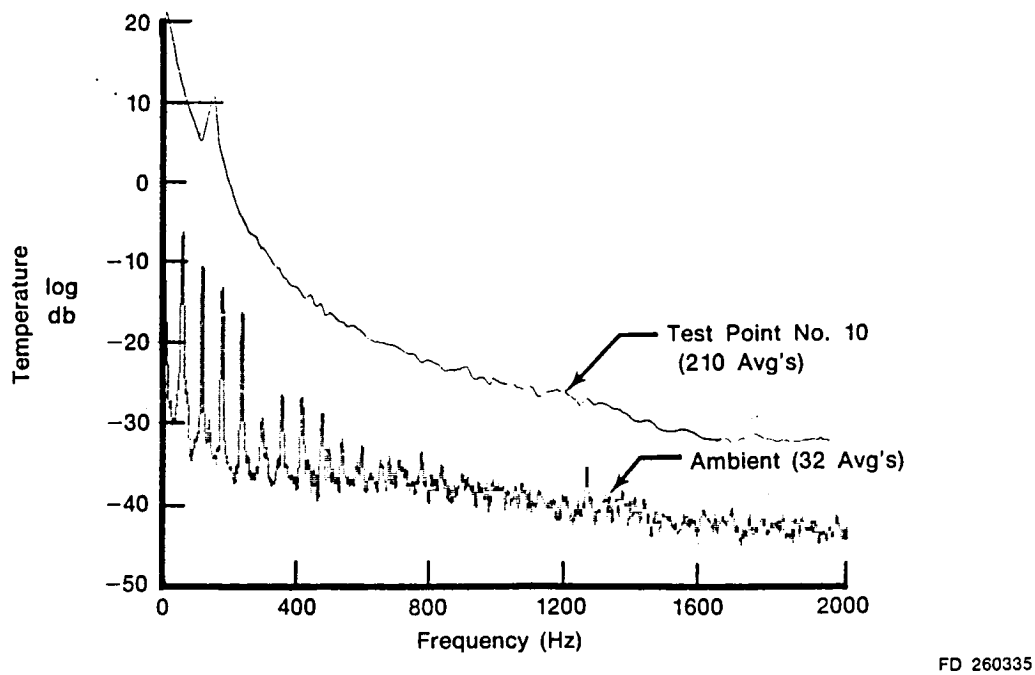

Figure 49. Power Spectral Density Plots of Uncompensated 76 μm (3 mil) Thermocouple Background Noise Compared with Its Uncompensated Output at Test Point N010 (Subscale Combustor Rig)

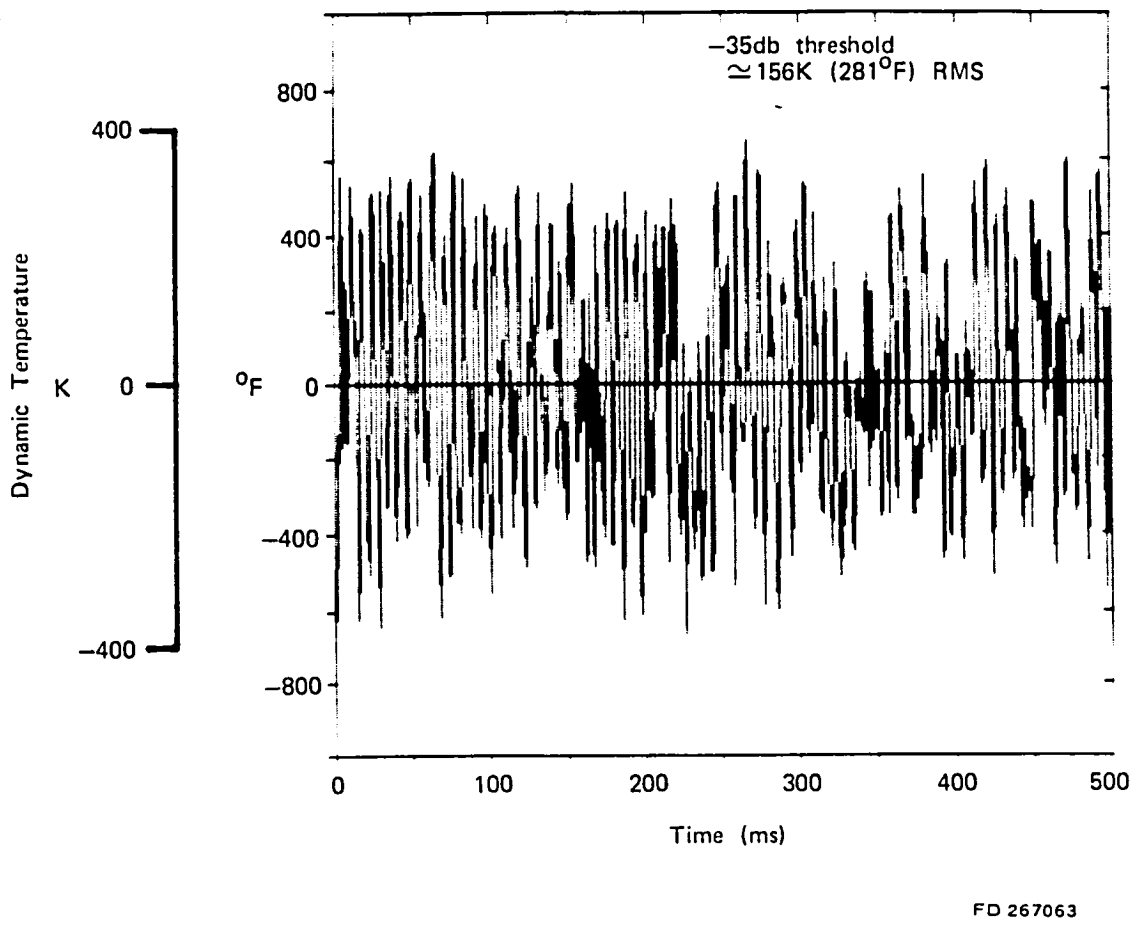

Figure 50. Instantaneous Temperature vs Time of Compensated 76 μm (3 mil) Thermocouple Output (−35 db Threshold-Subscale Combustor Rig Test Point No. 10)

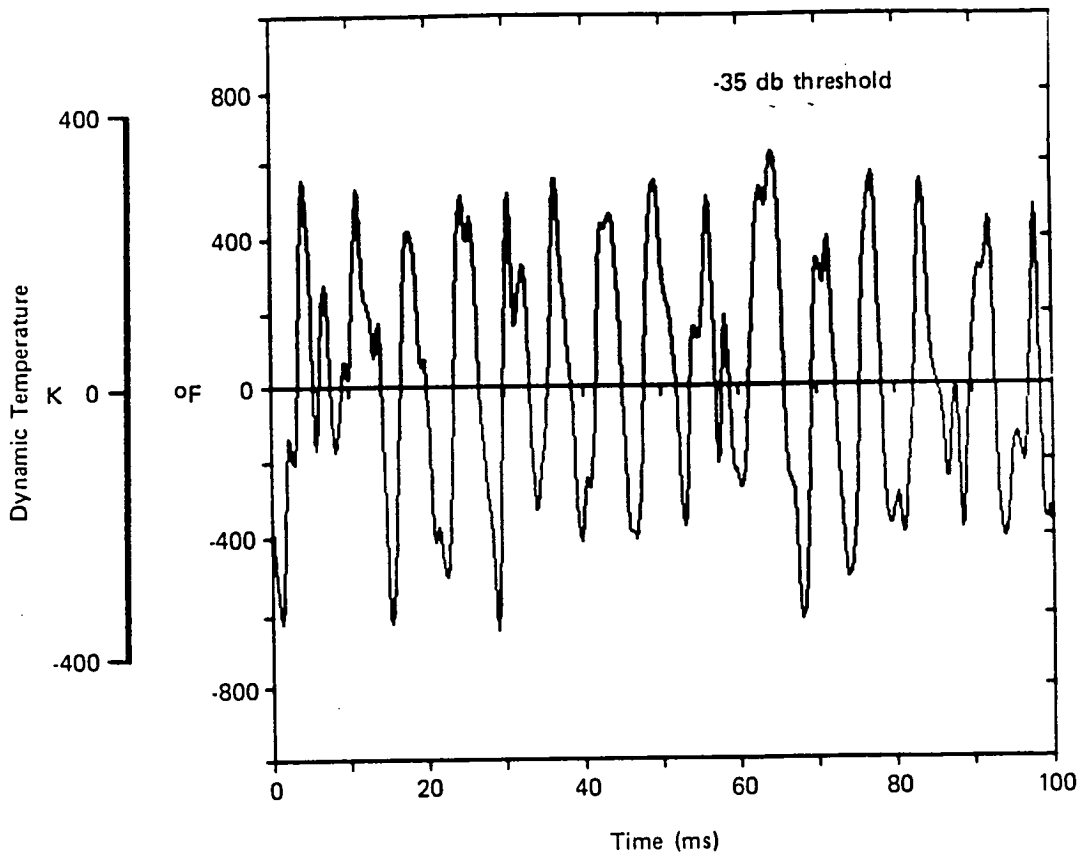

Figure 51. Expanded Time Segment from Figure 50

Figure 15 shows the compensation spectrum for the 76 μm t/c at test point No. 10. At 1000 Hz the gain correlation is about 36 db and at 2000 Hz about 43 db. Figures 50 and 51 show the 76 μm t/c compensated instantaneous time waveform for one entire data record (500 ms) and the first 100 ms of the data record. The compensated data show that the instantaneous temperature fluctuations are actually about 550K (1000°F) p-p with an rms value of around 156K (281°F) rms. The compensation spectrum was also applied to the 76 μm ambient background noise (Figure 52). The overall SNR of the compensated test data point to the compensated ambient was about 18.6 db (time domain signals).

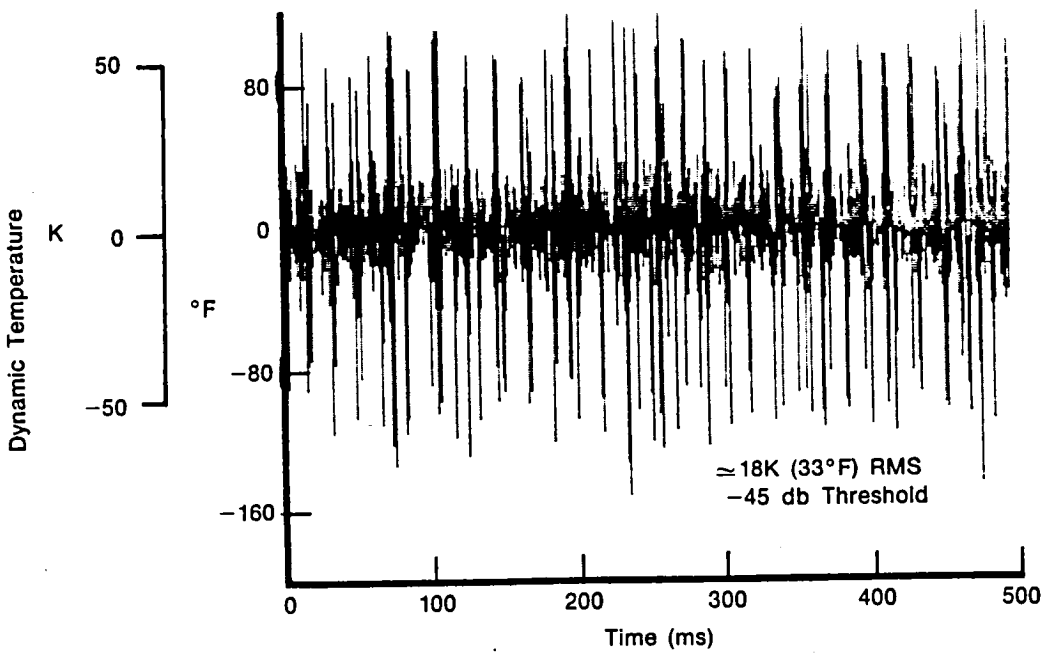

Figure 52. Instantaneous Temperature vs time of Compensated 76 μm (3 mil) Thermocouple Background Noise (−45 db SNR-Subscale Combustor Rig)

The compensated time domain data presented in Figures 50 and 51 were obtained using a data compensation threshold of −35 db. Figures 53 and 54 were processed with thresholds of −45 db and −70 db, respectively. Even with the lower thresholds, the resulting waveforms were well behaved (i.e., only slight increase in rms values and some higher frequency noise spikes). The PSD plots of the compensated 76 μm t/c for test point No. 10 and ambient are contained in Figure 55. Excluding power line harmonics, the SNR was >18 db up to 500 Hz, >13 db up to 1000 Hz, and >9.9 db out to 2000 Hz. Note that in the frequency band around 145 Hz, the SNR is excellent (≈ 43 db).

Prior to compensation, the linear PSD plot of the 76 μm t/c (Figure 56) indicates that the temperature fluctuations are generally randomly distributed with a low amplitude (2K (4°F) rms/ Hz) peak around 145 Hz. After compensating (Figure 57), the peak around 145 Hz is found to be about 21K (37°F) rms/ Hz and predominately characterizes the temperature fluctuations. The wideband random fluctuations present range from about 3K (5°F) rms/ Hz to 8K (15°F) rms/ Hz over the 1000 Hz analysis bandwidth. The data presented in Figures 56 and 57 are simply the square root of the PSD data presented in Figures 49 and 55. Figure 58 is the instantaneous (i.e., single record) PSD plot of the compensated time waveform.

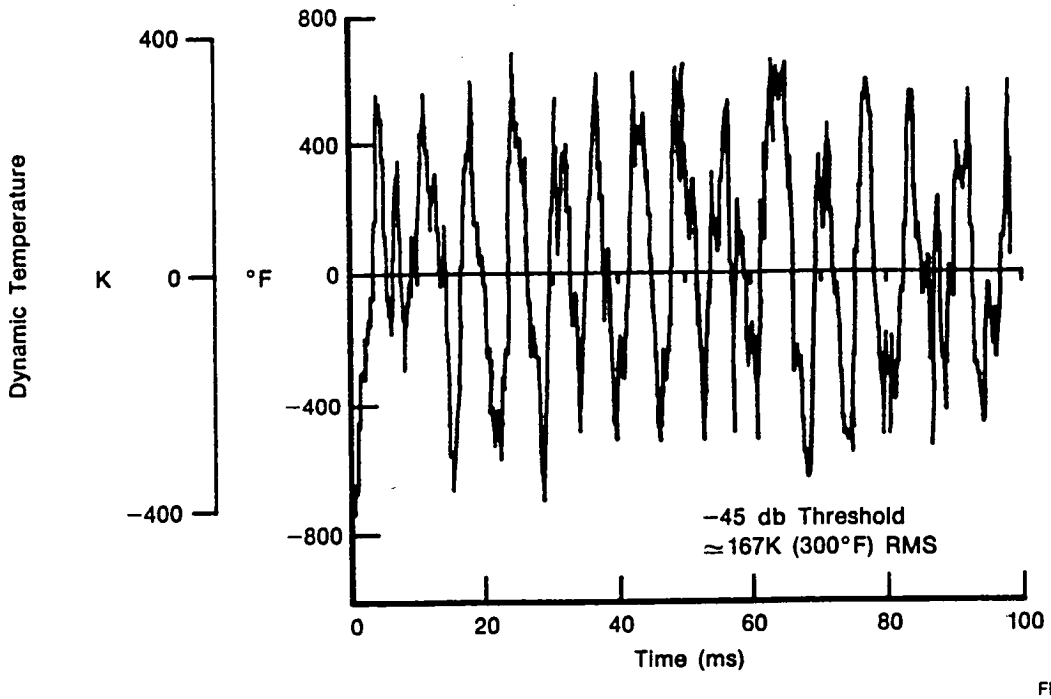

Figure 53. Instantaneous Temperature vs Time of Compensated 76 μm (3 mil) Thermocouple Output (−45 db Threshold-Subscale Combustor Rig Test Pont No. 10)

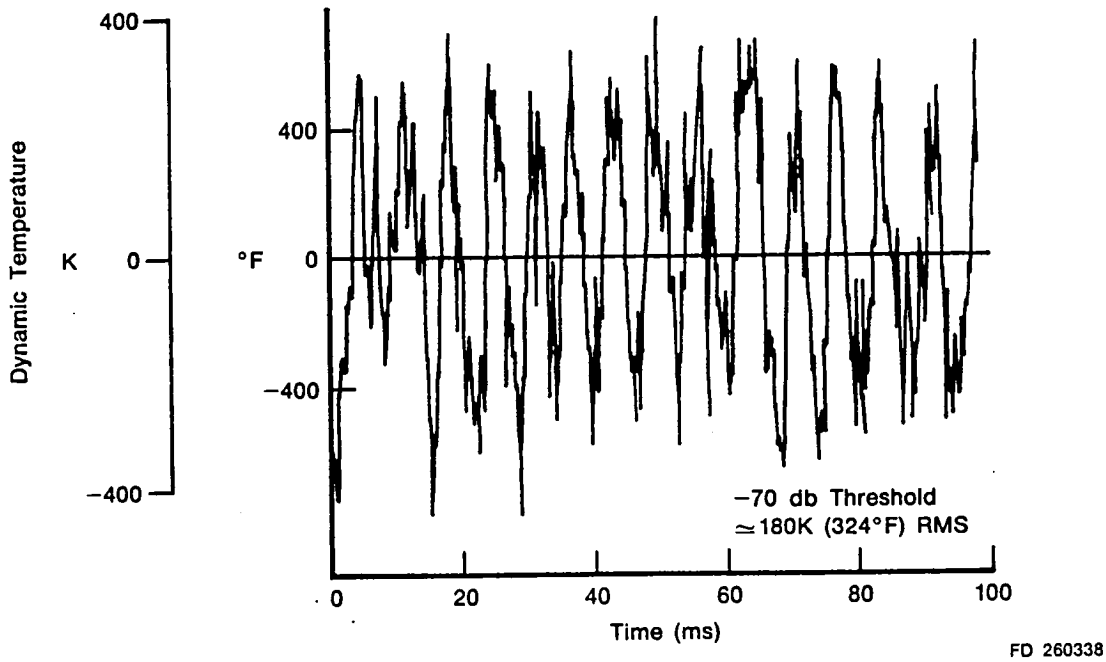

Figure 54. Instantaneous Temperature vs Time of Compensated 76 μm (3 mil) Thermocouple Output (−70 db Threshold-Subscale Combustor Rig — Test Pont No. 10)

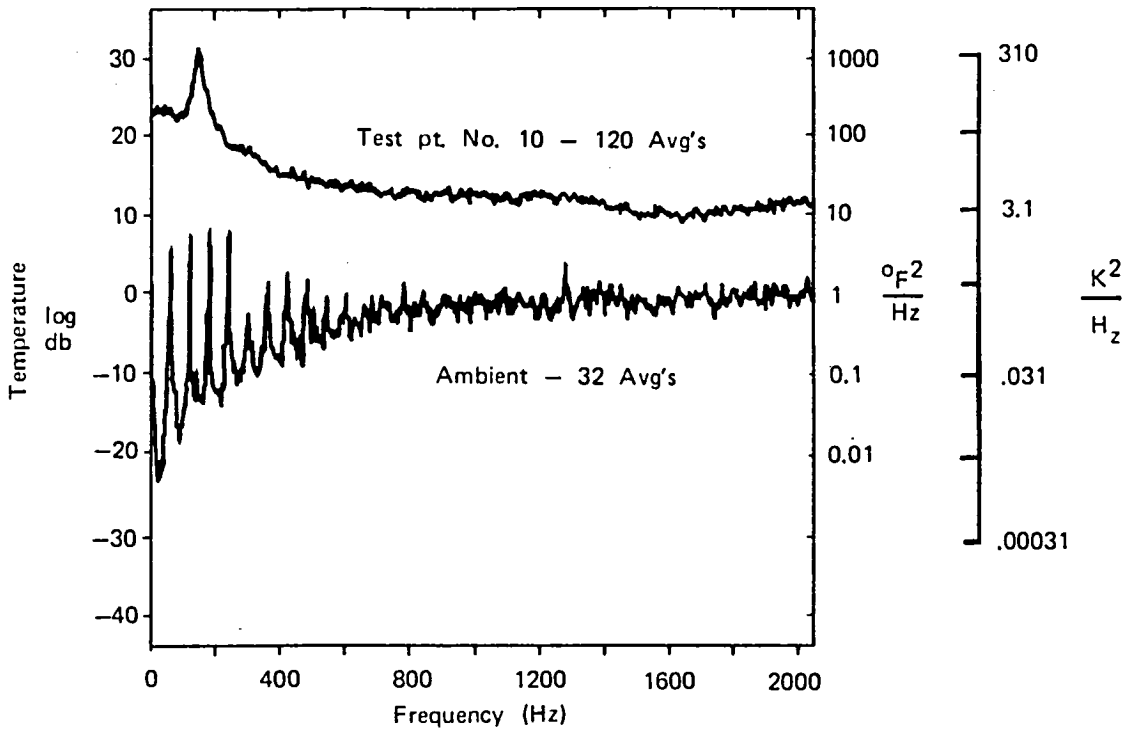

Figure 55. Power Spectral Density Plots of Compensated 76 μm (3 mil) Thermocouple Background Noise Compared with Its Compensated Output at Test Point No. 10 (Subscale Combustor Rig)

Comparing the PSD from a single record (Figure 58) with the 120 ensemble averaged PSD plot (Figure 55), it can be seen that the peak in the averaged PSD spectrum around 145 Hz is not a discrete frequency but a relatively narrow bandwidth peak in the random temperature fluctuations around this frequency. The characteristics of this peak appear to be similar to a classical structural resonance which has natural frequency and damping. In Figure 58, the singular peak in the instantaneous compensated spectrum around 680 Hz is not real data. It is attributed to errors generated during the FFT compensation process. By the time the instantaneous spectrum is made on a compensated time waveform, 3 FFT transforms plus 3 FFT windowing functions have been utilized.

For the combustor rig, data from the 76 μm t/c was successfully compensated to about 1250 Hz (the −3 db point of the system anti-aliasing filter) in the frequency domain presentation and about 600 Hz in the instantaneous time domain presentation. Better results, i.e., SNR and compensation over a larger bandwidth, were obtained in the frequency domain. This is because ensemble averaging is employed in the frequency domain and the compensation is more direct than for the time domain.

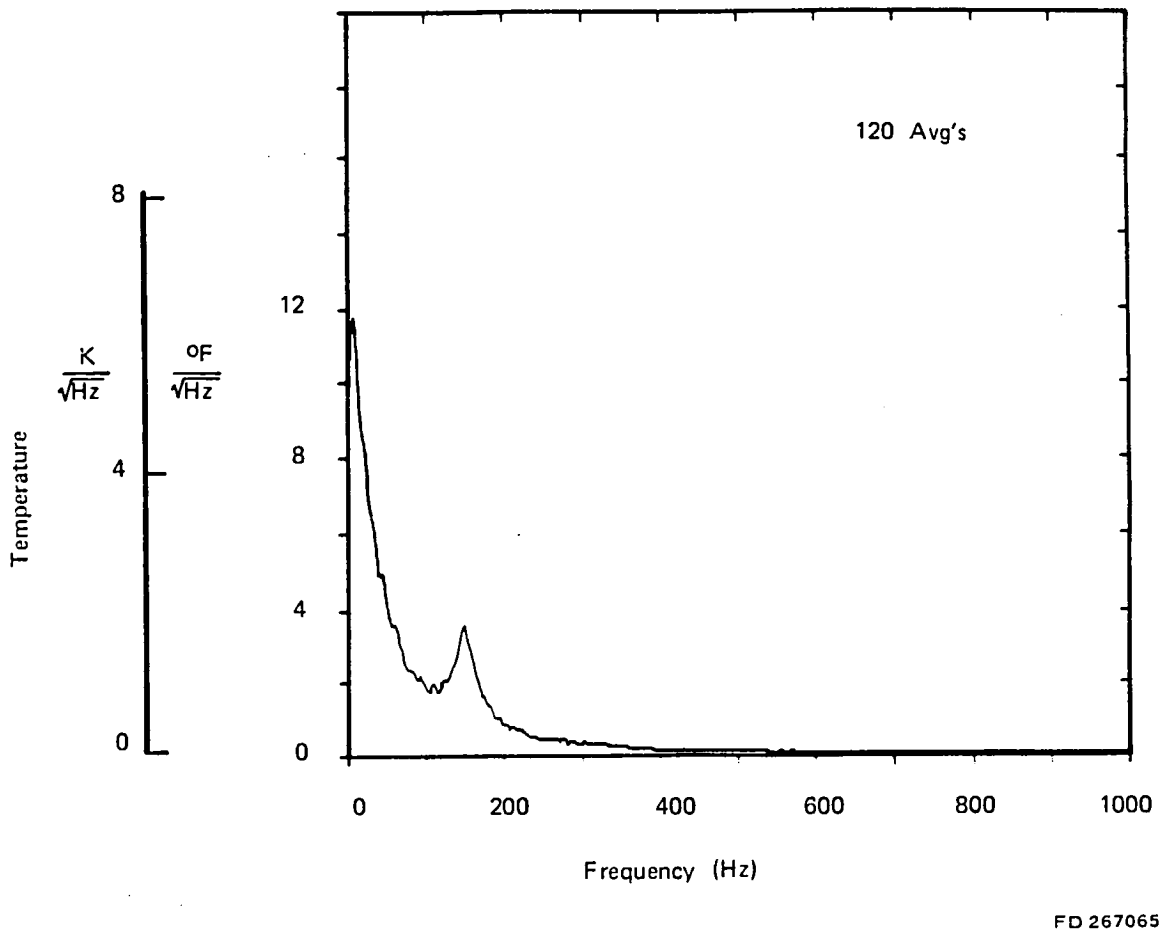

Figure 56. Linear Power Spectral Density Plot of Uncompensated 76 μm (3 mil) Thermocouple Output (Subscale Combustor Rig Test Point No. 10)

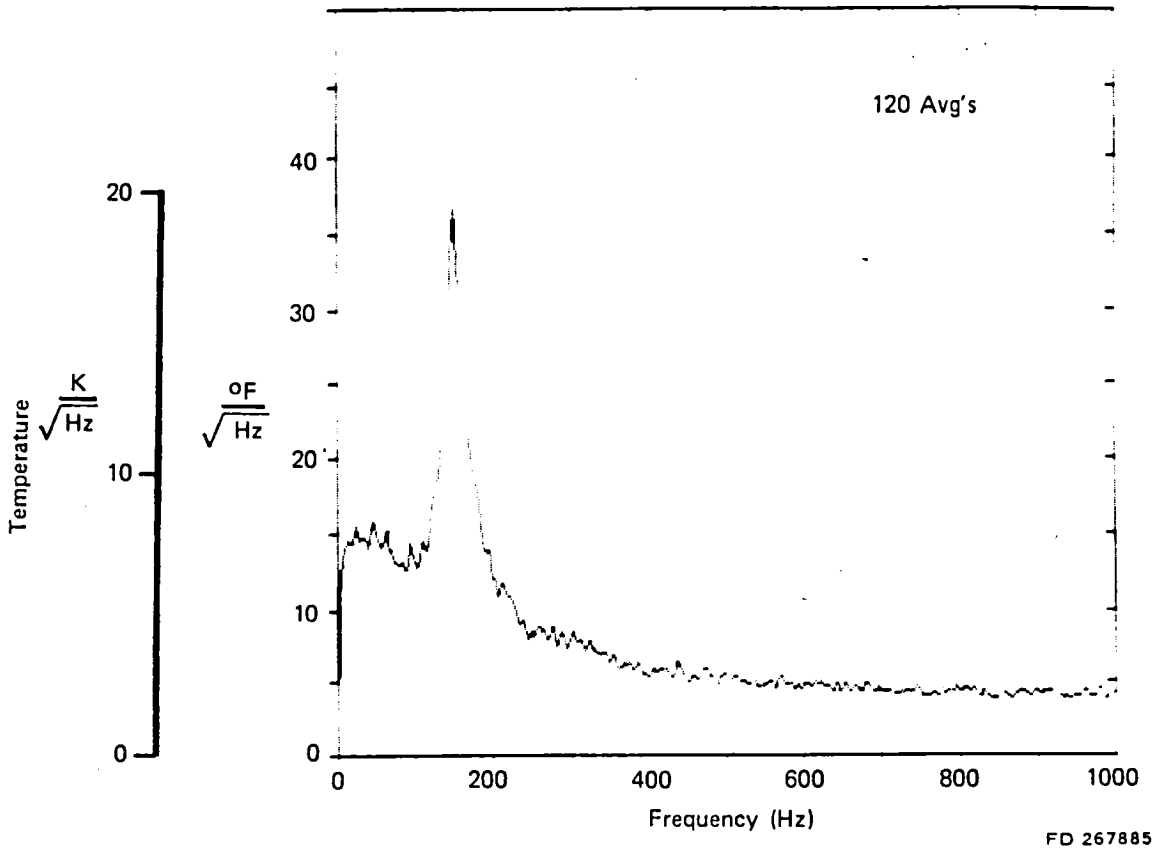

Figure 57. Linear Power Spectral Density Plot of Uncompensated 76 μm (3 mil) Thermocouple Output (Subscale Combustor Rig Test Point No. 10)

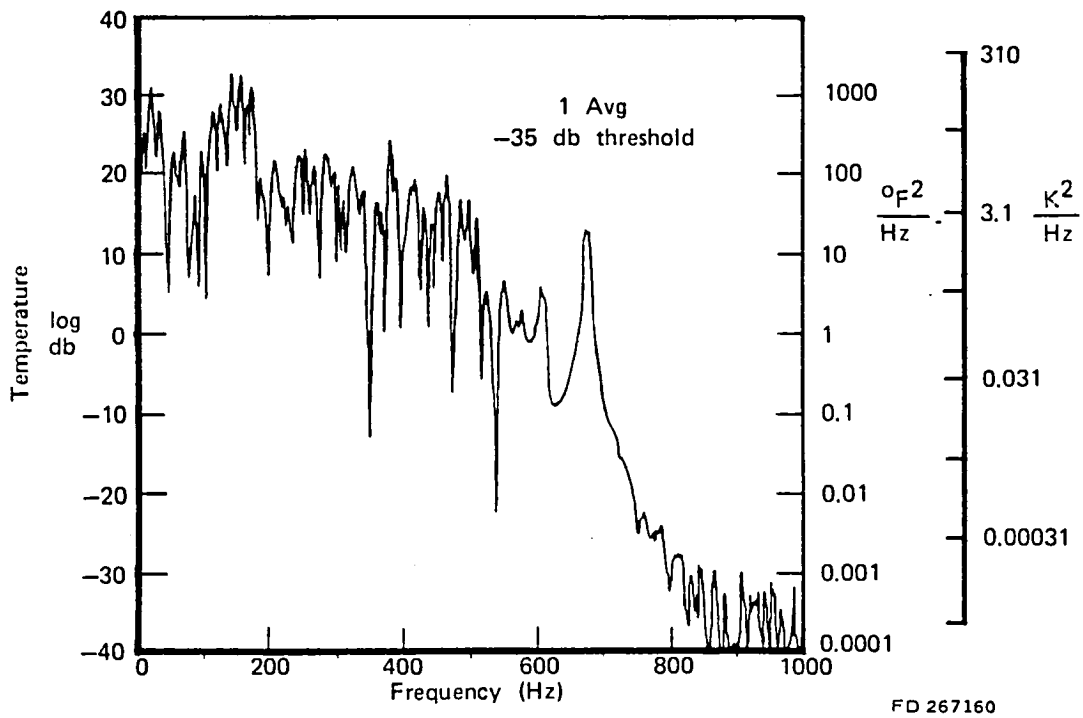

Figure 58. Instantaneous Power Spectral Density Plot of Compensated Time Waveform of 76 μm (3 mil) Thermocouple Output (Subscale Combustor Rig Test Point No. 10)

3. Full-Scale F100 Engine Tests

Test point No. 5 was processed. Test conditions were:

- Pressure 10.75 atms (158 psia)
- Mean temperature 1250K (1790°F)
- Fuel/air ratio 0.02
- Probe M_n 0.36

Figures 59, 60, 61, and 62 show the uncompensated instantaneous time waveforms of the 76 μm t/c and the 250 μm t/c for test point No. 5 and the ambient background noise. The overall SNR for the uncompensated time waveforms was 31 db for the 76 μm t/c and 26 db for the 250 μm t/c. Uncompensated, the 76 μm t/c was indicating about 222K (400°F) p-p and the 250 μm t/c about 55K (100°F) p-p.

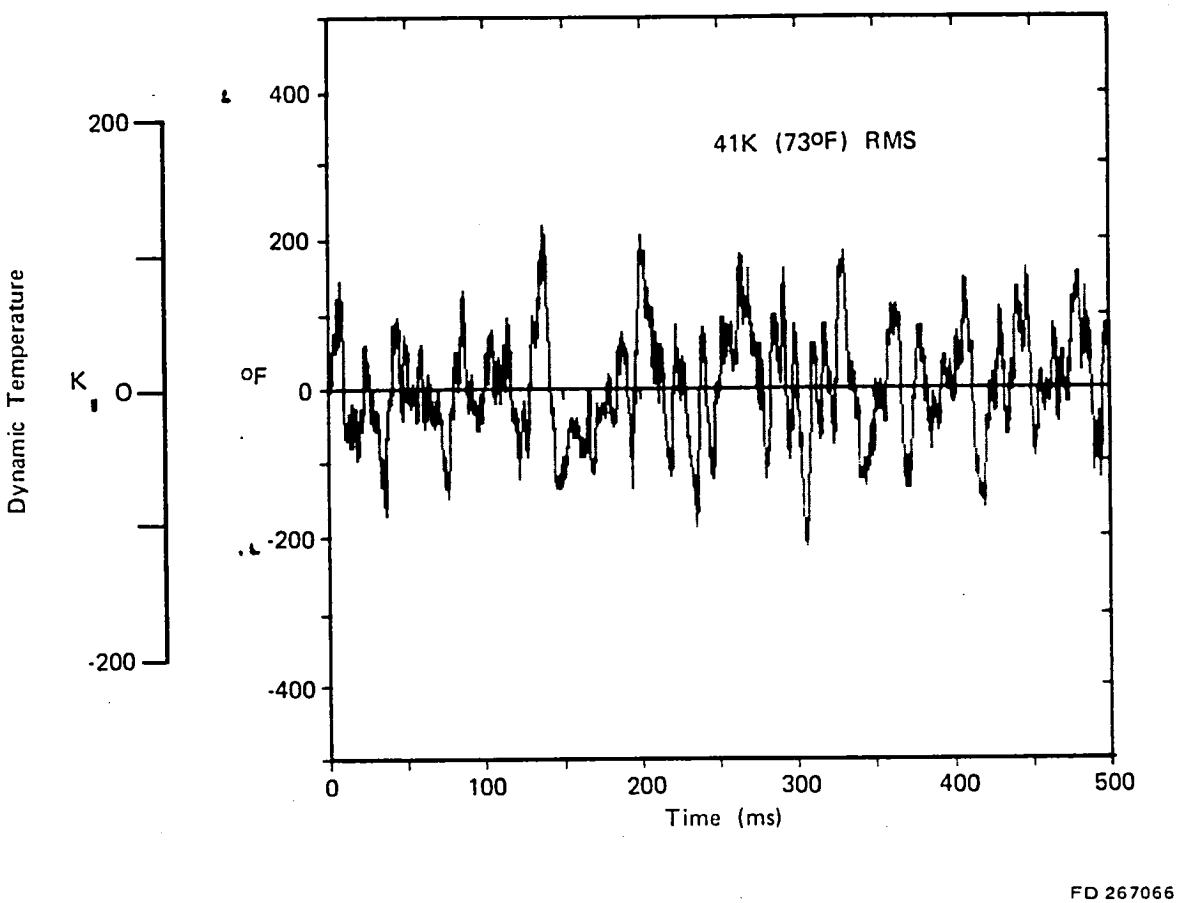

Figure 59. Instantaneous Temperature vs Time of Uncompensated 76 μm (3 mil) Thermocouple Output (F100 Engine Test Point No. 5)

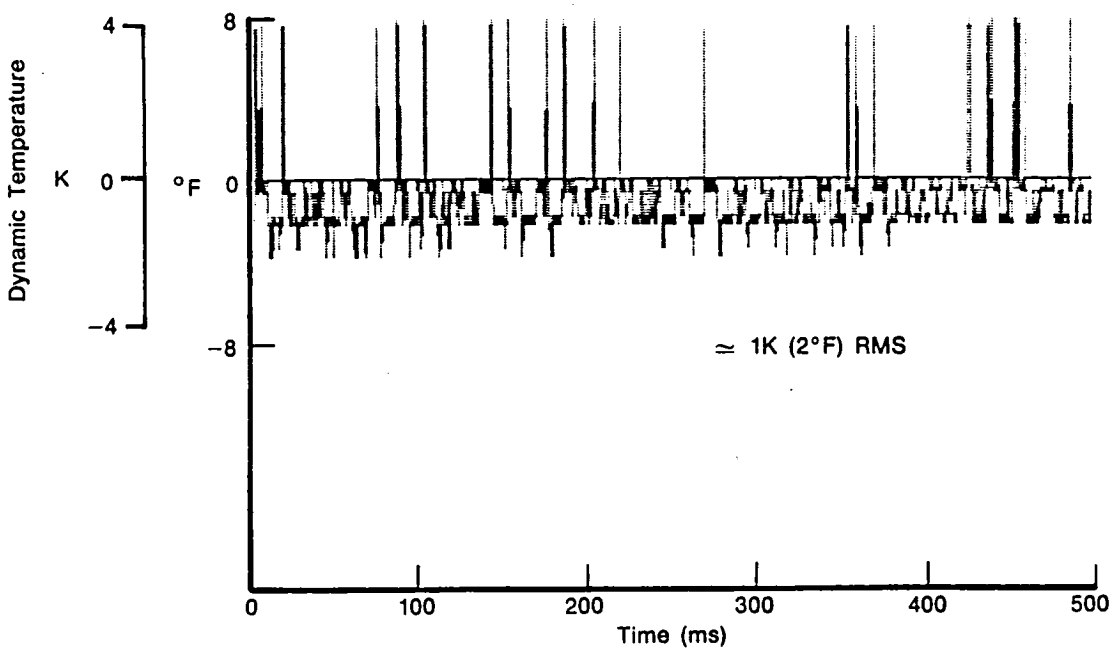

Figure 60. Instantaneous Temperature vs Time: Uncompensated Background Noise Measurement for 76 μm (3 mil) Thermocouple (F100 Engine Test)

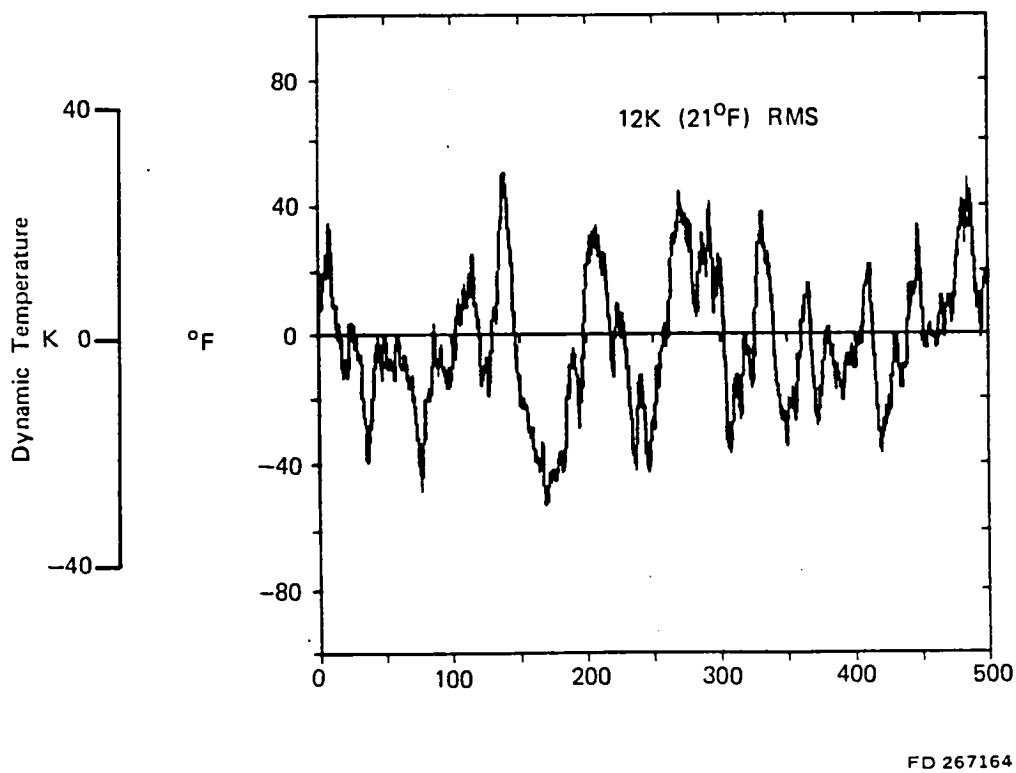

Figure 61. Instantaneous Temperature vs Time: Uncompensated 250 μm (10 mil) Thermocouple Output (F100 Engine Test Point No. 5)

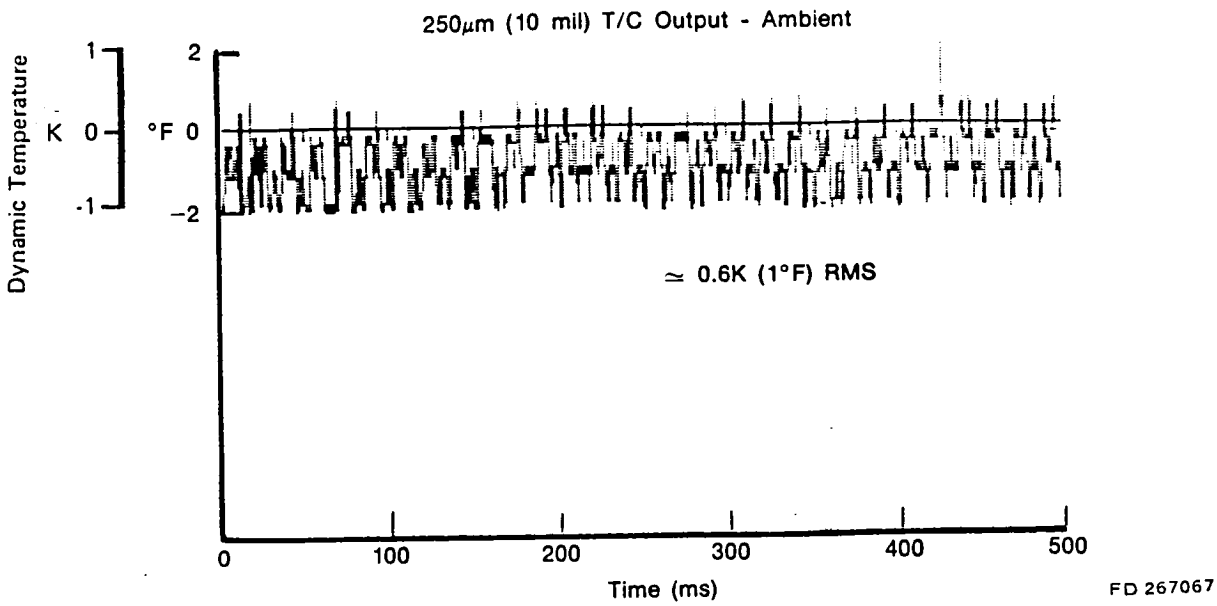

Figure 62. Instantaneous Temperature vs Time: Uncompensated Background Noise Measurement for 250 μm (10 mil) Thermocouple (F100 Engine Test)

Figures 63 and 64 are the PSD plots of the uncompensated 76 μm t/c and 250 μm t/c's for test point No. 5 and ambient. For the 76 μm t/c the SNR is very good; >24 db to 500 Hz, >18 db to 1000 Hz, and >12 db to 2000 Hz. For the 250 μm t/c neglecting the power line harmonics, the SNR is >20 db out to about 400 Hz and >12 db out to 1000 Hz.

The discrete frequency component which appears around 1850 Hz in the 250 μm PSD plot is felt to be mechanical in nature. Possibly, the 76 μm t/c was vibrating in contact with it (prior to its failure).

Figure 65 is the compensation spectrum for the 76 μm t/c for test point No. 5. The gain correction is about 32 db at 1000 Hz and 39 db at 2000 Hz. Figures 66, 67, and 68 are plots of the compensated instantaneous time waveforms of the 76 μm t/c for test point No. 5 and ambient. Figure 67 is a partial display of Figure 66. The overall SNR in the time domain of the compensated instantaneous time waveform for the 76 μm t/c is about 18 db as can be seen from the rms values of Figures 66 and 68. Following compensation, the temperature fluctuations were around 1333K (2400°F) p-p with an rms of about 218K (393°F) rms. The SNR of the compensated PSD spectrum was >26 db to 500 Hz, >20 db to 1000 Hz, and >14 db to 2000 Hz (Figure 69). As can be seen in Figures 69 and 70, the PSD signature is basically wideband random. There were no resonances present in the PSD plots. The low level (≃ 1.4K (2.5°F) rms/$\sqrt{\text{Hz}}$) fluctuations (Figure 70) are considered to be typical variations for a basically random signal.

The 250 μm t/c was compensated for comparison with the 76 μm t/c results. Its compensation spectrum is shown in Figure No. 71. For the limited investigations that were made, the ensemble averaged PSD plots (Figure No's. 63, 64, 69, 73, and 74) provide the most straight forward comparison of results between the compensated 76 μm and 250 μm signals. Any in depth comparisons of the time domain signals must account for differences in bandwidths and compensation thresholds.

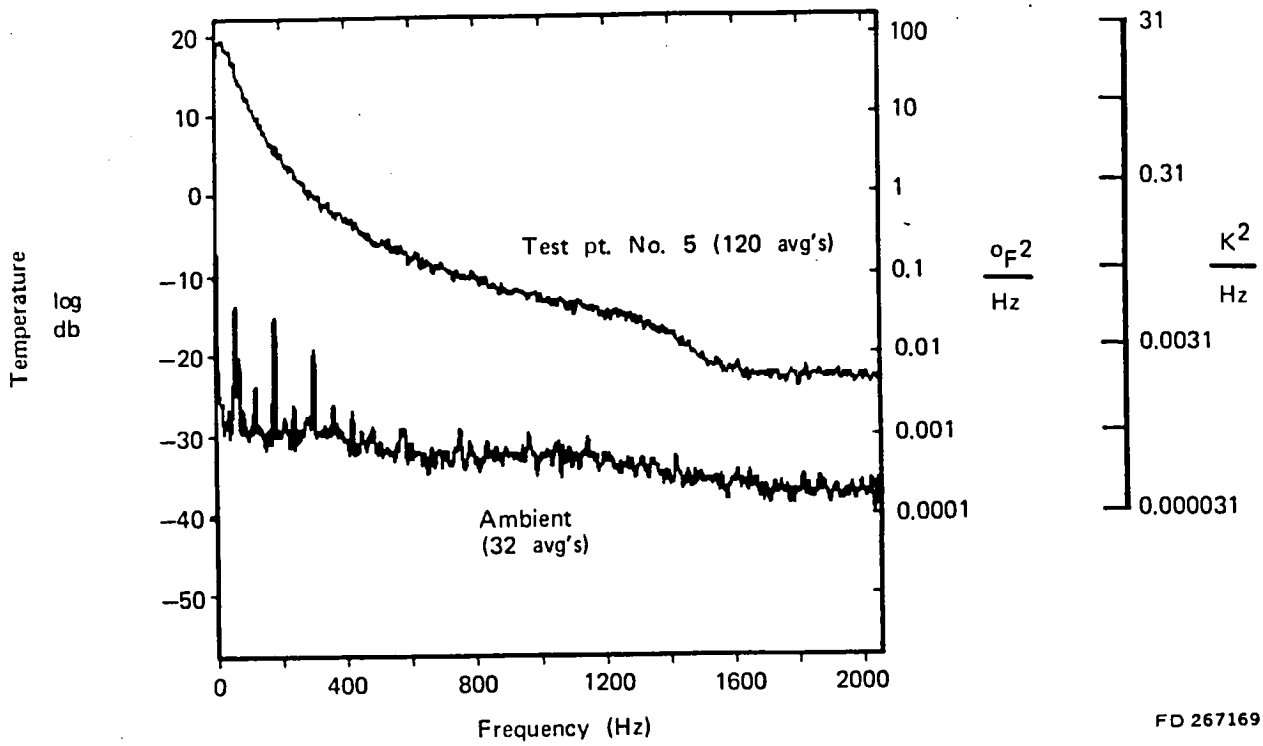

Figure 63. Power Spectral Density Plots of Uncompensated 76 μm (3 mil) Thermocouple Background Noise Compared with Its Compensated Output at Test Point No. 5 (F100 Engine Test)

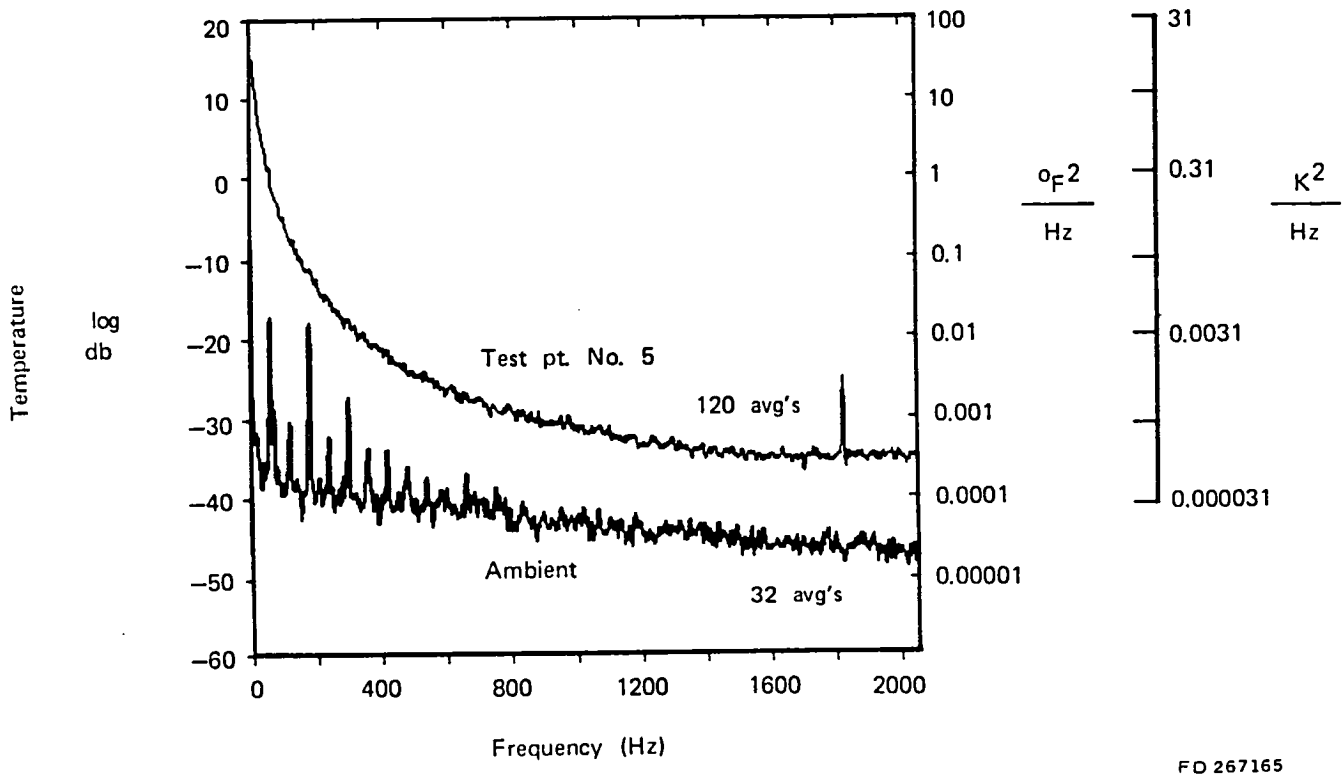

Figure 64. Power Spectral Density Plots of Uncompensated 250 μm (10 mil) Thermocouple Background Noise Compared to Its Uncompensated Output at Test Point No. 5 (F100 Engine Test)

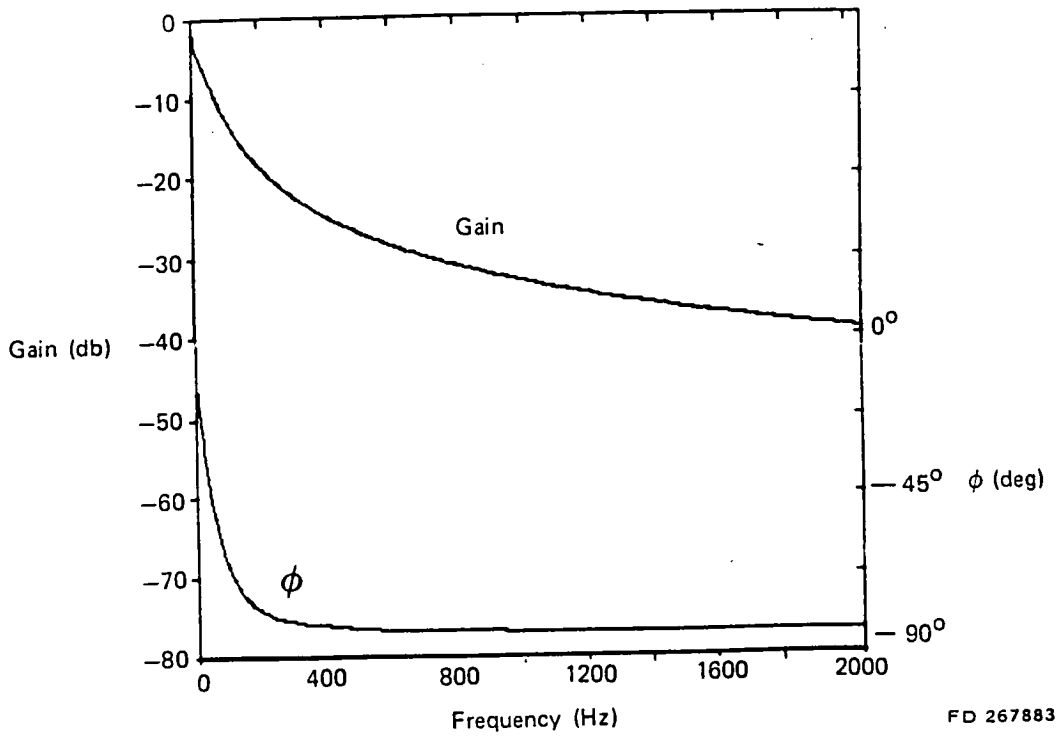

Figure 65. Compensation Spectrum for 76 μm (3 mil) Thermocouple Output for Test Point No. 5 (F100 Engine Test)

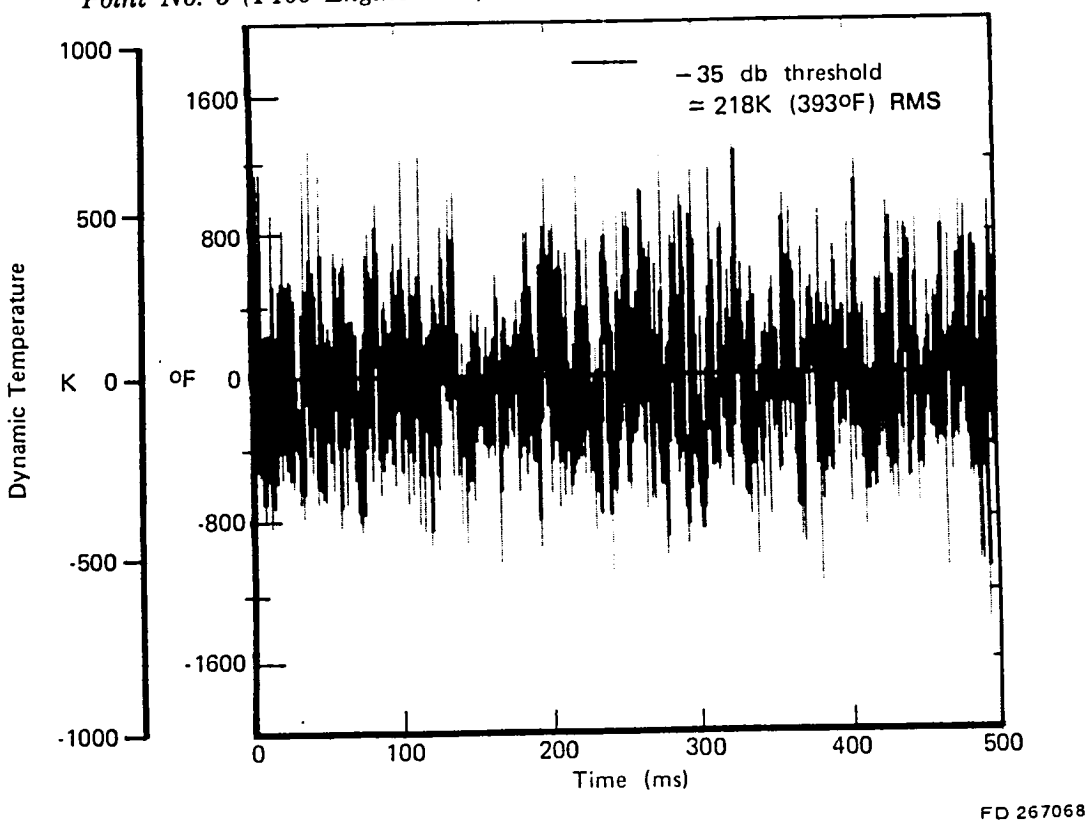

Figure 66. Instantaneous Temperature vs Time of Compensated 76 μm (3 mil) Thermocouple Output (F100 Engine Test Point No. 5)

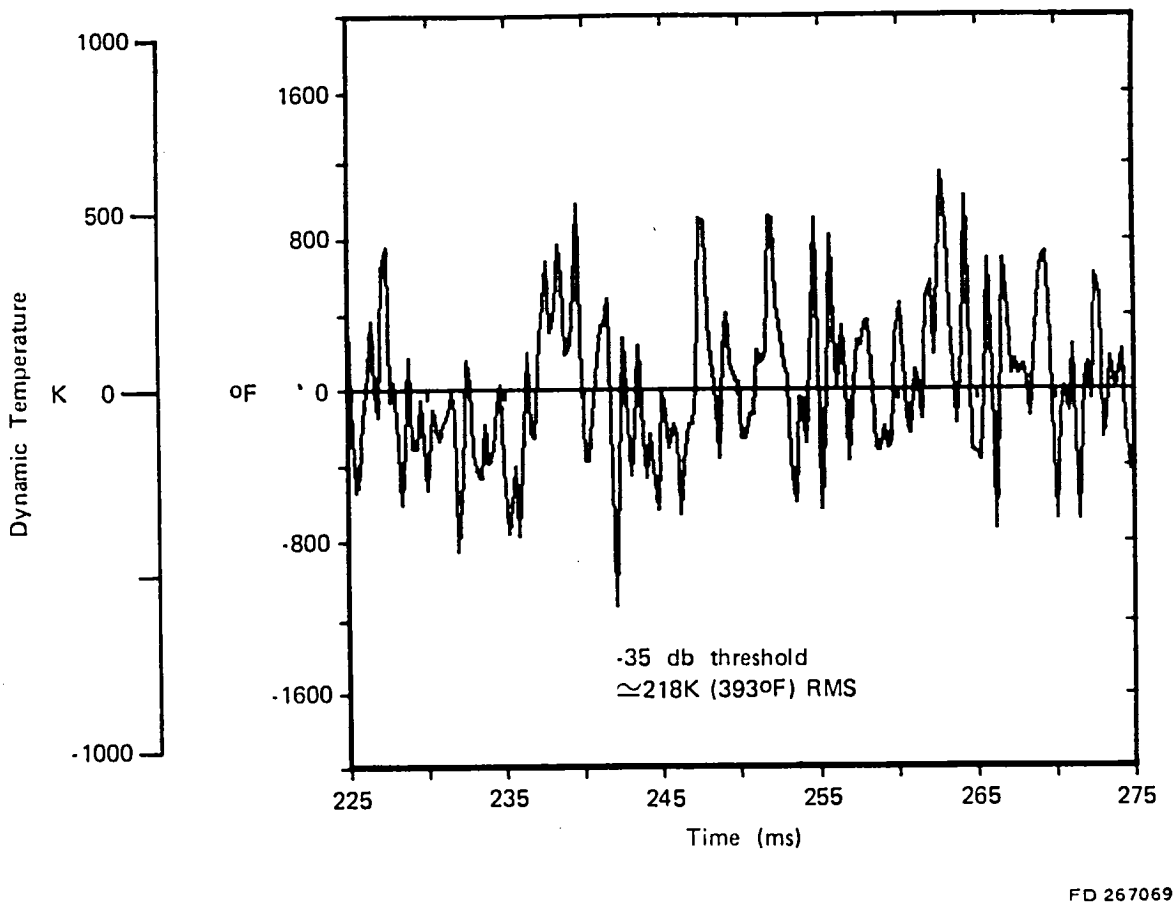

Figure 67. Expanded Time Segment from Figure No. 66

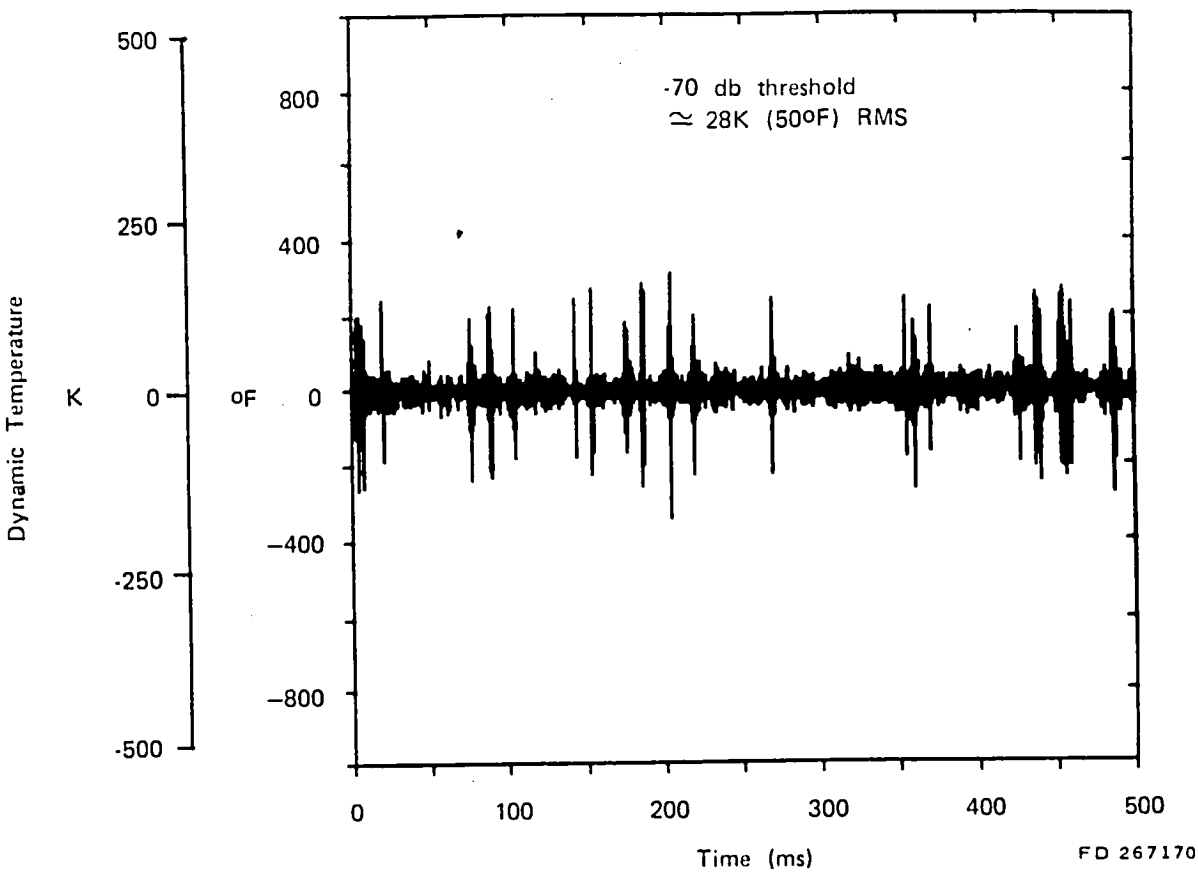

Figure 68. Instantaneous Temperature vs Time of Compensated 76 μm (3 mil) Thermocouple Background Noise (F100 Engine Test)

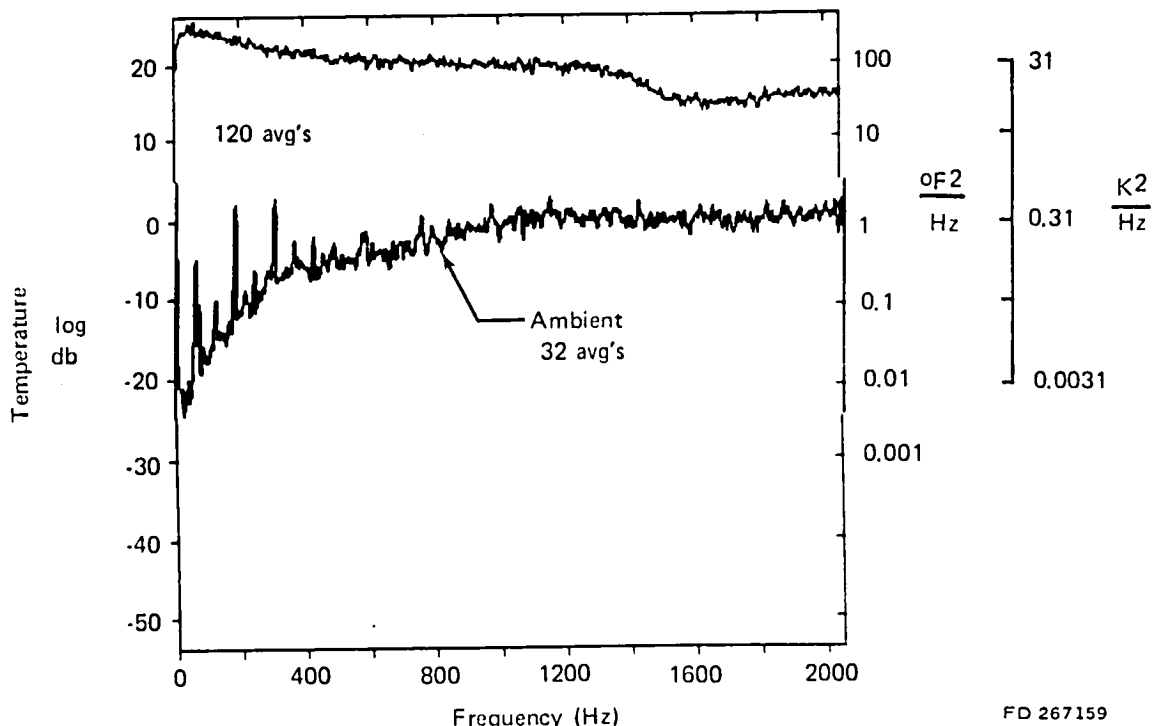

Figure 69. Power Spectral Density Plots of Compensated 76 μm (3 mil) Thermocouple Background Noise and Its Compensated Output at Test Point No. 5 (F100 Engine Test)

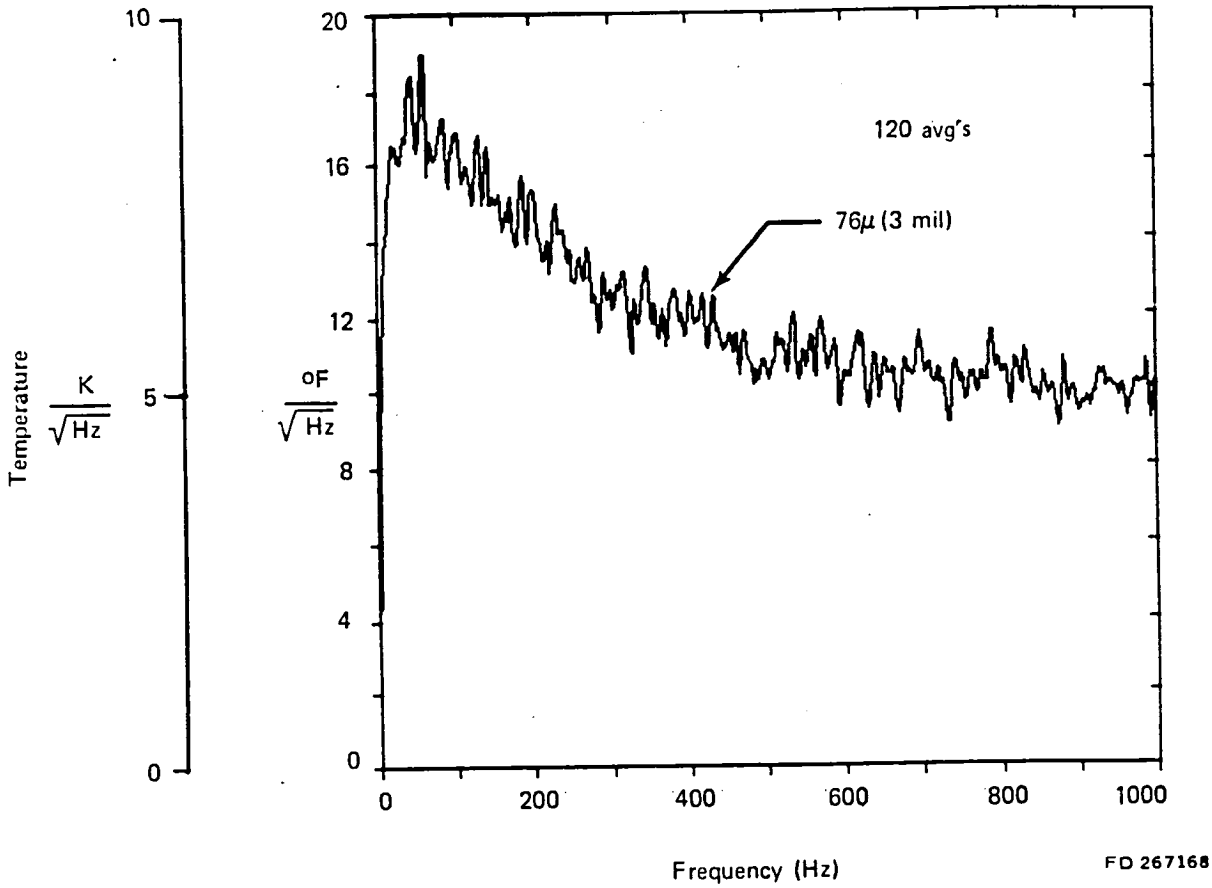

Figure 70. Linear Power Spectral Density Plot of Compensated 76 μm (3 mil) Thermocouple Output (F100 Engine Test Point No. 5)

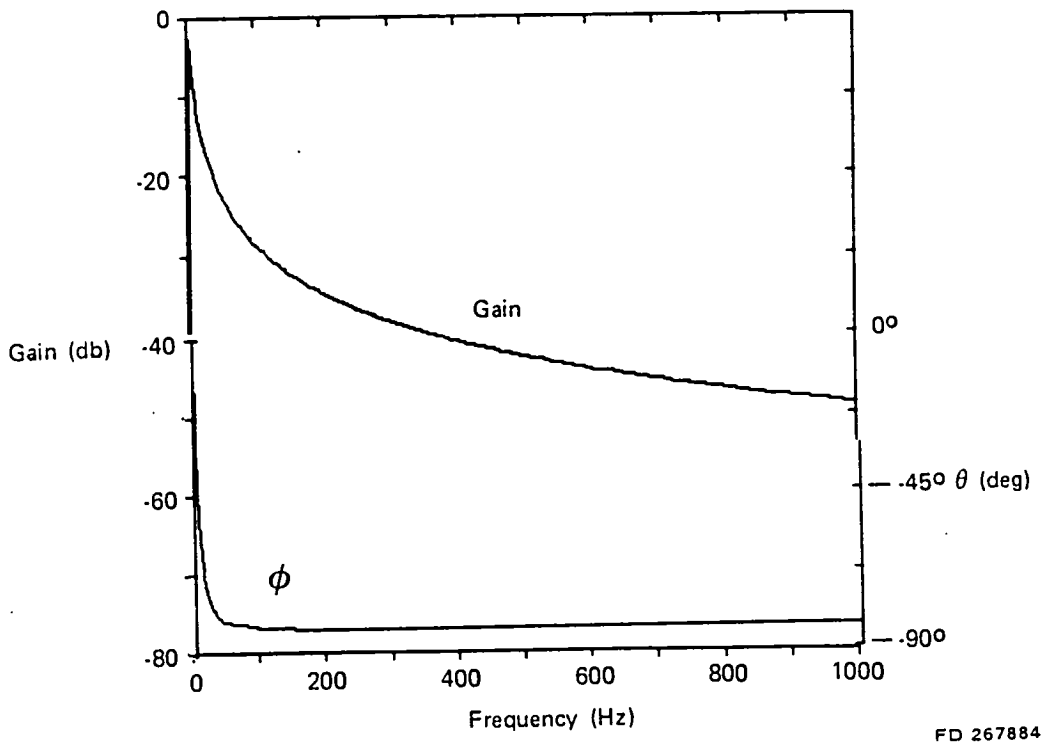

Figure 71. Compensation Spectrum for 250 μm (10 mil) Thermocouple Output for Test Point No. 5 (F100 Engine Test)

For the ensemble averaged compensated frequency domain data, the error between the 250 μm t/c and 76 μm t/c data was $<-6\%$ up to 100 Hz and $<-29\%$ up to 1000 Hz. At frequencies above the anti-aliasing filter setting (1250 Hz) there is an obvious error in the 250 μm results as evidenced in Figure 73 by the cross-over in the PSD functions around 1400 Hz.

There are two probable explanations for the observed cross-over in the PSD functions. (1) It is most likely due to lack of adequate dynamic range (and SNR) in the data acquisition and analysis system for the 250 μm t/c data. Comparing the compensation spectra for the two thermocouples at this data point (Figure No's. 65 and 71) it is evident that the output of the 250 μm t/c at the higher frequencies will be significantly lower (i.e., greater dynamic range required) than for the 76 μm t/c. The lack of dynamic range in the system would result in higher than actual outputs at the higher frequencies due to the system noise floor. When compensated, these frequencies would have erroneously high amplitudes. (2) The other possible source of the error is that the anti-aliasing filter for the 250 μm t/c did not set to 1250 Hz. It is normally in a by-pass mode (i.e., does not provide any filtering) and is automatically set by the computer prior to data acquisition. The anti-aliasing filter was properly set for the 76 μm data acquisition as evidenced by the abrupt roll-off in the uncompensated PSD plot in Figure 63. This characteristic roll-off is not readily apparent in the 250 μm PSD plot for test point No. 5 (Figure 64). With one signal filtered and the other not, the unfiltered signal would indicate higher following compensation (but only in the stop-band). For the filters used, and the characteristics of these particular data, at frequencies below $\simeq$1000 Hz there would be no differences attributable to the 76 μm signal being filtered and the 250 μm signal not being filtered. Above $\simeq$1000 Hz, the unfiltered results would be expected to indicate higher. Reason (1) is the most plausible. Note that in Figure 73 there is an upward slope in the compensated 76 μm PSD function which is tracking parallel to the 250 μm results beginning around 1550 Hz. This is an indication that it too has reached a noise floor and is being compensated too high in this region.

In judging the validity of the DGTMS (dual t/c) technique, identical results for the compensated 76 μm and 250 μm t/c signals over the entire bandwidth of the analysis would be highly indicative that the compensation technique is completely valid. For the less than identical results obtained, consideration must be given to the SNR'S of the two signals. In the bandwidth of good SNR ($>$30 db up to $\simeq$100 Hz) for both t/c's, the results are very good ($<6\%$ difference) and a significant gain compensation is being made to the 250 μm signal (up to 29 db). Results in the 100 Hz to 1000 Hz ($<29\%$ differences) are good considering the power SNR's and very high gain compensation factors employed. At 1000 Hz, the SNR of the uncompensated 250 μm t/c SNR is $\simeq$11 db and the gain correction is about 48 db. For the 76 μm t/c, the uncompensated SNR at 1000 Hz is about 20 db and the gain compensation is about 32 db.

Upon closer inspection of the differences in the two compensated PSD functions, it appears at first that the differences are not entirely explained by SNR. If the assumption is made that neither compensation spectra contained any errors, than if would be expected that the compensated 250 μm PSD function would be higher in amplitude if the 250 μm t/c signal had poorer SNR. Since the compensated 250 μm t/c PSD plot was lower in amplitude than the 76 μm t/c data, this would seem to indicate that the observed differences must be primarily associated with errors in the compensation spectra. However, from Figures 63 and 64 it can be seen that the absolute level of background noise for the 250 μm t/c is $\simeq$10 db lower than the background noise of the 76 μm t/c. Thus on final analysis it is concluded that in the 100 Hz to 1000 Hz bandwidth differences are most probably due to poor SNR in the 250 μm t/c data. In the bandwidth up to 100 Hz, where there is good SNR for both t/c's, the observed $<6\%$ differences are consistent with the predicted errors associated with the measurement accuracy of the t/c wire diameters (Table XII).

Figure 72 shows the compensated time waveform for 250 μm t/c for comparison with the compensated 76 μm t/c signal (Figure No. 67). The comparison is good considering the poorer SNR and lack of dynamic range in the 250 μm t/c data. The primary differences in these waveforms are due to the lack of the higher frequency components in the compensated 250 μm t/c waveform. As seen from Figures 67 and 72, the time phasing of the instantaneous signals is good at the lower frequencies. Using thresholds of −35 db and −65 db for the 76 μm and 250 μm respectively, the rms and p-p values of the compensated 250 μm t/c instantaneous time signal is about 25% lower than the compensated 76 μm signal. This magnitude of error is consistent with errors observed in the compensated PSD functions, i.e., an approximately constant error across the spectrum of a random signal with a constant phase angle (the phasing of all frequencies above ≃100 Hz ≃90°) would be expected to yield ≃ same error in the instantaneous waveform. Note that utilization of the relative threshold during the compensation process precludes obtaining signals compensated over the exact same bandwidth even if identical thresholds are specified. With the −65 db threshold used for the 250 μm t/c, it was compensated over the entire 2K Hz analysis bandwidth. The 76 μm t/c was compensated using a −35 db threshold which would yield a bandwidth of about 1250 Hz (Figure 63). As stated above, a more in depth unambiguous analysis of results in the time domain would require signals compensated to the same bandwidth. These data are not available from the limited processing accomplished under this contract.

In the F100 engine installation, data from the 76 μm (3 mil) t/c was sucessfully compensated to about 1250 Hz (the −3 db point of the antialiasing filter) and the 250 μm (10 mil) to about 1000 Hz in the time and frequency domains. The agreement between the compensated 76 μm and 250 μm data provided additional verification of the dual t/c approach developed under this contract.

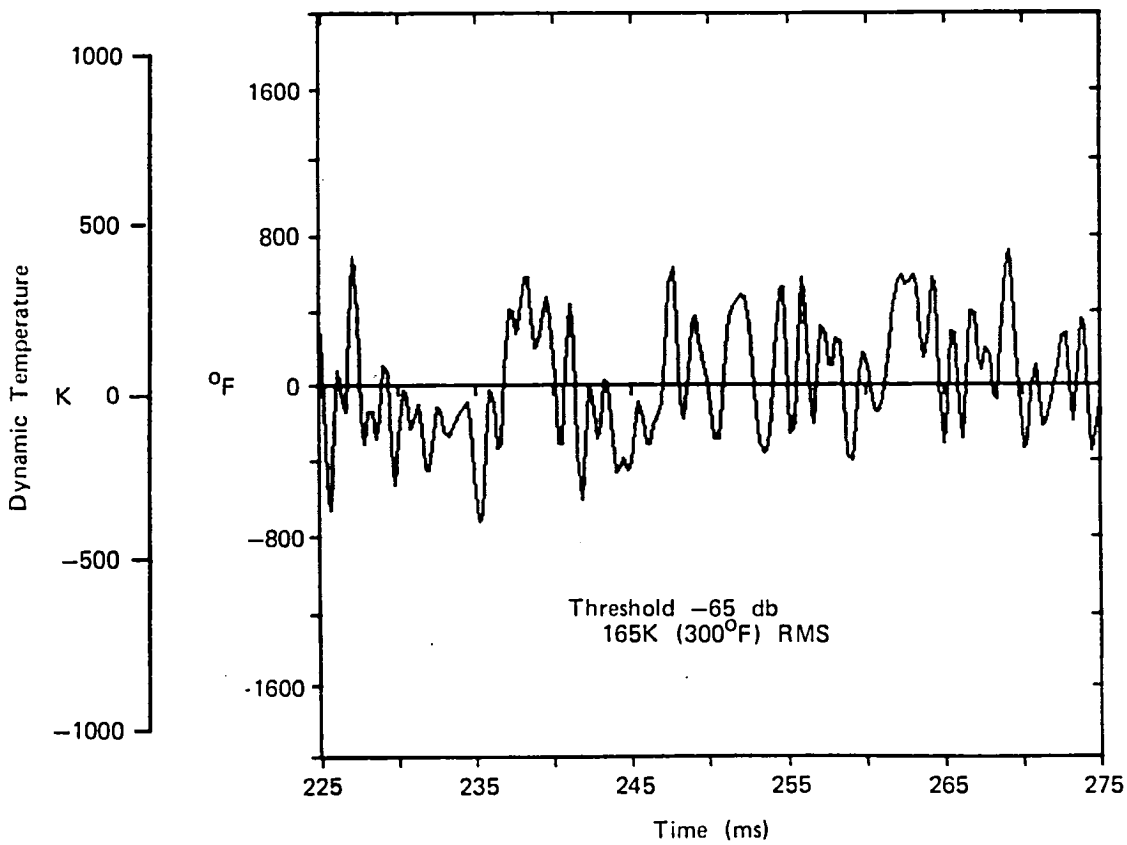

Figure 72. Instantaneous Temperature vs Time of Compensated 250 μm (10 mil) Thermocouple Output (F100 Test Point No. 5)

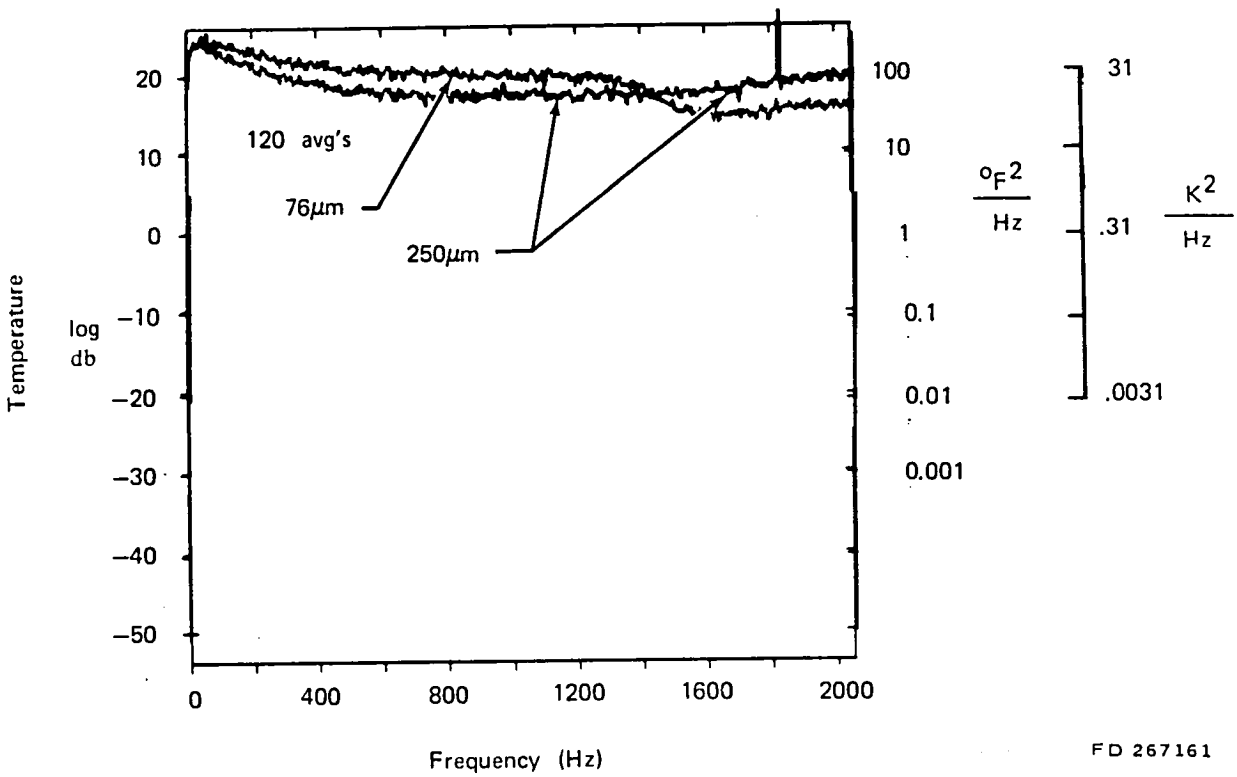

Figure 73. Power Spectral Density Plots of Compensated 76 μm (3 mil) Thermocouple Output Compared with Compensated 250 μm (10 mil) Thermocouple Output (F100 Engine Test Point No. 5)

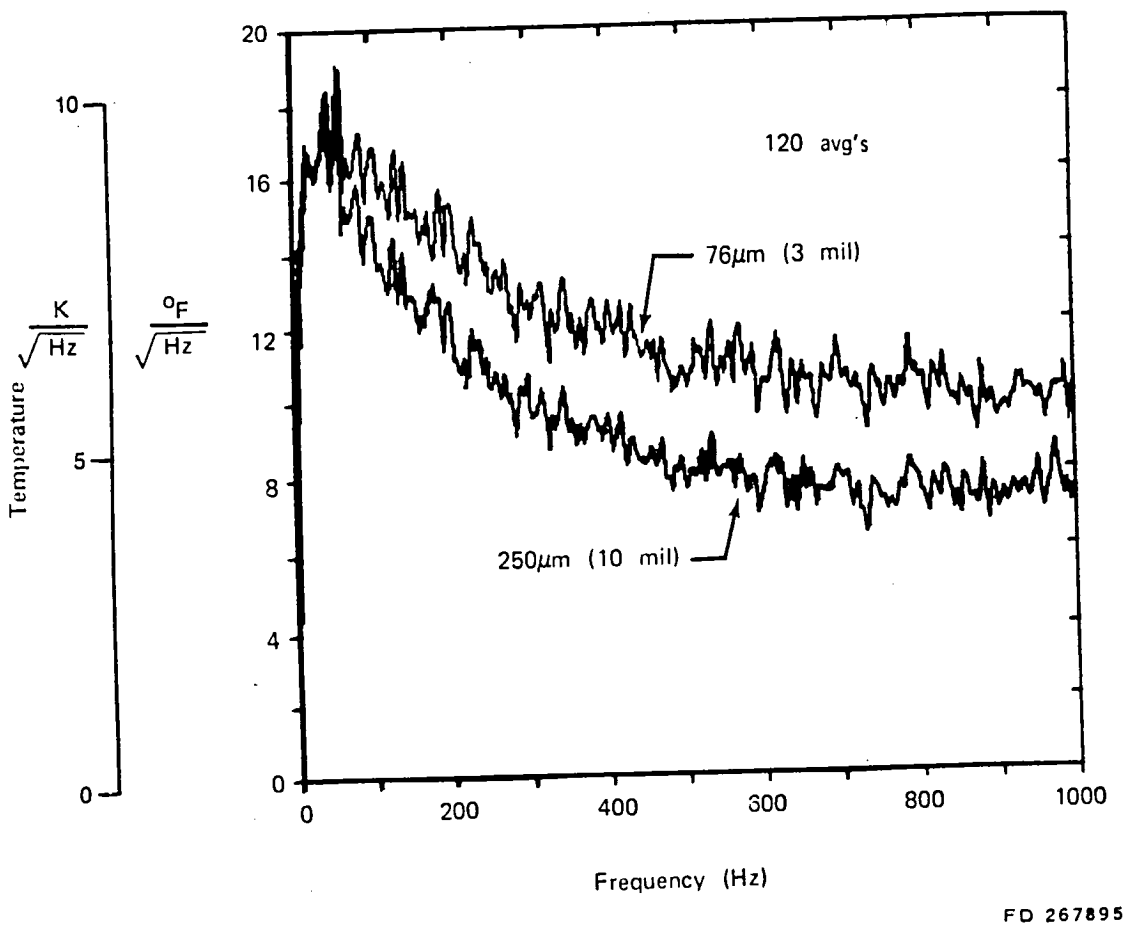

Figure 74. Linear Power Spectral Density Plots of Compensated 76 μm (3 mil) Thermocouple Output Compared with Compensated 250 μm (10 mil) Thermocouple Output (F100 Engine Test Point No. 5)

4. Summary

Dual wire t/c data from a subscale combustor rig and a full-sale F100 engine were acquired and successfully processed with the computer software developed under this contract. The technique was found to be very usable in the test stand environment. The data acquisition system was set-up on two occasions at two separate locations and data acquired without encountering any major problems or delays. The agreement between the compensated 76 μm (3 mil) t/c and the 250 μm (10 mil) on F100 engine test data was considered a significant achievement in verifying the dual wire approach for determining compensation spectra from the test data. Additional more in depth comparisons are recommended.

SECTION IV
SUMMARY OF RESULTS, CONCLUSIONS AND RECOMMENDATIONS

Methods for measuring the dynamic temperature fluctuations from a gas turbine combustor were surveyed, and from the methods described in the literature, a two-wire thermocouple concept was chosen for detailed design, fabrication and testing. Detailed analysis of the concept revealed that transient conduction effects were significant for mechanical designs which would meet contract durability goals. A method of analysis which included both convective and conductive heat transfer was formulated. The key feature of the analysis method was modeling the thermocouple element as a cylinder in crossflow, a configuration which was obtained experimentally using welded thermocouple elements with beadless junctions.

Two probes were fabricated and tested. The first test series was done in an atmospheric pressure laboratory burner. The second test series was done in an F100 engine. Thermocouple response spectra, compensation spectra and uncompensated and compensated waveforms were obtained for both test series. Simulation of the finite element thermocouple model with analog electrical circuits verified the analysis method. Extensive investigations into possible error sources defined the accuracy of the measurement technique for instantaneous and averaged data.

Several aspects of this investigation should be continued to increase confidence in the measurement technique. At the beginning of the contract, experimental methods were sought to directly verify the compensation method. It is desirable to (1) obtain a dynamic temperature source of known signal character (for example, a pure sine wave of known frequency and amplitude), and (2) compare the input, known signal with the compensated thermocouple response. Direct experimental verification of this type would erase any doubts present in application of the technique. Direct experimental verification of the performance of the dynamic gas temperature measurement system is outside the scope of the current contract. The first recommendation for further work is, therefore, to define and conduct a controlled experiment which will yield a direct comparison between known input temperature signals and compensated thermocouple output.

A second area requiring further investigation concerns probe durability and obtaining increased probe life. The F100 engine test series demonstrated about one hour probe life for the present design. As described in the Task IV section of this report, the structural design of the probe was more than adequate for conditions in the engine. It is believed that the sensor element durability is extremely sensitive to particulate content in the airstream, especially during engine transients, and, at this time particulate content in the airstream is the hypothesis for failure. Increase in probe durability could be obtained by reducing sensor element and support wire lengths. Also, it is recommended that (1) the ceramic stick be modified at its tip to allow more complete packing of ceramic cement into the holes; and (2) the support wires be left straight rather than bent. Attempting to bend the support wires to mount the two elements in the same plane at probe centerline may have caused unacceptable stress concentrations and inadvertently aided probe failure. Fabrication and use of a probe retraction mechanism would also alleviate effects of particulates which occur during transients.

SECTION V
APPENDICES

A. LITERATURE SURVEY

References Received Prior to Contract Start

1. Yule, A. J., D. S. Taylor, and B. A. Chigier, "On-Line Digital Compensation and Processing of Thermocouple Signals for Temperature Measurement in Turbulent Flames," AIAA 16th Aerospace Sciences Meeting, 16-18 January 1978, Paper No. 78-30.

2. Shepard, E., and I. Warshawsky, "Electrical Techniques for Time Lag Compensation of Thermocouples Used in Jet Engine Gas Temperature Measurements," ISA Proceedings, 1952, pp. 149-154.

3. Allen, J., "Evaluation of Fast Response Temperature Sensor," P&WA Internal Memo, FR-4365, 12 March 1971.

4. Dils, R. R., and P. S. Follansbee, "Wide Bandwidth Gas Temperature Measurements in Combustor and Combustor Exhaust Gases," 1976, ISA ASI 76245 (307-328).

5. Dils, R. R., and P. S. Follansbee, "Heat Transfer Coefficients Around Cylinders in Crossflow in Combustor Exhaust Gases," Journal of Engineering for Power, Trans. ASME, October 1977, p. 497.

6. Dils, R. R., "Dynamic Gas Temperature Measurements in Gas Turbine Transition Duct Exit," Journal of Engineering for Power, Trans. ASME, Series A, Vol. 95, No. 3, 1973, p. 265.

7. Dils, R. R., "Measurement of Engine Temperature at the Front Plane of a JT8D-1 Turbine Inlet Nozzle Guide Vane; Sensor Design and Analysis, P&WA Internal Report 68-037, 10 September 1968.

8. "Rugged Fast-Response Temperature Probe," NASA Technical Briefs, Winter 1979, pp. 531 and 532.

9. Friedman, R., Fourth Symposium (International) on Combustion, p. 259, Baltimore, The Williams & Wilkins Company, 1953.

10. Leah, A. S., and W. Carpenter, Fourth Symposium (International) on Combustion, p 274, Baltimore, The Williams & Wilkins Company, 1953.

11. Olsen, L. O., "Catalytic Effects of Thermocouple Materials," National SAE Aeronautics Meeting, New York, 1962, paper 524G.

12. Marshall, R. L., R. R. Strange, D. G. Sanders, P&WA/CPD, East Hartford Private Communication, 1981.

13. Kaskan, W. E., Sixth Symposium (International) on Combustion p. 16, New York, Reinhold, 1956.

14. Fristrom, R. M., and A. A. Westenberg, "Flame Structure," Chapters 8, 9, 13, 14, New York, McGraw-Hill, 1965.

15. Allan, J., "Thermocouple Design Manual," SMRFR 1660, Florida, Pratt & Whitney Aircraft, 1973.

16. "Measurement of Engine Temperature Sensor Design Analysis," Middletown, CT, P&WA 68037, 1968.

17. P&WA Design Manual, pp. 23.2.5 and 23.2.6.

18. Moffat, R. J., "Gas Temperature Measurement," Temperature, its Measurement and Control in Science and Industry, Vol. 3, 1962.

19. Collins, J. O., and W. W. Robinson, "Data Processing Handbook," P&WA/GPD Internal Report SMR FF-6165, 15 December 1973.

20. Eckbreth, A. C., et. al., "Review of Laser Raman and Fluorescence Techniques for Practical Combustion Diagnostics," Task I Report, EPA Contract 68-02-2176.

21. Borkowski, C. J., et. al., "A New Method of Johnson Noise Thermometry," Rev. Sci. Instr. 45, No. 2 (February 1974) p. 151.

22. See, for example, Marsden, R. S., "The Electrical Noise Turbulent Flames," Fourth Symposium (International) on Combustion, 1953, p. 683, or Calcote, H. F., "Ion Production and Recombination in Flames," Eighth Symposium (International) on Combustion, 1962, p. 184.

23. Glaser, F. M., "Comparison of the Time Response of Various Thermocouple Probes," P&WA Experimental Test Department Short Memorandum Report No. 4186, February 1966.

24. Bradley, D. and K. J. Matthews, "Measurement of High Gas Temperatures With Fine Wire Thermocouples," Journal of Engineering Science, Vol. 10, No. 4, 1968, pp. 299-305.

25. Stickney, T. M., "Recovery of Time-Response Characteristics of Six Thermocouple Probes in Subsonic and Supersonic Flow," NACA Tech. Note 3455, July 1955.

26. Glawe, G. E., and R. C. Johnson, "Experimental Study of Heat Transfer to Small Cylinders in a Subsonic, High-Temperature Gas Stream," NACA Tech. Note 3934, May 1957.

Literature Survey References Received

1. Stradle, W. C., and M. Muthukrishnan, "Thermocouple Time Constant Measurement by Cross Power Spectra," AIAA Journal, Vol. 14, No. 11, pp. 1642-1644, November 1976.

2. Davis, M. R., "General Response of Resistance Thermometers and Thermocouples in Gases at Low Pressures," AIAA Journal, Vol. 10, No. 4, pp. 546 and 547, April 1972.

3. Schlader, A. F., P. Rouiller, and J. Odgers, "Some Considerations of the Measurement of Temperatures Within Aircraft Combustion Chambers, Using a Calorimetric Probe," Proceedings of an International Propulsion Symposium, Coll. of Aeronautics, 15-17 April 1969, pp. 363-381.

4. Rein, C. R., and J. R. O'Loughlin, "Measurement of Error of Temperature Sensors in Flowing Gases," AIAA Journal, Vol. 10, No. 7, pp. 954-956, July 1972.

5. Schwedland, R. P., and M. F. Hall, "Instrumenting a Stoichiometric Turbine Development Engine," Instrumentation for Airbreathing Propulsion: Proceedings of the Symposium, Monterey, CA, 19-21 September 1972, MIT Press, 1974, pp. 387-396.

6. Schacher, G. E., and C. W. Fairall, "Producing Small Scale Temperature Fluctuations in an Airstream," Rev. Sci. Instrum., Vol. 49, No. 10, October 1978.

7. Chigier, N. A., "Instrumentation Techniques for Studying Heterogeneous Combustion," Prog. Energy Combustion Sci., Vol. 3, pp. 175-189, 1977. Pergamon Press. Printed in Great Britain.

8. Lockwood, F. C., and A. O. Odidi, "Measurement of Mean and Fluctuating Temperature and Ion Concentration in Round Free-Jet Turbulent Diffusion and Premixed Flames," Symp. on Combust. 15th Int. Proc., Tokyo, Japan, 25-31 August 1974. pp. 561-571, published by Combustion Inst., Pittsburgh, PA, 1975.

9. Panteleev, A. A., and V. A. Trushin, "Determination of Unsteady Gas-Stream Temperature Using Slow-Response Thermocouples," Soviet Astronautics, Vol. 19, No. 1, 1976, pp. 125-130.

10. Miles, R. B., "Resonant Doppler Velocimeter, "Appl. of Nonintrusive Instru. in Fluid Flow Research," AGARD Conf. Proc. No. 193, May 1976, Paper No. 19.

11. Glawe, G. E., R. Holanda, and L. N. Krause, "Standardized Gas-Temperature Probes," NASA Tech. Briefs B78-10392, Fall 1978.

12. Durao, D. F. G., and J. H. Whitelaw, "Instantaneous Velocity and Temperature Measurements in Oscillating Diffusion Flames," Contemo. Physics, Vol. 17, No. 3, May 1976, pp. 249-274.

13. Kamper, R. A., "Survey of Noise Thermometry," Symp. on Temperature, 5th, Washington, DC, 21-24 June 1971, Proceedings, ISA, 1972, pp. 349-354.

14. Actis, A., A. Cibrario, and L. Crovini, "Methods of Noise Thermometry Above 400°C," Symp. on Temperature, 5th, Washington, DC, 21-24 June 1971, Proceedings, ISA, 1972, pp. 355-364.

15. Buchele, D. R., "Effect of Radiometric Errors on Accuracy of Temperature Profile Measurement by the Spectral-Scanning Method," Symp. on Temperature, 5th, Washington, DC, 21-24 June 1974, Proceedings, ISA, 1972, pp. 645-656.

16. Cezairliyan, A., "Measuring Transient High Temperatures by Optical Pyrometry," Symp. on Temperature, 5th, Washington, DC, 21-24 June 1971, Proceedings, ISA, 1972, pp. 657-664.

17. Lapworth, K. C., L. A. Allnutt, and J. R. Pendlebury, "Short Duration Temperature Measurements by Infra-Red Emission-Absorption," Symp. on Temperature, 5th, Washington, DC, 21-24 June 1971, Proceedings, ISA, 1972, pp. 665-676.

18. Innes, G. L., "Use of Edge-Tone Resonators as Gas Temperature Sensing Devices," Symp. on Temperature, 5th, Washington, DC, 21-24 June 1971, Proceedings, ISA, 1972, pp. 689-700.

19. Lynnworth, L. C., and E. H. Carnevale, "Ultrasonic Thermometry Using Pulse Techniques," Symp. on Temperature, 5th, Washington, DC, 21-24 June 1971, Proceedings, ISA, 1972, pp. 715-732.

20. Reed, R. P., "Branched Thermocouple Circuits in Underground Coal Gasification Experiments," 1976, ISA 76244, pp. 295-306.

21. Glawe, G. E., H. A. Will, and L. R. Krause, "A New Approach to the Pulsed Thermocouple for High Gas Temperature Measurements," 1976, ISA 76246, pp. 329-336.

22. Baker, P. D. and R. A. Mason, "Recent Developments in Sensors for the Gas Turbine Engine," ASME Paper 78-GT-52 presented at Gas Turbine Conf. and Products Show, London, England, 9-13 April 1978.

23. Glawe, G. E., R. Holanda, and L. N. Krause, "Recovery and Radiation Corrections and Time Constants of Several Sizes of Shielded and Unshielded Thermocouple Probes for Measuring Gas Temperature," NASA-LeRC, NASA Tech. Paper 1099, 1978.

24. Vonada, J. A., "A Thermal Investigation of AFAPL Turbine Engine Heat Transfer Test Facility," Air Force Prop. Lab. Tech. Report AFAPL-TR-77-52, December 1974.

25. Kretschmer, D., and A. F. Schlader, "The Pulsed Thermocouple for Gas, Turbine Application," ASME Gas Turbine Conf., New Orleans, LA, 21-25 March 1976, Paper No. 76-GT-1.

26. Warshawsky, I., "Instrumentation for Propulsion Systems Development," Congress and Exposition, Detroit, MI, 27 February through 3 March 1978.

27. Roberts, H. C., "The Vibrating Filament Temperature Measuring System," ISA Conf. Proceedings, 26 Annual, Part 4, Chicago, IL, 1971, pp. 801.1-801.4, No. 71-801.

28. Karrer, H. E., "The Piezoelectric Resonator as a Temperature Sensor," ISA Conf. Proceedings, 26th Annual, Part 4, pp. 802.1-802.4, No. 71-802.

29. Bailey, R. G., "Fluid Oscillator Temperature Sensor," ISA Conf. Proceedings, 26th Annual, Part 4, pp. 803.1-803.7, No. 71-803.

30. Garelick, L., and E. Hauptmann, "Linearizing Thermocouple Amplifiers," ISA Conf. Proceedings, 26th Annual, Part 4, pp. 852.1-852.6, No. 71-852.

31. Smits, A. J., A. E. Perry, and P. H. Hoffmann, "The Temperature Response to Temperature Fluctuations of a Constant Current Hot-Wire Anemometer," Journal of Physics E — Scientific Instruments, Vol. VII, September 1978, pp. 909-914.

32. Small, L. L., "Turbine Engine Sensors for High Temperature Applications," Fluidics Quarterly, Vol. 4, April 1972, pp. 59-67.

33. Gray, P., and D. Thompson, "An Experimental Investigation of Thermocouple Response Times in Static Gas Environments," International Journal of Heat and Mass Transfer, Vol. 18, October 1975, pp. 1207-1211.

34. Barnes, J. H., "The measurement of Gas Temperature Using the Gas Jet Generator," Inst. of Mech. Eng. Proc. Part I, Vol. 184, No. 6, 1969-70, pp. 107-120

35. Zalmanzon, L. A., "Fluidic Methods of Measurements and Development of Sensors (Review)," Automat Remote Control, Vol. 9, September 1970, pp. 1490-1499.

36. London, G. E., "Gas Temperature and Heat Flux in Short-Lined Gasdynamic Processes," Heat Transfer — Soviet Research, Vol. 7, May-June 1975, pp. 152-157.

37. Penner, S. S., and T. Jersky, "Use of Lasers for Local Measurement of Velocity Components, Species, Densities, and Temperatures," Annual Review of Fluid Mechanics, Vol. 5, 1973, pp. 9-30.

38. Reader, G. T., "Aspects of Pulsating Combustion," Intersociety Energy Conversion Conference, 13th, San Diego, CA, August 1978, pp. 548-557.

39. Coghe, A., V. Ghezzi, S. Pasini, "Optical Temperature Measurements in a Continuous Flow Combustion Chamber," Intern. Symp. on Airbreathing Engines, 2nd, March 1974, Sheffield, England.

40. Gupta, A. K., and J. M. Beer, "On Combustion Generated Noise From Turbulent Diffusion Gaseous Flames," Applied Acoustics, Vol. 11, No. 1, January 1978, pp. 35-55.

41. Smith, J. R., and W. H. Giedt, "Flow Field Temperature Distribution Determination Using Rotational Raman Spectroscopy," International Heat Transfer Conf., 5th, Proceedings, Tokyo, Japan, September 1974, Vol. 5, pp. 239-243, Paper No. MA1.1.

42. Cook, W. J., and M. A. Renaud, "Analysis and Interpretation of the Response of Coated Thin — Film Heat Flux Gases," International Heat Transfer Conf., 5th, Proceedings, Tokyo, Japan, September 1974, Vol. 5, pp. 283-287, Paper No. MA2.3.

43. Dubrovskii, O. V., "Analysis of Low-Frequency Pulsations in Gas Turbine Combustion Chambers," translation of Teploenergetika (USSR), 1961, Vol. 8, No. 8, pp. 32-37.

44. Antonov, A. N., and M. S. Sladkevick, "Experimental Investigation of a High-Temperature Jet," Fluid Dynamics, Vol. 13, No. 5, September-October 1975, pp. 761-764.

45. Farag, I. H., "Temperature Profiles in Combustion Gases by Inversion: Review and Approach," ASME Paper No. 79-HT-21 for Meeting 6-8 August 1979.

46. Vagnin, S. P., and Yu. A. Yakobi, "Measurement of the Temperature of Gas Media Containing Carbon Dioxide by the Laser-Probing Method," J. Eng. Physics, Vol. 35, No. 1, July 1978, pp. 769-772.

47. Krylovich, V. I., and A. D. Soloduklin, "Acoustic Method of Investigating Nonstationary Heat Convection in Cylindrical Layers of Gases and Liquids," J. Eng. Physics, Vol. 31, No. 6, December 1976, pp. 1477-1482.

48. Chigier, N. A., "Instrumentation Techniques for Studying Heterogeneous Combustion," Combustion Inst. Cent. States Sect. Spring Meet, NASA-Lewis, 28-30 March 1977.

49. Lee, C. S., and J. E. Kim, "Frequency Response Technique for Measuring the Thermal Conductivity of Gases at Low Pressures," Pac. Chem. Eng. Congr., 1st, Kyoto, Japan, 10-14 October 1972, Part 3, Paper 15-2, pp. 150-159.

50. Simbirskii, D. F., "Characteristics of the Dynamic Calibration of an Instrument for Measuring the Instantaneous Temperatures of Gas Flows," Foreign Technology Div. Wright-Patterson AFB, OH, 24 August 1967, Report No. FTD-HT-23-874-67.

51. Nesterikhin, Yu. Ye., "Methods of High-Speed Measurements in Gas Dynamics and Plasma Physics," NASA, Washington, DC, September 1968, Report No. NASA-TT-F-12202.

52. Arbib, H. A., Y. Goldman, and Y. Manheimer-Timnat, "The Influence of Pressure on Combustion Intensity," Int. Colloquium on Gasdynamics of Explosions and Reactive Systems, 6th, Stockholm, Sweden, 22-26 August 1977, Acta Astronautica, Vol. 5, November-December 1978, pp. 1221-1230.

53. Ruffino, G., "Progress in Laboratory High Temperature Measurement," High Temperatures — High Pressures, Vol. 9, No. 3, 1977, pp. 253-267.

54. Pelepeichenko, I. P., "Operations of Heat Detector-Corrector System in Conditions of Nonstationary Convection-Gas Temperature Measurements," Aviatsionnyi Institute, Kharkov, UK, USSR, Priborostroenie, Vol. 20, No. 6, 1977, pp. 114-116.

55. Menshikov, V. I., "A Method for Measuring Gas — Stream Temperature Using Two Thermocouples," Institute Geokhimil, Irkutsk, USSR, Inzhenerno-Fizicheskii Zhurnal, Vol. 31, November 1976, pp. 794-799.

56. Shaleav, A. M., and A. L. Kholodenko, "Change in Thermocouple Readings Under the Influence of a Flow of Charged Particles," Metallofizika, No. 57, 1975, pp. 84-93.

57. Obrien, W. J., "Temperature Measurement for Gas Turbine Engines," SAE Automotive Eng. Congress and Exp., Detroit, MI, 24-28 February 1975, 10 pgs.

58. Pelepeichenko, I. P., and Iu. N. Dotsenko, "Allowing for Thermocouple Error Caused by a Protective Shield," Priborostroenie, Vol. 16, No. 10, 1973, pp. 102-104.

59. Baas, P. B., and K. Mai, "Trends in Design in Gas Turbine Temperature Sensing Equipment," Symp. on Temperature, 5th, Washington, DC, 21-24 June 1971, Proceedings, Part 3.

60. Dotsenko, Iu. N., "Thermocouple Circuits for Measurement of Unsteady Temperatures in Gases by the Two-Thermoreceiver Method and Analysis of Thermocouple Circuit Errors," Samoletostroenie i Tekhnika Vozdashnogo Flota, No. 28, 1972, pp. 20-25.

61. Dotsenko, Iu. N., I. P. Pelepeichenko, and V. G. Volkov, "Determination of Alignment Parameter of a Compensating Network in the Gas Turbine Engine," Samoletstroenie i Tekhnika Vozdushnogo Flota, No. 25, 1971, pp. 46-50.

62. Bekaert, G., "A Fluidic Oscillator for Temperature Measurement," International Federation of Automatic Control, Symp. on Fluidics, 2nd, Prague, Czechoslovakia, 28 June through 2 July 1971.

63. Baum, D. W., S. P. Gill, W. L. Shimmin, and J. D. Watson, "Thermal Noise Emissions from a Hot Gas," ARTEC Associates, Inc. Hayward, CA, March 1981, Report No. FR-153.

64. Bergman, P., and W. K. Bullivant, "A Compression Heating Device for Agent Tolerance Studies: III, Thermocouple Response Study," Fort Detrick, Frederick, MD, Technical Memo, January 1968, Report No. SMUFD-TM-127.

65. Gruszczynski, J. S., C. J. Harris, D. A. Rogers, and W. R. Warren, "Fast Response Total Radiation Gage for Measurement of Radiant Emission from High Temperature Gas," GE Co., Philadelphia, PA, Missile and Space Div., Report No. R 63SD11, January 1963.

B. PLATINUM/RHODIUM ALLOY PROPERTIES

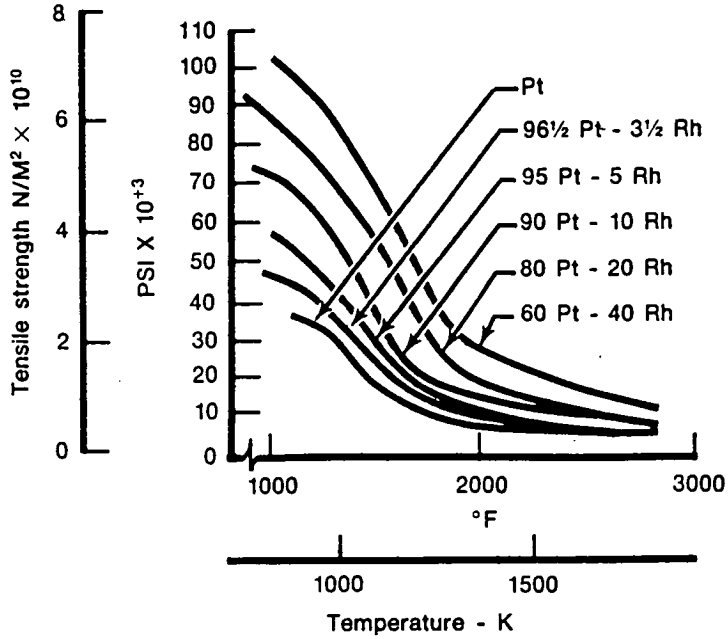

FD 238840

Figure B.1. Platinum/Rhodium Alloy Strength

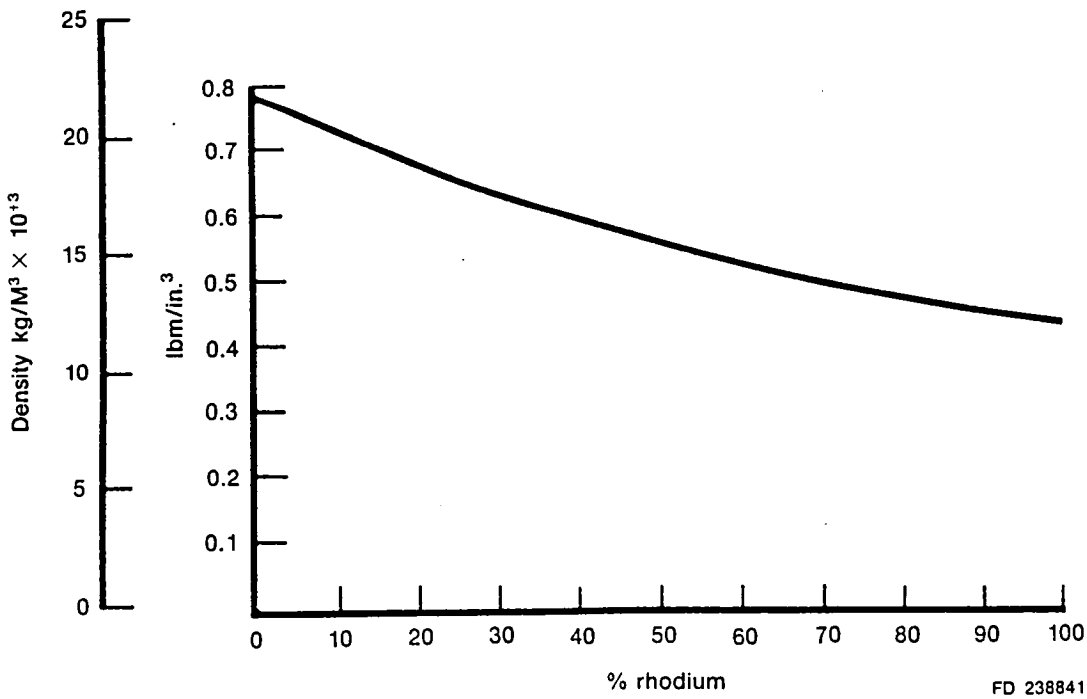

FD 238841

Figure B.2. Platinum/Rhodium Alloy Density

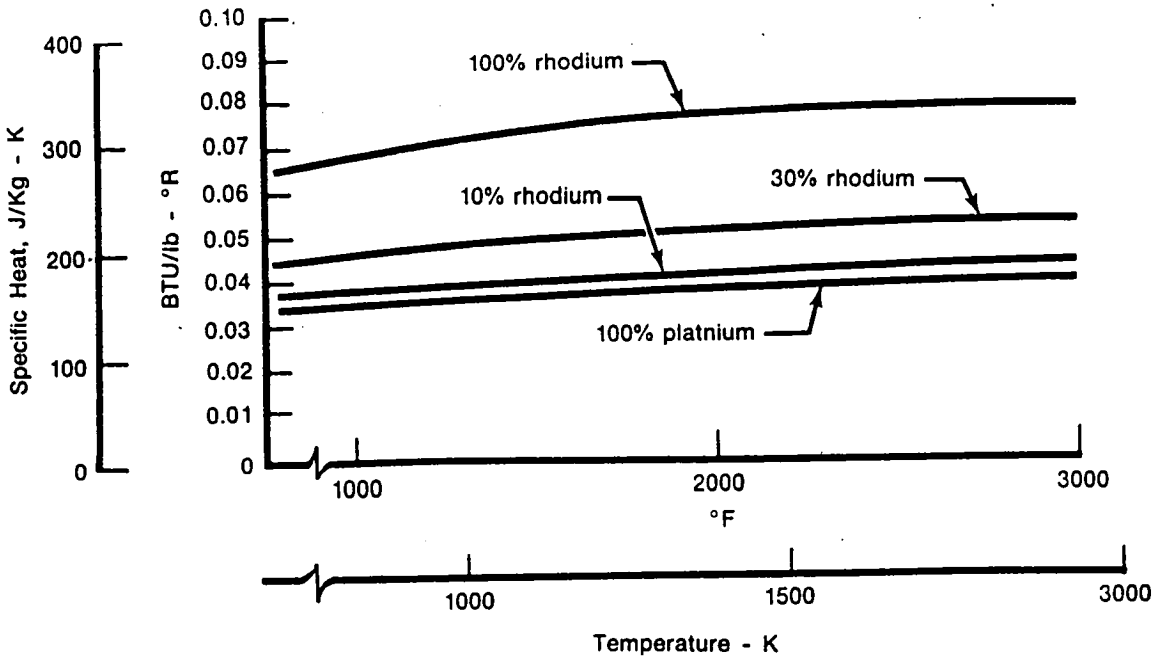

Figure B.3. Platinum/Rhodium Alloy Specific Heat

FD 238842

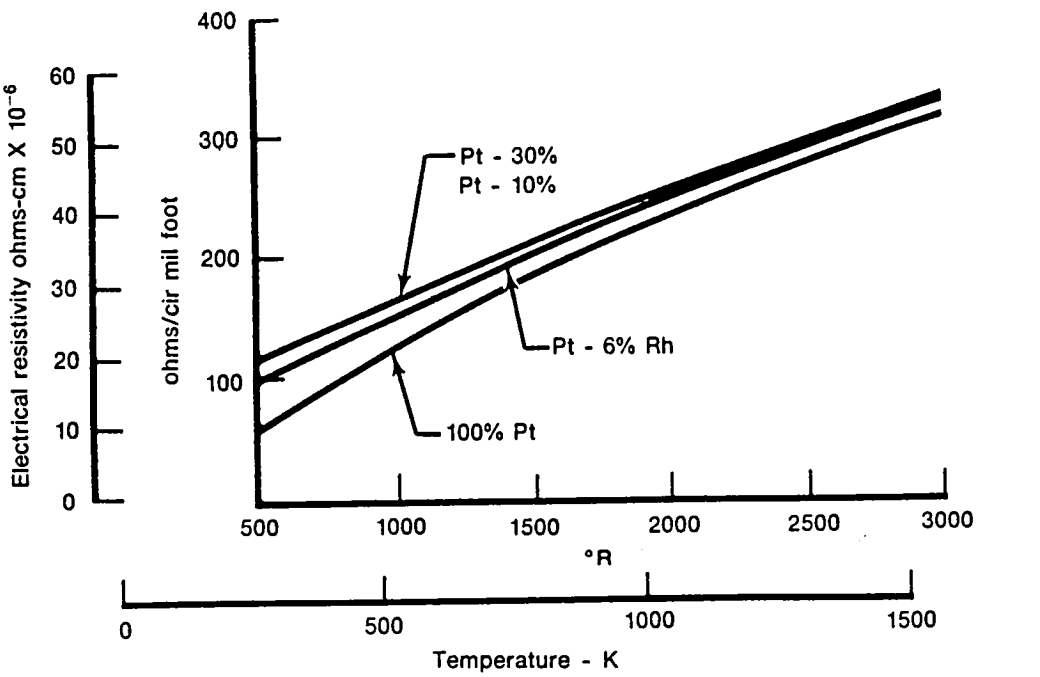

FD 238844

Figure B.4. Platinum/Rhodium Alloy Electric Resistivity

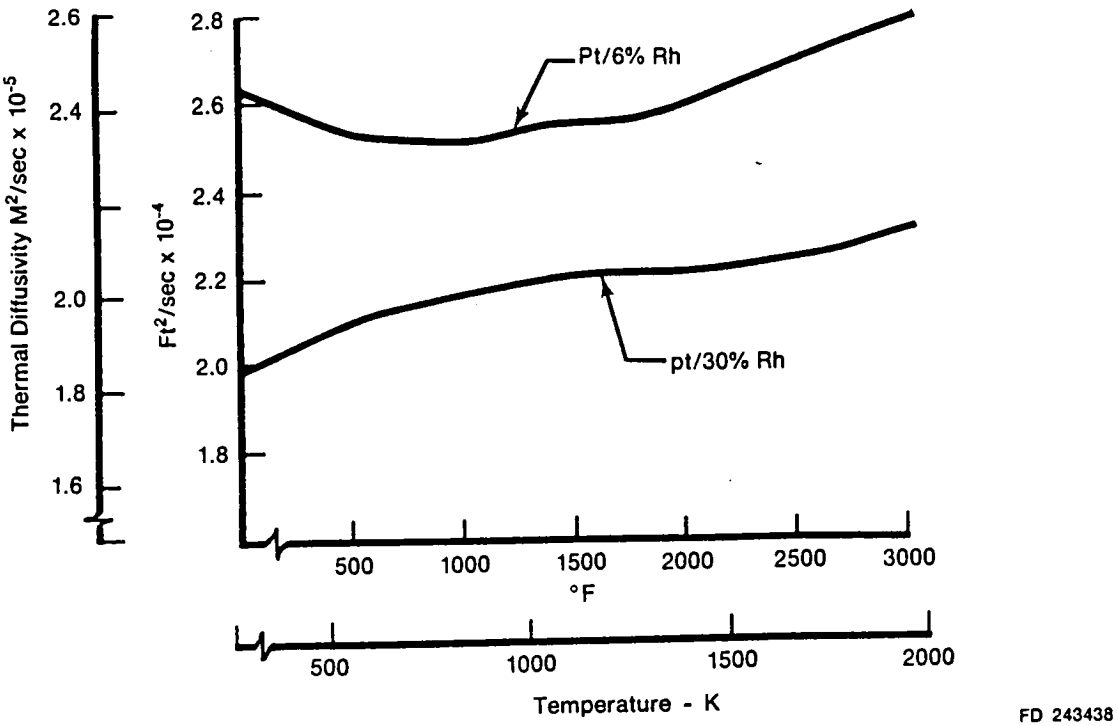

Figure B.5. Platinum/Rhodium Alloy Thermal Diffusivity

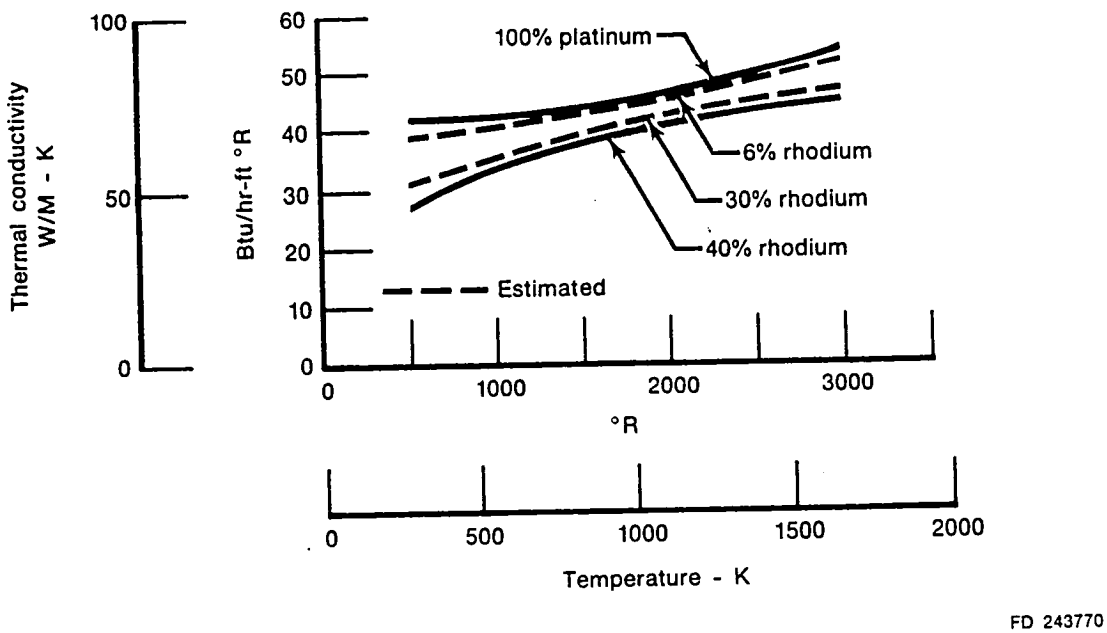

Figure B.6. Platinum/Rhodium Alloy Thermal Conductivity

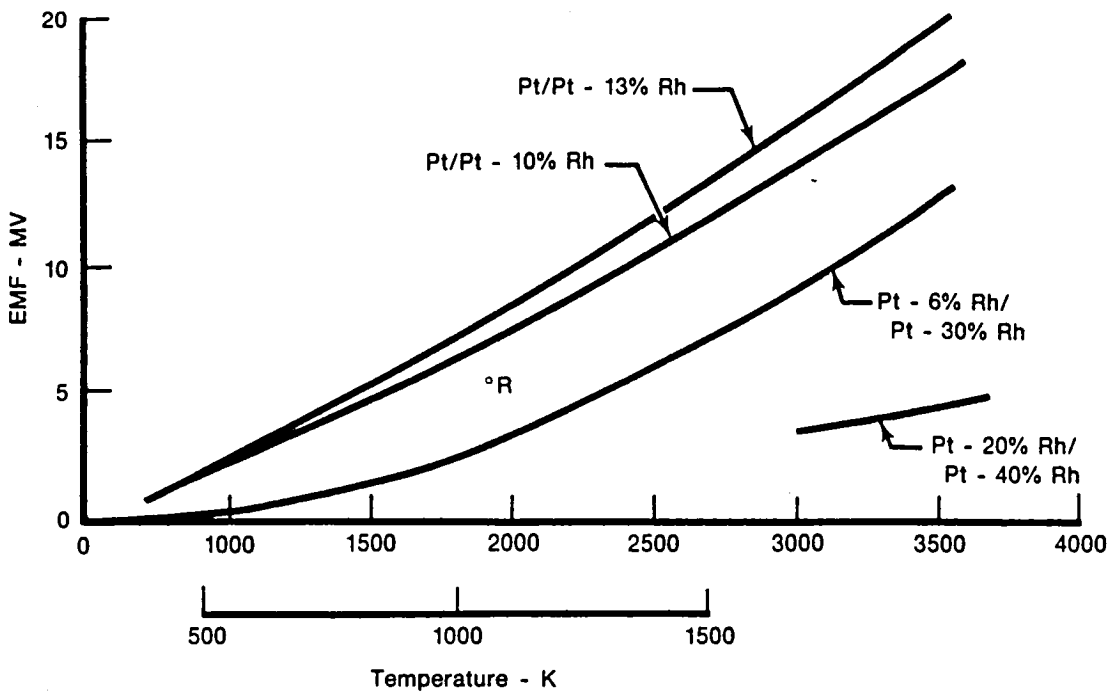

Figure B.7. Platinum/Rhodium Alloy Thermal EMF

C. COMBUSTION GAS PROPERTIES

The following properties are for the combustor gases at the combustion exit of the F100 engine:

Figure C.1. Specific Heat Ratio (γ)
Figure C.2. Specific Heat (C_p)
Figure C.3. Thermal Conductivity
Figure C.4. Viscosity

The properties are presented over the temperature range (0-2000K) and fuel/air ratio range (0.01 to 0.03) which encompasses the F100 operating range. In addition, the properties are independent of pressure over the F100 operating range.

In addition, the density and sonic velocity can be calculated using perfect gas equations and a molecular weight of 28.95. The equations are:

Density, $\rho = 3.4816 \times 10^{-3} \frac{P}{T}$

where: ρ = Kg/M^3
T = K
P = N/M^2

or

$\rho = 2.69825 \frac{P}{T}$

where: ρ = lb/ft^3
T = °R
P = PSIA

Sonic Velocity, $C = 16.96 \sqrt{\gamma T}$

where: C = m/sec
γ = Dim-less
T = K

or

$C = 41.454 \sqrt{\gamma T}$

where: C = ft/sec
γ = Dim-less
T = °R

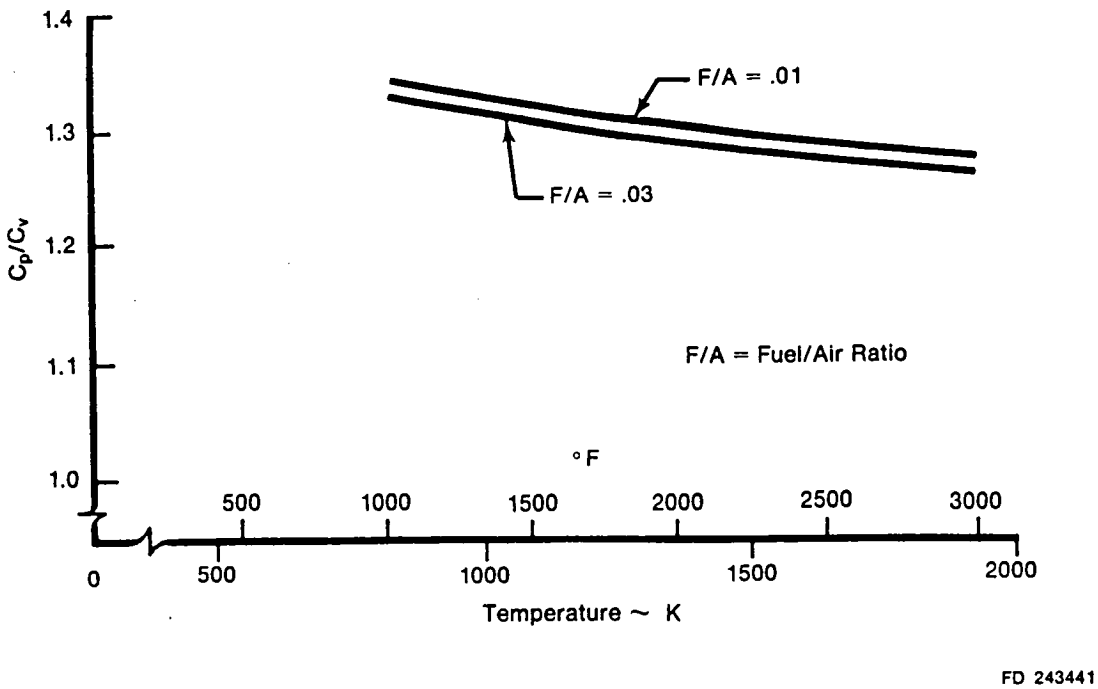

Figure C.1. Combustion Gas Specific Heat Ratio

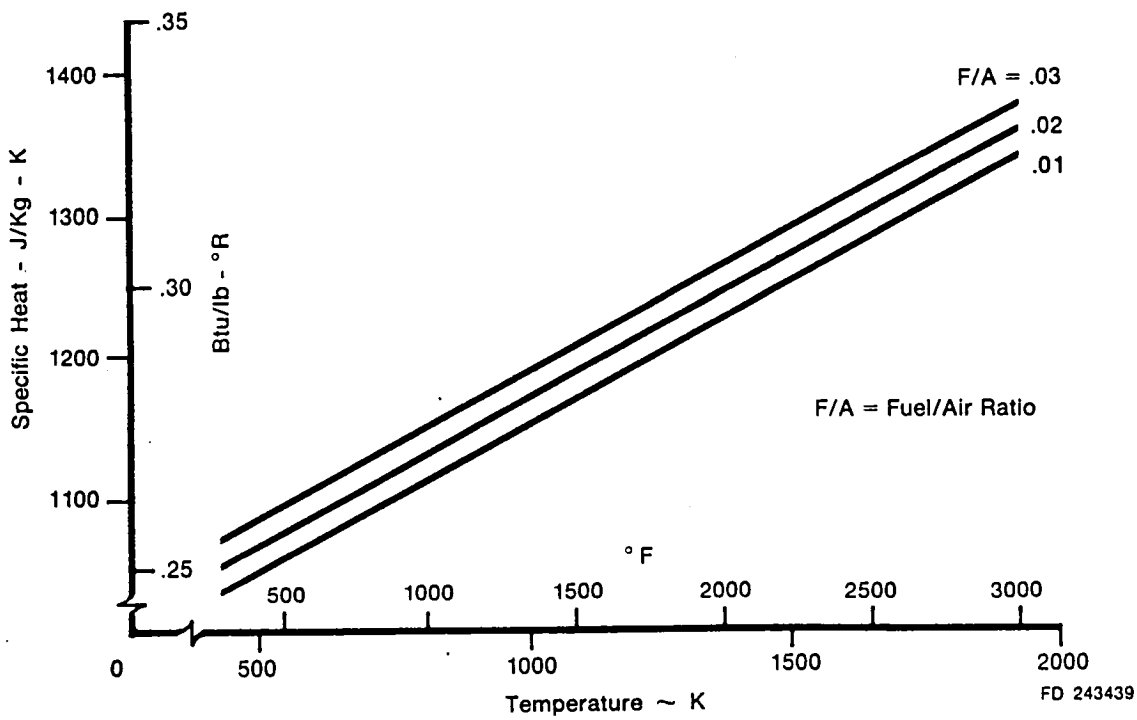

Figure C.2. Combustion Gas Specific Heat

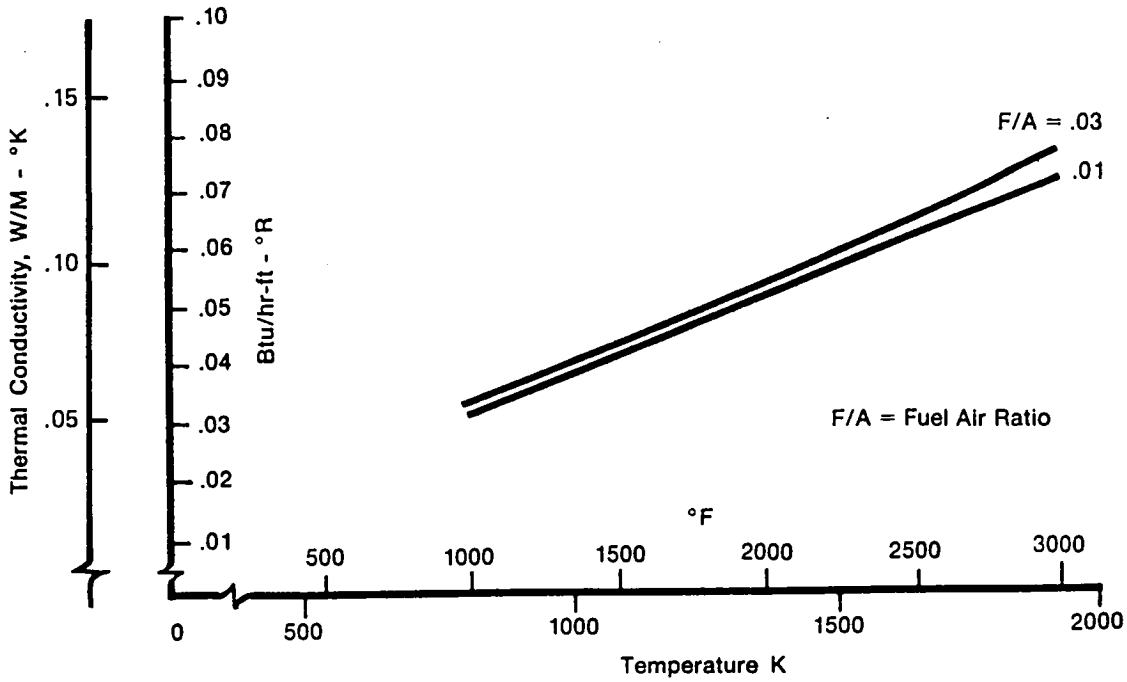

Figure C.3. Combustion Gas Thermal Conductivity

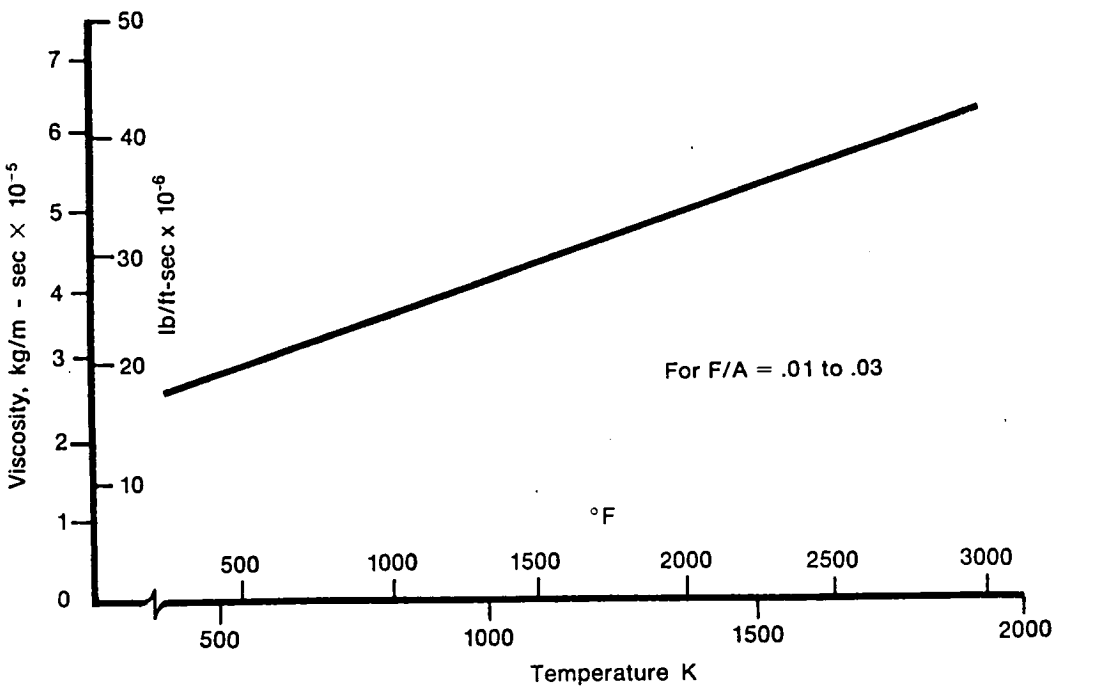

Figure C.4. Combustion Gas Viscosity

D. PROBE DRAWINGS

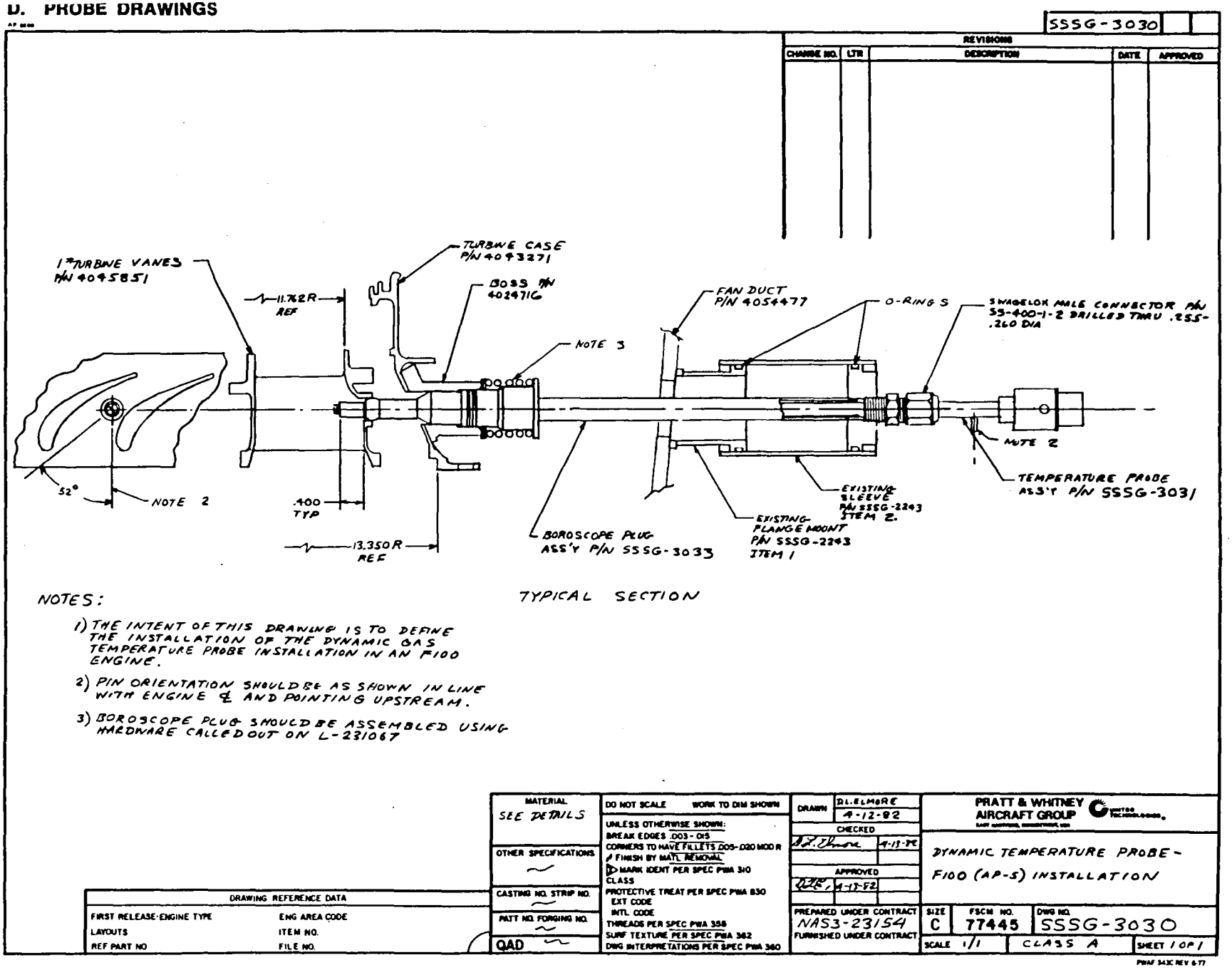

Figure D.1. Dynamic Temperature Probe — F100 (AP-5) Installation

FD 243445

SSSG-303I

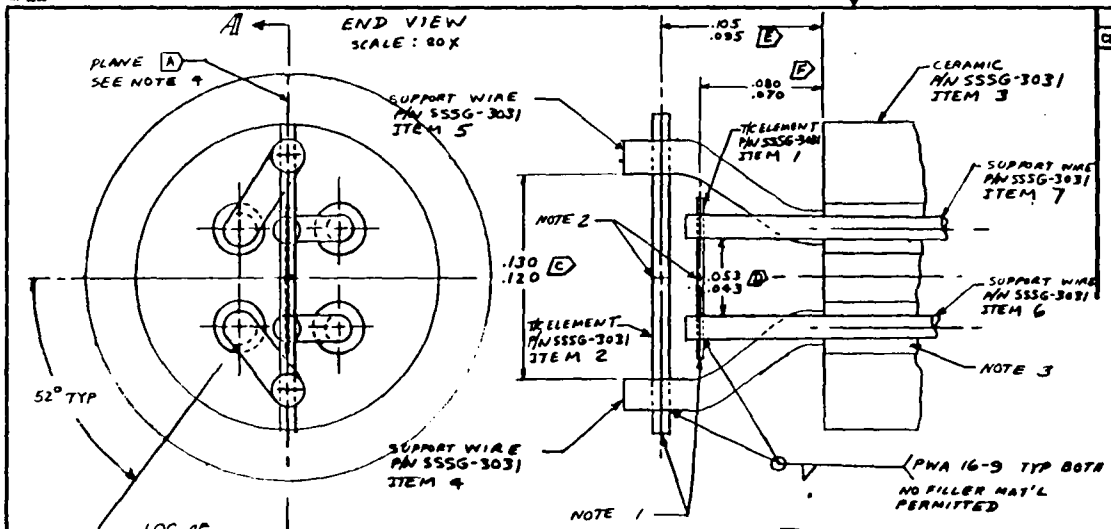

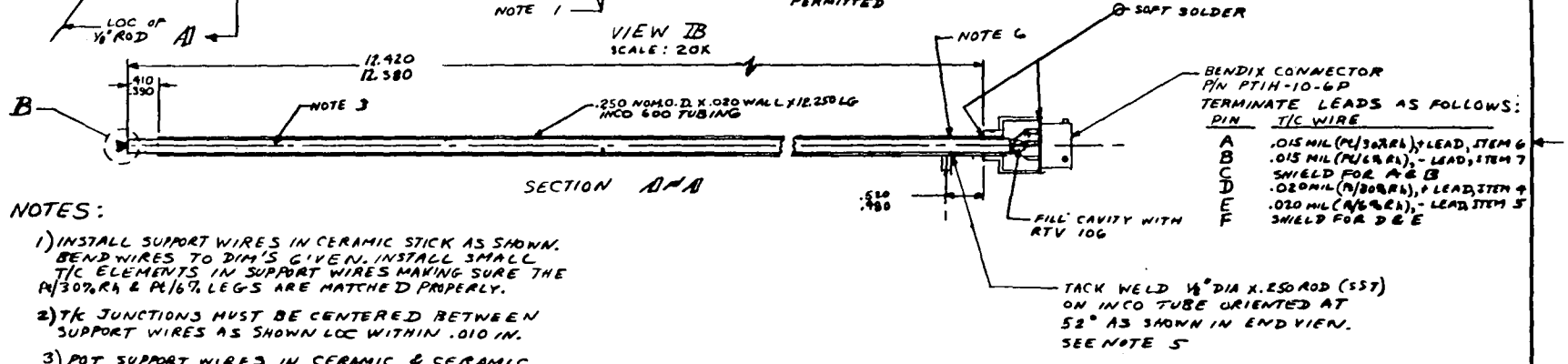

SECTION AAA

REVISIONS				
CHANGE NO.	LTR	DESCRIPTION	DATE	APPROVED

NOTES:

1) INSTALL SUPPORT WIRES IN CERAMIC STICK AS SHOWN. BEND WIRES TO DIM'S GIVEN. INSTALL SMALL T/C ELEMENTS IN SUPPORT WIRES MAKING SURE THE Pt/30% Rh & Pt/6% LEGS ARE MATCHED PROPERLY.

2) T/C JUNCTIONS MUST BE CENTERED BETWEEN SUPPORT WIRES AS SHOWN LOC WITHIN .010 IN.

3) POT SUPPORT WIRES IN CERAMIC & CERAMIC IN INCO TUBE WITH SERMETEL P-1, AIR DRY FOR 30 MIN @ RM. TEMP, OVEN BAKE 1 HR. @ 150°F, INCREASE OVEN TEMP TO 650°F FOR 1HR, OVEN COOL.

4) FINAL ASS'Y REQUIRES THAT T/C ELEMENTS BE LOCATED IN THE SAME PLANE (A) WITHIN .005 IN.

5) ROD INDICATES ENGINE ℄ AND SHOULD BE POINTING UPSTREAM IN ENG ASS'Y.

6) TACK WELD 5 WIN T/C ON INCO TUBE O.D USING BX-6504 3 SOFT T/C WIRE CABLE. CABLE LENGTH IS 30 FEET TERMINATED WITH A MALE MARLIN T/C CONNECTOR.

7) MEASURE FINAL DIM'S C, D, E, & F & RECORD

DRAWING REFERENCE DATA	
FIRST RELEASE-ENGINE TYPE	ENG AREA CODE
LAYOUTS	ITEM NO.
REF PART NO	FILE NO.

MATERIAL	SEE DETAILS
OTHER SPECIFICATIONS	~
CASTING NO. STRIP NO.	
PATT NO. FORGING NO.	
QAD	~

DO NOT SCALE WORK TO DIM SHOWN

UNLESS OTHERWISE SHOWN:
BREAK EDGES .003 - .015
CORNERS TO HAVE FILLETS .006 - .020 MOD R
FINISH BY MATL REMOVAL
MARK IDENT PER SPEC PWA 340
CLASS
PROTECTIVE TREAT PER SPEC PWA 830
EXT CODE
INTL CODE
THREADS PER SPEC PWA 35S
SURF TEXTURE PER SPEC PWA 342
DWG INTERPRETATIONS PER SPEC PWA 360

DRAWN	D.L. ELMORE	9-13-82
CHECKED	D.F. [illegible]	9-13-82
APPROVED	[illegible]	9-0-82

PREPARED UNDER CONTRACT NAS3-23159
FURNISHED UNDER CONTRACT

PRATT & WHITNEY AIRCRAFT GROUP
UNITED TECHNOLOGIES

DYNAMIC GAS TEMPERATURE PROBE ASS'Y FOR F100

SIZE	FSCM NO.	DWG NO.
C	77445	SSSG-3031
SCALE 1/1	CLASS A	SHEET 1 OF 8

PWAF 343C REV 6-77

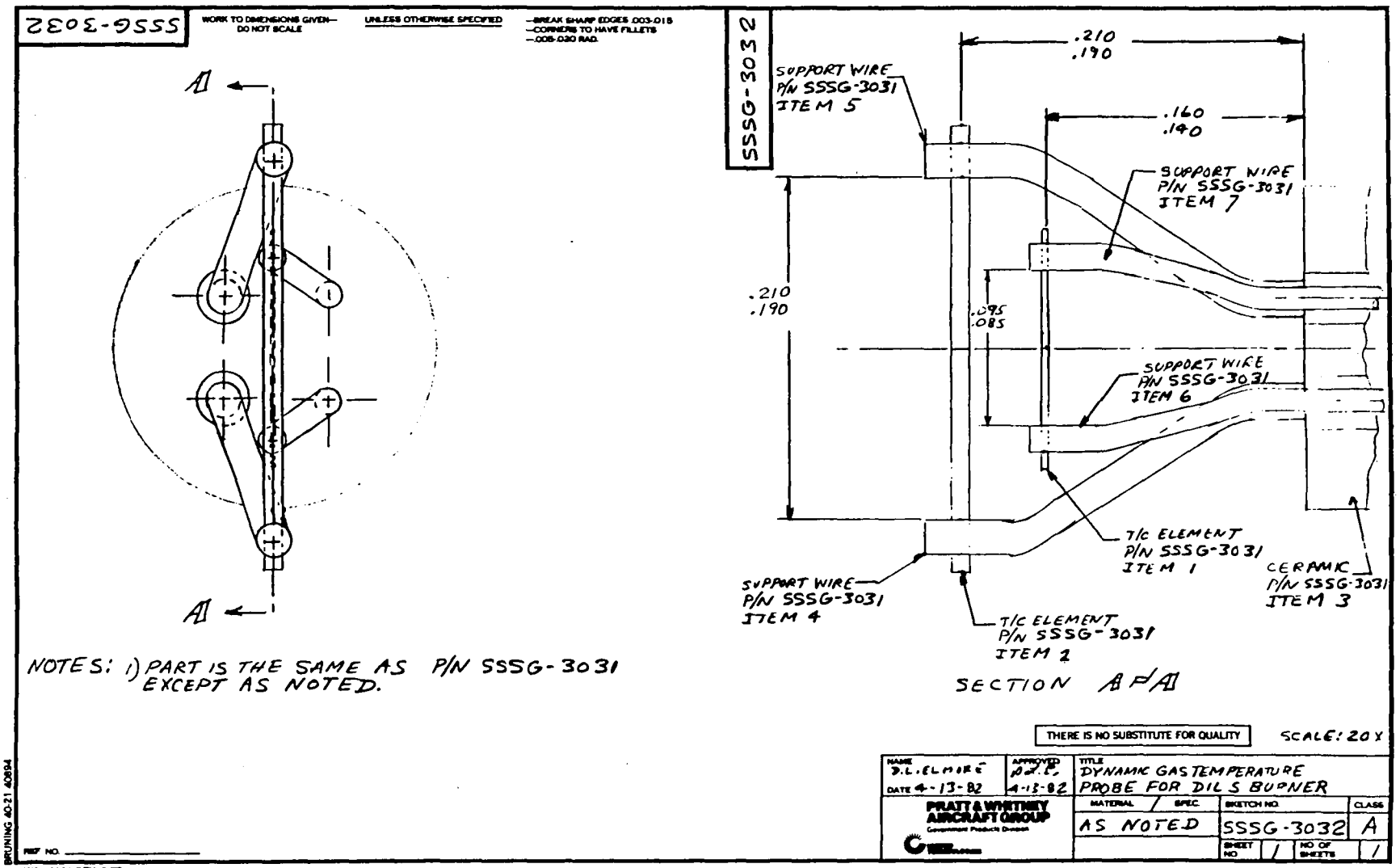

Figure D.3. Dynamic Gas Temperature Probe for Subscale Combustor

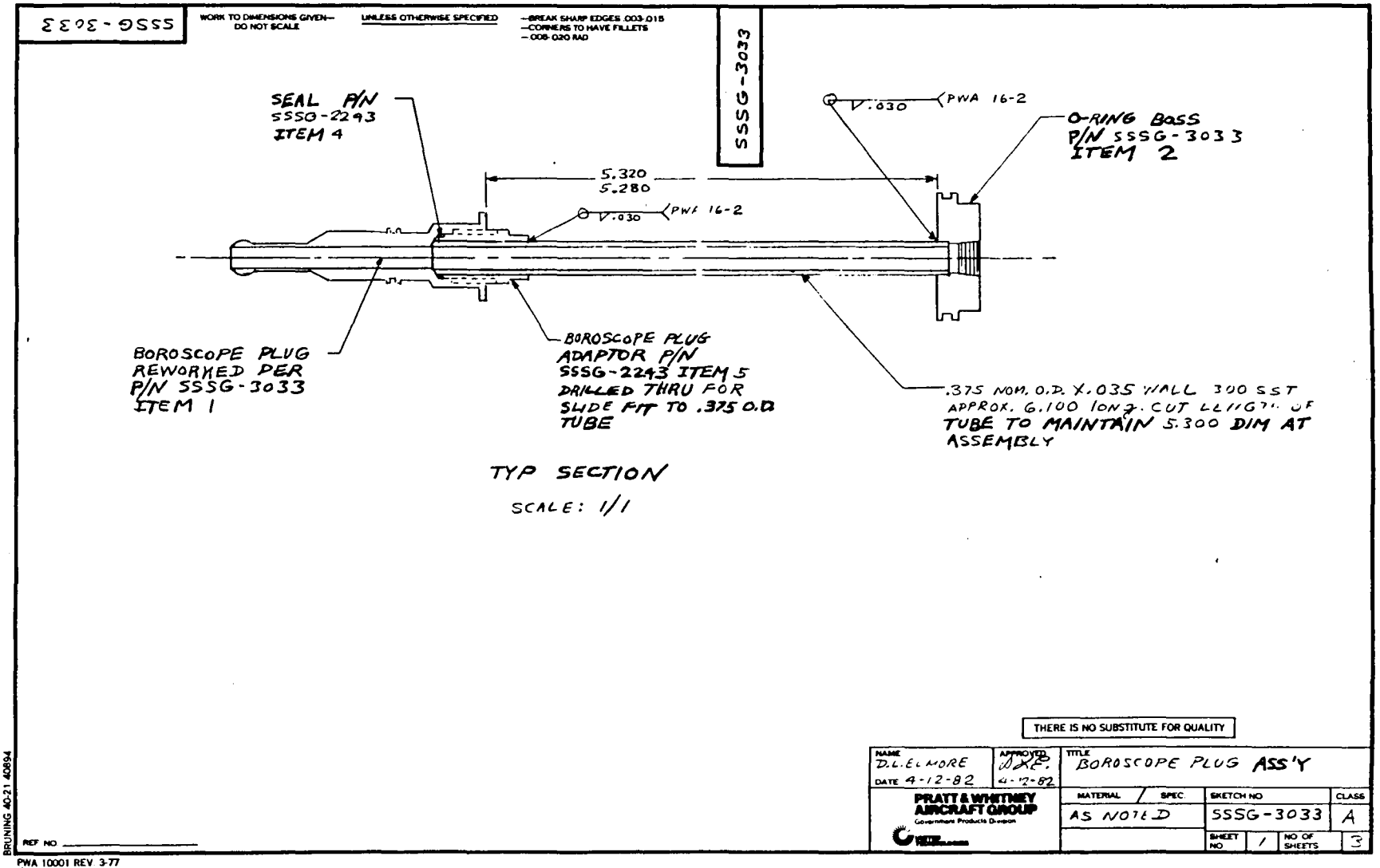

Figure D.4. Borescope Plug Assembly

E. DERIVATION OF ELECTRICAL ANALOG OF NINE NODE FINITE ELEMENT THERMOCOUPLE MODELS

For the finite element electrical schematic shown in Figure E-1, the current flow equations for each node can be defined as follows:

$$C_0 \frac{dE_9}{dt} = \frac{1}{R_1}(E_8 - E_9) + \frac{1}{R_0}(E_G - E_9)$$

$$C_1 \frac{dE_8}{dt} = \frac{1}{R_1}(E_9 + E_7 - 2E_8) + \frac{1}{R_3}(E_G - E_8)$$

$$C_1 \frac{dE_7}{dt} = \frac{1}{R_1}(E_8 + E_6 - 2E_7) + \frac{1}{R_3}(E_G - E_7)$$

$$C_2 \frac{dE_6}{dt} = \frac{1}{R_1}(E_7 - E_6) + \frac{1}{R_2}(E_5 - E_6) + \frac{1}{R_4}(E_G - E_6)$$

$$C_3 \frac{dE_5}{dt} = \frac{1}{R_2}(E_4 + E_6 - 2E_5) + \frac{1}{R_5}(E_G - E_5)$$

$$C_3 \frac{dE_4}{dt} = \frac{1}{R_2}(E_3 + E_5 - 2E_4) + \frac{1}{R_5}(E_G - E_4)$$

$$C_3 \frac{dE_3}{dt} = \frac{1}{R_2}(E_2 + E_4 - 2E_3) + \frac{1}{R_6}(E_G - E_3)$$

$$C_3 \frac{dE_2}{dt} = \frac{1}{R_2}(E_1 + E_3 - 2E_2)$$

$$C_3 \frac{dE_1}{dt} = \frac{1}{R_2}(E_2 + E_0 - 2E_1)$$

Rearranging the electrical current flow equations in the same form as the equivalent thermal equations results in the following sets of equation pairs:

Node 1

$$\frac{\Delta_2}{\alpha}\frac{dT_1}{\Delta t} = (T_0 + T_2 - 2T_1)$$

$$R_2 C_3 \frac{dE_1}{dt} = (E_0 + E_2 - 2E_1)$$

Node 2

$$\frac{\Delta_2}{\alpha}\frac{dT_2}{\Delta t} = (T_1 + T_3 - 2T_2)$$

$$R_2 C_3 \frac{dE_2}{dt} = (E_1 + E_3 - 2E_2)$$

Node 3

$$\frac{\Delta_2}{\alpha}\frac{dT_3}{\Delta t} = (T_2 + T_4 - 2T_3) + \frac{2h'\,\Delta^2}{kD}(T_G - T_3)$$

$$R_2 C_3 \frac{dE_3}{dt} = (E_2 + E_4 - 2E_3) + \left(\frac{R_2}{R_6}\right)(E_G - E_4)$$

Node 4

$$\frac{\Delta_2}{\alpha}\frac{dT_4}{\Delta t} = (T_3 + T_5 - 2T_4) + \frac{4h'\,\Delta^2}{kD}(T_G - T_4)$$

$$R_2 C_3 \frac{dE_4}{dt} = (E_3 + E_5 - 2E_4) + \left(\frac{R_2}{R_5}\right)(E_G - E_4)$$

Node 5

$$\frac{\Delta_2}{\alpha}\frac{dT_5}{\Delta t} = (T_4 + T_6 - 2T_5) + \frac{4h'\,\Delta^2}{kD}(T_G - T_5)$$

$$R_2 C_3 \frac{dE_5}{dt} = (E_4 + E_6 - 2E_5) + \left(\frac{R_2}{R_5}\right)(E_G - E_5)$$

Node 6

$$\frac{1}{2\alpha}\left(\frac{D^2\Delta\delta}{d^2} + \delta^2\right)\frac{\Delta T_6}{\Delta t} = (T_7 - T_6) + \frac{\delta D^2}{\Delta d^2}(T_5 - T_6)$$

$$+ \frac{2}{kd^2} = (h'D\Delta\delta + hd\delta^2)(T_G - T_6)$$

$$R_1 C_2 \frac{dE_6}{dt} = (E_7 - E_6) + \left(\frac{R_1}{R_2}\right)(E_5 - E_6) + \left(\frac{R_1}{R_4}\right)(E_G - E_6)$$

Node 7

$$\frac{\delta_2}{\alpha}\frac{\Delta T_7}{\Delta t} = (T_6 + T_8 - 2T_7) + \frac{4h'\,\delta_2}{kD}(T_G - T_7)$$

$$R_1 C_1 \frac{dE_7}{dt} = (E_6 + E_8 - 2E_7) + \left(\frac{R_1}{R_3}\right)(E_G - E_7)$$

Node 8

$$\frac{\delta_2}{\alpha}\frac{\Delta T_8}{\Delta t} = (T_7 + T_9 - 2T_8) + \frac{4h'\delta^2}{kd}(T_G - T_8)$$

$$R_1 C_1 \frac{dE_8}{dt} = (E_7 + E_9 - 2E_8) + \frac{R_1}{R_3}(E_G - E_8)$$

Node 9

$$\frac{\delta^2}{\alpha}\frac{\Delta T_9}{\Delta t} = (T_8 - T_9) + \frac{2h\delta^2}{kd}(T_G - T_9)$$

$$R_1 C_0 \frac{dE_9}{dt} = (E_8 + E_9) + \frac{R_1}{R_0}(E_G - E_9)$$

On inspection of the equation pairs, the equivalent dimensionless coefficent groups can be equated for the thermal and electrical networks to produce the following identities:

$$R_2 C_3 = \frac{\Delta^2}{\alpha}$$

$$\frac{R_2}{R_6} = \frac{2h'\Delta^2}{kD}$$

$$\frac{R_2}{R_5} = \frac{4h'\Delta^2}{kD}$$

$$R_1 C_2 = \frac{1}{2\alpha}\left(\frac{D^2\Delta\delta}{d^2} + \delta^2\right)$$

$$\frac{R_1}{R_2} = \frac{\delta}{\Delta}\frac{D^2}{d^2}$$

$$\frac{R_1}{R_4} = \frac{2}{kd^2}(h'D\Delta\delta + hd\delta^2)$$

$$R_1 C_1 = \frac{\delta^2}{\alpha} \text{ and } R_1 C_0 = \frac{\delta^2}{2\alpha}$$

$$\frac{R_1}{R_3} = \frac{4h\delta^2}{kd} \text{ and } \frac{R_1}{R_0} = \frac{2h'\delta^2}{kd}$$

If a value of C_1 is selected, then the remaining RC values can be calculated as follows:

$$R_1 C_1 = \frac{\delta^2}{\alpha} \text{ and } R_1 = \frac{1}{C_1}\frac{\delta^2}{\alpha}$$

$$C_0 = \frac{C_1}{2}$$

$$R_3 = \frac{R_1 kd}{4h\delta^2}$$

$$R_4 = R_1 \left[\frac{1}{\frac{2}{kd^2}(h'D\Delta\delta + hd\delta^2)} \right]$$

where $h' = h \left(\frac{d}{D}\right)^{1/2}$

$$R_2 = R_1 \left(\frac{\Delta^2}{\delta D^2}\right)$$

$$C_2 = \frac{1}{R_1 2\alpha}\left(\frac{D^2\Delta\delta}{d^2} + \delta^2\right)$$

$$R_5 = R_2 \left(\frac{kD}{4h'\Delta^2}\right)$$

$$R_6 = 2R_5$$

$$C_3 = \frac{\Delta^2}{R_2\alpha}$$

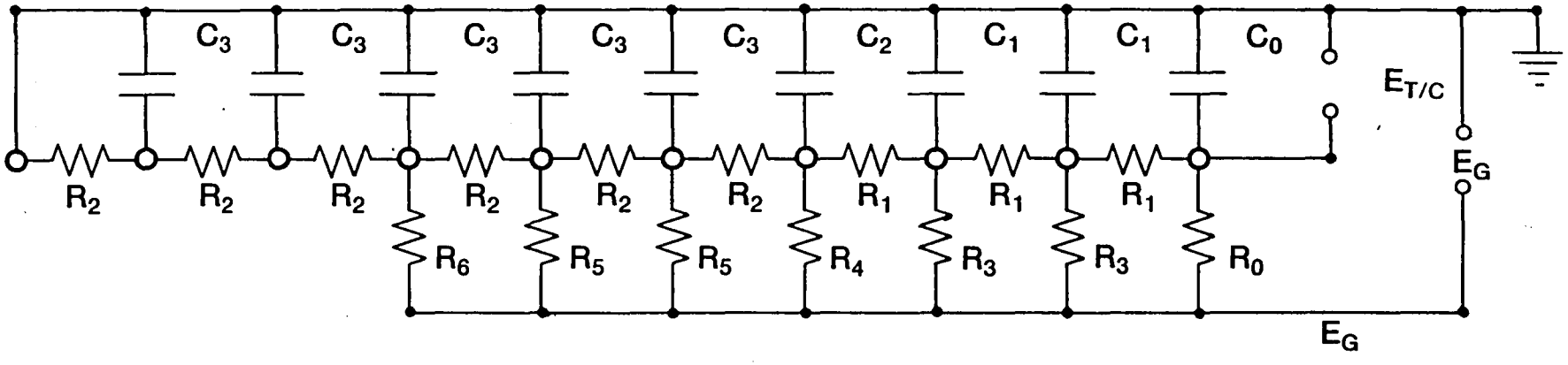

Figure E.1. RC Analog Network Simulation

F. LIST OF SYMBOLS

Symbol	*Description*	*Units*
A	Constant infinite element transfer function equations $= D^2 \Delta/8 \alpha \Delta T$	Meters-sec/K
a_n	Amplitude of the gas temperature at frequency f_n	K
$a_n(f)$	a_n as a function of frequency	K
a_1	Amplitude of the small 76 μm (0.003 in.) thermocouple element	K
a_2	Amplitude of the large 254 μm (0.010 in.) thermocouple element	K
B	Constant infinite element transfer function equation $= d^2 \delta/8 \alpha \Delta T$	Meters-sec/K
C	Constant infinite element transfer function equation $= D^2/4 \Delta$	Meters
C_{1-3}	Capacitance of electrical analog RC newtork component	μ farads
C_n	Radian frequency $= 2 \pi f_n$	Radians/sec
C_{pw}	Specific heat of thermocouple wire	Cal/grams-K
D	Large thermocouple element diameter at junction	Meters
d	Small thermocouple element diameter at junction	Meters
E	Constant infinite element transfer function equations $= d^2/4 \delta$	Meters
E	Young's Modulus	Newton/Meters^2
E_g	Electrical analog circuit emf corresponding to gas temperature	Volts
$E_{T/C}$	Electrical analog circuit emf corresponding to thermocouple temperature	Volts
F	Constant infinite element transfer function equations $= \Gamma D^{1/2} \Delta/2 \alpha$	Meters
F/A	Free Stream gas fuel-air ratio	Dim-less
FTIT	F100 engine third turbine vane gas probe temperature	K

Symbol	*Description*	*Units*
f	Frequency	Hz
f_n	nth frequency window in frequency space	Hz
G	Constant infinite element transfer function equations $= \Gamma\ d^{1/2}\ \delta/2\ \alpha$	Meters
G	Thermocouple signal gain	Dim-less
G_a	Design safety factor for vibrational stress	Dim-less
$G_{11}(f)$	Measured FFT Autospectral density function of smaller diameter t/c	K^2/Hz Phase — degrees
$G_{12}(f)$	Measured FFT cross-spectral density function between small and large diameter t/c's	K^2/Hz Phase — degrees
$S_1(f)$	Measured FFT spectrum of smaller diameter t/c	K Phase — degrees
g	Acceleration of gravity	Meters/sec^2
H	Probe ceramic height	Meters
H(f)	Measured transfer function (FFT frequency response function) of larger diameter t/c with respect to smaller diameter t/c	Gain — dim-less Phase — degrees
h^+, h_g	Convective film coefficient of t/c element	Watt/m^2K
h^-	Convective film coefficient of t/c support wire	Watt/m^2K
I	Moment of inertia	$Meters^4$
j	Time index	Seconds
k_c	Thermal conductivity of the probe ceramic	Cal/sec-Meter-K
k_g	Thermal conductivity of the gas	Cal/sec-Meter-K
k_w	Thermal conductivity of the thermocouple wire	Cal/sec-Meter-K
L	Length of the probe thermocouple support wire	Meters
l	One half of the length of the probe thermocouple element wire	Meters
M or M_n	Free stream gas Mach number	Dim-less
m	Probe mass/unit length	grams/Meter

Symbol	*Description*	*Units*
n	Cyclic frequency — subscript	Hz
N	Number of ensemble averages	Dim-less
Nu	Convective heat transfer Nusselt number for the thermocouple wire	Dim-less
P or P_T	Gas total pressure	Newton/Meter^2
P_{rg}	Gas Prandtl number	Dim-less
$R_0 \rightarrow R_5$	Resistance of electrical analog RC network components	ohms
S	Probe stress	Newton/Meters^2
SNR	Thermocouple signal-to-noise ratio	Dim-less
T,T_g, T_T	Gas total temperature	K
T_B	Probe ceramic base temperature	K
T_n	Instantaneous temperature of thermocouple wire at frequency n	K
T_P	Probe ceramic tip temperature	K
T_{Xpeak}	Maximum peak in instantaneous temperature of thermocouple wire at spacial location X	K
t_0	Arbitrary time reference	Seconds
$U_g$or V	Gas free stream velocity	Meters/sec
X	Spacial index — subscript	Dim-less

Symbol	*Greek Symbols*	*Units*
α	Thermal diffusivity of the thermocouple wire	Meters^2/sec
Γ	Aerodynamic parameter which is defined as = $0.48\ k_g\ P_{rg}^{1/3}\ U_g^{1/2}/(\mu_g/\rho_g)^{1/2}\ \rho_w\ C_{pw}$	Meters$^{3/2}$/sec
γ	Gas stream ratio of specific heats	Dim-less
γ^2	Coherence function	Dim-less

Symbol	Greek Symbols	Units
Δ	Finite element model spacing of the thermocouple support wire	Meters
ΔT	Temperature difference	K
Δt	Time step	sec
δ	Finite element model spacing of thermocouple element wire	Meters
ϵ_{error}	Transfer function error	%
ζ	Transfer function (gain and phase) of the thermocouple wire with respect to the gas temperature at frequency f_n	Gain — dim-less Phase — degrees
η	Fin efficiency function = $\sqrt{4\ Nu\ kg/D^2\ kc}$	1/Meters
η_{1n}	Phase shift of the 76 μm (0.003 in.) thermocouple with respect to gas temperature at frequency f_n	Degrees
η_{2n}	Phase shift of the larger diameter thermocouple with respect to gas temperature at frequency f_n	Degrees
θ_{1n}	Peak amplitude of the smaller diameter thermocouple at frequency f_n	K
$\theta_1(f)$	θ_{1n} as a function of frequency	K
θ_{2n}	Peak amplitude of the larger diameter thermocouple at frequency f_n	K
$\theta_2(f)$	θ_{2n} as a function of frequency	K
λ_i	Stress constant for cantilever beam	Dim-less
λ_{1n}	Phase shift of smaller diameter thermocouple at frequency f_n with respect to arbitrary time t_0	Degrees

Symbol	*Greek Symbols*	*Units*
$\lambda_1(f)$	λ_{1n} as a function of frequency	Degrees
λ_{2n}	Phase shift of larger diameter thermocouple at frequency f_n with respect to arbitrary time t_0	Degrees
$\lambda_2(f)$	λ_{2n}as a function of frequency	Degrees
σ	Boltzmann constant	J/K
μ_g	Gas stream viscosity	Grams/Meter-sec
ρ_w	Density of the thermocouple wire	Grams/Meter^3
ρ_g	Density of the gas stream	Grams/Meter^3
ϕ_n	Phase shift of the gas temperature with respect to arbitrary time t_0 at frequency f_n	Degrees
$\phi(f)$	ϕ_n as function of frequency	Degrees
ψ	Fin efficiency	Dim-less
$\gamma^2_{12}(f)$	Measured FFT ordinary coherence function between larger diameter t/c and smaller diameter t/c	Dim-less

DISTRIBUTION LIST FOR
CONTRACT NAS3-23154

INSTRUMENTATION R&D BRANCH

Each addressee will receive one copy of Volume I only, unless indicated otherwise.

*NASA Lewis Research Center
21000 Brookpark Road
Cleveland, OH 44135
Attn: G. Fralick, M.S. 77-1
(50 copies)

*NASA Lewis Research Center
21000 Brookpark Road
Cleveland, OH 44135
Attn: Leonard W. Schopen, M.S. 501-11

*NASA Scientific and Technical
Information Facility
P.O. Box 33
College Park, MD 20740
Attn: Acquisitions Branch
(22 copies)

*NASA Lewis Research Center
21000 Brookpark Road
Cleveland, OH 44135
Attn: Library, M.S. 60-3
(2 copies)

*NASA Lewis Research Center
21000 Brookpark Road
Cleveland, OH 44135
Attn: Report Control Office, M.S. 5-5
(2 copies)

General Electric Company
Aircraft Engine Group
Evendale, OH 45215
Attn: Wayne Shaffernocker, MSH-78
Ronald Weise, MSH-78

Stanford University
Stanford, CA 94305
Attn: Dr. R. J. Moffat
Asst. Prof., Mech. Engr.
Dir. Thermoscience
Measurement Center

*Air Force Wright Aeronautical
Laboratory
Wright Patterson AFB, OH 45433
Attn: R. Cox/POTC

*Air Force Wright Aeronautical
Laboratory
Wright Patterson AFB, OH 45433
Attn: Everett E. Bailey/AFWAL/NASA-PO

*Air Force Wright Aeronautical
Laboratory
Wright Patterson AFB, OH 45433
Attn: Deborah Finnerty/POTC

*Air Force Wright Aeronautical
Laboratory
Wright Patterson AFB, OH 45433
Attn: M. Roquemore/POSF

Roto Data, Inc.
10200 Anderson Way
Cincinnati, OH 45242
Attn: David Davidson

UTRC/OATL
Pratt & Whitney Aircraft
Main Plant
P.O. Box 2691
West Palm Beach, FL 33402
Attn: John T. Carroll

Lewis Engineering Company
238 Wate Street
Naugatuck, CT 06770
Attn: C. B. Stegner

*Arnold Engineering
Development Center
Arnold Air Force Station, TN 37389
Attn: Marshall Kingery

*Volumes I and II.

Hitec Corporation
Nardone Industrial Park
Westford, MA 01886
Attn: Steve Wnuk

General Electric Company
Aircraft Engine Group
1000 Western Avenue
Lynn, MA 01910
Attn: George Leperch, A129dD

General Electric Company
Aircraft Equipment Division
50 Fordham Road
Wilmington, MA 01887
Attn: Ronald J. Casagrande

Allison Gas Turbine Operations
General Motors Corporation
Box 894
Indianapolis, IN 46206
Attn: John Custer, W-16

Allison Gas Turbine Operations
General Motors Corporation
Box 894
Indianapolis, IN 46206
Attn: Ken Cross

Allison Gas Turbine Operations
General Motors Corporation
Box 894
Indianapolis, IN 46206
Attn: David Willis

Allison Gas Turbine Operations
General Motors Corporation
Box 894
Indianapolis, IN 46206
Attn: Ralph Fox

Battelle Columbus Laboratories
505 King Avenue
Columbus, OH 43201
Attn: Ross G. Luce, Energy &
Thermal Tech. Section

Teledyne CAE
1350 Laskey Road
Toledo, OH 43612
Attn: R. Hugh Gaylord

Garrett Turbine Engine Company
P.O. Box 5217
Phoenix, AZ 85010
Attn: N. Fred Pratt

FluiDyne Engr. Corporation
5900 Olson Memorial Highway
Minneapolis, MN 55422
Attn: T. Matsuura

AVCO Corporation
Lycoming Division
550 South Main Street
Stratford, CT 06497
Attn: E. Twarog, Mgr.
Electronics and Instr.

Thermonetics Corporation
1028 Garnet Avenue
San Diego, CA 92109
Attn: H. F. Poppendiek

Battelle Columbus Laboratories
505 King Avenue
Columbus, OH 43201
Attn: M. M. Lemcoe

Peter K. Stein
5602 East Monterosa
Phoenix, AZ 85018

Pratt & Whitney Aircraft
Main Plant
P.O. Box 2691
West Palm Beach, FL 33402
Attn: John Prosser (MS C-04)

National Bureau of Standards
Washington, DC 20234
Attn: Ray Dils

*National Bureau of Standards
Washington, DC 20234
Attn: George Burns
Inst. for Basic Research

General Electric Company
P. O. Box 8
Schenectady, NY 12301
Dr. David Skelley
Bldg. K-1, Rm. 3B24

Mechanical Technology, Inc.
968 Albany-Shaker Road
Latham, NY 12110
Attn: R. Hohenberg

Boeing Aerospace Company
Engineering Laboratories
Seattle, WA 98124
Attn: Darrell R. Harting

Engelhard
Engelhard Industries Div.
228 East 10th Street
Newport, KY 41075
Attn: Ronald G. Braun

Williams Research
2280 West Maple Road
Walled Lake, MI 48088
Attn: Henry Moore, Head
Instr. Dept.

Virginia Polytechnic Institute
and State University
Mechanical Engineering Dept.
Blacksburg, vA 24061
Attn: W. F. O'Brien, Jr.

*Naval Post Graduate School
Department of Aeronautics (Code 67)
Monterey, CA 93940
Attn: Prof. R. P. Shreeve

Pennsylvania State University
233 Hammond Building
University Park, PA 16802
Attn: Prof. B. Lakshminarayana

Kulite Semiconductor Products, Inc.
1039 Hoyt Avenue
Ridgefield, NJ 07657
Attn: John R. Hayer

Bolt Beranek and Newman, Inc.
50 Moulton Street
Cambridge, MA 02138
Attn: Richard E. Hayden

Caterpillar Tractor Company
Technical Center, Building F
100 Northeast Adams Street
Peoria, IL 61629
Attn: Mr. Donald Wilson

*Air Force Wright Aeronautical
Laboratory
Wright Patterson AFB, OH 45433
Attn: Mr. Charles Bentz/POTC
Hot Section Technology

AVCO Corporation
Lycoming Division
550 South Main Street
Stratford, CT 06497
Attn: Mr. K. Collinge
IRAD Mechanical Projects
Manager

Eaton Corporation
Box 766
Southfield, MI 48037
Attn: Mr. Lamont Eltinge
Director of Research

Public Service Electric & Gas Company
80 Park Plaza
Newark, NJ 07101
Attn: Dr. Melvin L. Zwillenberg
Research & Development Dept.

Raychem Corporation
300 Constitution Drive
Menlo Park, CA 94025
Attn: Dr. David C. Chappelear
Director of Corporate
Research & Development

Fabrication Development Laboratory
Owens/Corning Fiberglas
Technical Center
Granville, OH 43023
Attn: Mr. Hugh W. Bradley, Jr.

Xerox Electro-Optical Systems
1616 North Fort Myer Drive, 16th Floor
Arlington, VA 22209
Attn: Mr. Clifford I. Cummings
Manager, Intelligence &
Reconnaissance

Construction Materials Support Group
Owens/Corning Fiberglas
CMG Process Technology Laboratory
Granville, OH 43023
Attn: Mr. J. W. Scott

NASA Headquarters
Washington, DC 20546
Attn: M/Paul N. Herr

Massachusetts Institute of Technology
Cambridge, MA 02139
Attn: Dr. Alan Epstein
Rm. 31-266

Sverdrup (AEDC)
Arnold AFB, TN 37389
Attn: Paul McCarty

Rosemont, Inc.
Mail Stop F-15
P.O. Box 959
Burnsville, MN 55337
Attn: Mr. Larry N. Wolfe

Thermogage, Inc.
330 Allegany Street
Frostburg, MD 21532
Attn: Charles E. Brookley

Hycal Engineering
12105 Los Nietos Road
Sante Fe Springs, CA 90670
Attn: William Clayton

Medtherm Corporation
P.O. Fox 412
Huntsville, AL 35804
Attn: Larry Jones

Rocketdyne
6633 Canoga Avenue
Canoga Park, CA 91304
Attn: Dr. John C. Lee

Combustion Engineering
Dept. 9005-03D1
Windsor, CT 06095
Attn: John Fishburn

RdF Corporation
23 Elm Avenue
Hudson, NH 03051
Attn: Frank Hines

Babcock & Wilcox R&D Division
P.O. Box 835
Alliance, OH 44601
Attn: Harold Wahle

JEC Lasers, Inc.
253 Crooks Avenue
Paterson, NJ 07503
Attn: Mr. John Wasko

*NASA Langley Research Center
Hampton, VA 23665
Attn: R. E. Wright, Jr. (MS-234)

Babcock & Wilcox R&D Division
P.O. Box 835
Alliance, OH 44601
Attn: John Berthold

Applied Sensors International
7834 Palace Drive
Cincinnati, OH 45242
Attn: Richard Stillmaker

Carnegie-Mellon University
Dept. of Mechanical Engineering
Pittsburgh, PA 15213
Attn: Dr. Norman Chigier
Professor William J. Brown